EXPERIMENTAL INVESTIGATIONS ON POWDER MIXED ELECTRO-DISCHARGE MACHINING (PMEDM) OF INCONEL 718: STUDY OF PARAMETRIC EFFECT AND MACHINING PERFORMANCE OPTIMIZATION

Thesis submitted by

SANTOSH KUMAR SAHU

Doctor of Philosophy (Engineering)

Mechanical Engineering Department
Faculty Council of Engineering & Technology
Jadavpur University
Kolkata-700032, India

2018

JADAVPUR UNIVERSITY
KOLKATA-700032

Index No. **D-7/E/589/16**

1. Title of the thesis:

   Experimental Investigations on Powder Mixed Electro-Discharge Machining (PMEDM) of Inconel 718: Study of Parametric Effect and Machining Performance Optimization

2. Name, Designation and Institution of the Supervisor/s:

   Dr. Goutam Nandi
   Associate Professor, Mechanical Engineering Department,
   Jadavpur University, Kolkata-700032, West Bengal

   Dr. Saurav Datta
   Associate Professor, Department of Mechanical Engineering,
   National Institute of Technology, Rourkela-769008, Odisha

3. List of Publications:

   Santosh Kumar Sahu, Thrinadh Jadam, Saurav Datta, Goutam Nandi, (July 2018) *Effect of using SiC powder added dielectric media during electro-discharge machining of Inconel 718 super alloys*, **Journal of the Brazilian Society of Mechanical Sciences and Engineering**, 40: 330. DOI: 10.1007/s40430-018-1257-7 ***(Published Online)***

   Santosh Kumar Sahu, Saurav Datta, (2019) *Experimental studies on graphite powder mixed electro-discharge machining of Inconel 718 super alloys: comparison with conventional electro-discharge machining*, **Proceedings of the Institution of Mechanical Engineers**, **Part E: Journal of Process Mechanical Engineering**, 33(2): 384-402.
   DOI: 10.1177/0954408918787104

4. List of Patents: NA

5. List of Presentation in National/International:

   Santosh Kumar Sahu, Thrinadh Jadam, Saurav Datta, Debabrata Dhupal, Goutam Nandi, Application of SiC powder added in kerosene dielectric media for electro-discharge machining of Inconel 718 super alloys: effects of powder concentration, **International Conference on Materials Processing and Characterization (ICMPC 2018)**, held during March 16-18, 2018, organized by GRIET, **Hyderabad**.

   Santosh Kumar Sahu, Saurav Datta, Goutam Nandi, Siba Sankar Mahapatra, Study of parametric effect and machining-induced surface integrity during EDM of Inconel 718 super alloys, **National Conference on Mechanical**, **Production and Industrial Engineering (NCMPIE 2018)** sponsored by Madhya Pradesh Council of Science and Technology (MPCST), organized by Department of Mechanical Engineering, St. Aloysius Institute of Technology (SAIT), **Jabalpur** (MP-482002) during August 31-September 01, 2018.

CERTIFICATE

Date _____

This is to certify that the thesis entitled ***Experimental Investigations on Powder Mixed Electro-Discharge Machining (PMEDM) of Inconel 718: Study of Parametric Effect and Machining Performance Optimization*** submitted by ***Shri Santosh Kumar Sahu*** who got his name registered on **21/09/2016** for the award of **Ph.D. (Engineering)** degree of **Jadavpur University** is absolutely based upon his own work under the supervision of ***Dr. Goutam Nandi*** and ***Dr. Saurav Datta***, and neither his thesis nor any part of the thesis has been submitted for any degree/diploma or any other academic award anywhere before.

Dr. Goutam Nandi
Associate Professor
Mechanical Engineering Department
Jadavpur University
Kolkata-700032
Email: gnandi87@gmail.com

Dr. Saurav Datta
Associate Professor
Department of Mechanical Engineering
National Institute of Technology, **Rourkela**
Rourkela-769008 (Odisha)
Email: sdatta@nitrkl.ac.in

Acknowledgement

This dissertation is a milestone in my academic career. I am grateful to many people who have guided and supported me throughout the research tenure and provided assistance for this venture. Foremost, I would like to express my sincere gratitude to my Ph. D. supervisors: Principal Supervisor ***Dr. Goutam Nandi***, Associate Professor, Mechanical Engineering Department, **Jadavpur University**, Kolkata and Co-Supervisor ***Dr. Saurav Datta***, Associate Professor, Department of Mechanical Engineering, **National Institute of Technology Rourkela** (Odisha). I am always grateful for their patience, motivation, enthusiasm, and immense knowledge. Their guidance helped me in various ways during my research and in the course of writing this dissertation.

Dr. Saurav Datta is a gracious mentor who demonstrates that rigorous scholarship can and must be accessible to everyone, that social change is central to intellectual work and as such, scholars have a responsibility to use the privileges of academia to imagine and create a better world. I could not have imagined having a better supervisor and mentor for my Ph. D.

Besides my supervisors, I would like to express my deepest gratitude to the members of the Internal Research Committee (IRC): ***Prof. Dipankar Bose***, Professor, National Institute of Technical Teachers Training and Research (NITTTR), Kolkata, ***Dr. Subhash Chandra Panja***, Associate Professor, Mechanical Engineering Department, and ***Prof. Bijan Sarkar***, Professor, Production Engineering Department, Jadavpur University, Kolkata for their insightful comments and constructive suggestions during busy semesters.

I would also like to express my deepest gratitude to our professors of the Department of Mechanical Engineering, Jadavpur University, Kolkata, for showing me by example through course works how to think, teach, and teach others to think. In this context, I would like to mention the contributions of ***Prof. Asish Bandyopadhyay***, Professor, Mechanical Engineering Department, Jadavpur University, Kolkata, a person with an amicable and positive disposition, who has always made himself available to clarify my doubts despite his busy schedules and to enable me learning from his research expertise. Thank you so much sir for all your help and support.

I am also highly obliged to ***Prof. Suranjan Das***, our Honorable Vice-Chancellor, ***Prof. Chiranjib Bhattacharjee***, Dean, Faculty Council of Engineering and Technology, ***Prof Gautam Majumdar***, Head, Department of Mechanical Engineering, Jadavpur University, Kolkata for their academic support and concern about requirements to carry out the research work in the university.

Special thank goes to all faculty and staff-members: Mechanical Engineering Department, Jadavpur University, Kolkata, and Mechanical Engineering Department, National Institute of Technology, Rourkela, for their vital support, kind and generous help during the progress of my work which formed the backbone of this research work.

The thesis would not have come to a successful completion, without the help of ***Prof. Debabrata Dhupal***, Professor and HOD, ***Prof. Debadutta Mishra***, Department of Production Engineering, Veer Surendra Sai University of Technology (VSSUT) Burla, Odisha. I am

particularly thankful to ***Mr. Prasanta Kumar Samal***, Junior Instructor for providing technical support to carry out my experimental work in the EDM set up. He was always very kind and patient; always willing to lend his service whenever I approached him. I, therefore, must acknowledge and appreciate him for all his efforts.

I greatly appreciate ***Dr. Chitta Ranjan Deo***, Associate Professor, Department of Mechanical Engineering and ***Dr. Sudhansu Ranjan Das***, Associate Professor, Department of Production Engineering, VSSUT, Burla for their generous times spend for me. I would like to express my special thanks to ***Dr. Das*** for being a great soul. I find him always ready to help others with a smile.

I would like to convey my heartiest thanks to my friends: ***Dr. Nikhil Kumar***, Ex. Ph.D. Scholar, Jadavpur University, Kolkata, ***Mr. Suman Chatterjee***, ***Mr. Thrinadh Jadam***, Ph.D. Scholars, National Institute of Technology, Rourkela and ***Dr. Priyadarshi Tapas Ranjan Swain***, Assistant Professor, Department of Mechanical Engineering, VSSUT, Burla for their continuous support and encouragement throughout my research endeavor.

I greatly appreciate and convey my heartfelt thanks to the persons for sharing their enthusiasm and comments on my work: ***Mr. Binay Kumar Paul*** and ***Mr. Biswajit Dey***, Ex. M. Tech. Scholars, Department of Mechanical Engineering, National Institute of Technology, Rourkela.

The greatest gift I ever had, came from God, I call them **MAA** and **BAPA**, I owe a lot to my Parents ***Shri Udayanath Sahu*** and ***Smt. Rupabati Sahu***, for their inseparable support and encouragements at every movement of my life and yearned to see this achievements practically come true. They are the people who show me the joy of the intellectual pursuit ever since I was born on the earth. I will be always thankful to my parents because they both have done everything for me, including sacrificing their joys to make me happy. I also feel pleased to strong acknowledge the support received from my elder six sisters, thirteen nephews and nieces in every possible way to see the completion of this research work. I would also like to thank them.

Specially, I would like to thank my wife ***Swarnalipi Sahoo (Leema)*** who has always been there cheering me up and stood by me throughout good times and bad. Generally people say no man succeeds without a good woman behind him. Wife or mother, if it is both, she is twice blessed indeed. In that aspect, I am indeed very lucky.

Last but not the least; I will always be thankful to my son ***Chidatma Chetan Sahu (Kanha)*** for giving his cute smiles and doing all the naughty activities, which always release all stresses from my mind.

Above all, I owe it all to ***Almighty God*** for granting me the wisdom, health and strength to undertake this research task and enabling me to its completion.

SANTOSH KUMAR SAHU

Abstract

Inconel 718 is a nickel based super alloy widely applied in aerospace, automotive and defense industries. Low thermal conductivity, extreme high temperature strength, strong work-hardening tendency make the alloy '*difficult-to-cut*'. In contrast to traditional machining, non-conventional route like Electro-Discharge Machining (EDM) is relatively more advantageous to machine this alloy. However, low thermal conductivity of Inconel 718 restricts EDM to perform well.

In order to improve EDM performance of Inconel 718, Powder-Mixed Electro-Discharge Machining (PMEDM) was reported in the present dissertation. PMEDM was carried out by adding graphite powder to the dielectric medium (EDM oil) in consideration with varied peak discharge current. The morphology and topographical features of the machined surface including surface roughness, crack density, white layer thickness, metallurgical aspects (phase transformation, crystallite size, micro-strain, and dislocation density), material migration, residual stress as well as micro-indentation hardness etc. were studied and compared to that of conventional EDM. Additionally, effects of peak discharge current were discussed on influencing different performance measures of PMEDM. Material removal efficiency and tool wear rate were also examined. Use of graphite powder-mixed EDM was experienced better in performance for improved material removal rate, superior surface finish, reduced tool wear rate, and reduced intensity as well as severity of surface cracking. Lesser extent of carbon migration onto the machined surface as observed in powder-mixed EDM in turn reduced possibility of formation of hard carbide layers. As compared to conventional EDM graphite powder-mixed EDM exhibited relatively less micro-hardness and residual stress at the machined surface. Maximum improvement in MRR was observed (~13.08%) at 30A. The most satisfactory surface finish was obtained at 20A (R_a ~49.15% reduced than conventional EDM). The minimum tool wear rate was noticed at 30A (~92.68% less than conventional EDM).

In continuation to the previous work, EDM of Inconel 718 was carried out further using SiC powder-mixed kerosene as dielectric media. Apart from considering peak discharge current, and pulse-on duration; particle concentration were also varied to evaluate the performance of EDM process. Based on L_9 Orthogonal Array (OA) design of experiment, material removal efficiency, surface roughness, surface crack density, and white layer thickness were measured. Effects of process parameters along with powder concentration were studied on influencing various EDM responses. Finally, an optimal setting of parameters (peak discharge current, and pulse-on time), followed by an optimal powder concentration was determined to achieve satisfactory EDM output in purview of machining efficiency, and surface integrity of the EDMed part. Utility theory coupled with Taguchi method was utilized to evaluate the optimal process environment. Within selected experimental domain, the most appropriate parametric combination was determined: [I_P= 25A, T_{on}= 1000µs and powder concentration 4g/l].

Keywords: Inconel 718; super alloy; Electro-Discharge Machining (EDM); Powder-Mixed Electro-Discharge Machining (PMEDM); Orthogonal Array (OA); surface crack density; white layer thickness; Utility theory; Taguchi method

Content

Particulars	Page No.
Title Page	i
Summary Sheet	ii
Certificate	iii
Acknowledgment	iv
Abstract	vi
Content	vii
List of Figures	viii-ix
List of Tables	x
Abbreviations	xi
1. Background and Rationale	**1-12**
1.1 Introduction	1
1.2 State of Art	2
1.3 Problem Statement: Coverage of the Present Dissertation	7
2. Experimental Details	**13-19**
3. Application Potential of Graphite Powder-Mixed EDM: Comparison with Conventional EDM	**20-42**
3.1 Characterization of Graphite Powder Particles	20
3.2 Surface Integrity	22
3.2.1 Surface Morphological Characteristics	22
3.2.2 XRD Test Results: Metallurgical Characteristics	25
3.2.3 Analysis of EDS and Micro-Hardness Test Results	33
3.3 Effects of Peak Discharge Current	35
4. EDM of Inconel 718 with SiC Powder-Mixed Kerosene Dielectric Media: Effects of Powder Concentration	**43-61**
4.1 Characterization of SiC Powder Particles	43
4.2 Surface Integrity: Morphology and Topography	45
4.3 Prediction of Optimal Setting: Effects of Process Factors	50
5. Summary and Conclusions	**62-64**
5.1 Conclusions	62
5.2 Scope for Future Work	64
References	**65-69**
Appendix I	70-73
Appendix II	74
Appendix III	75
Appendix IV	76-78
Resume of Mr. SANTOSH KUMAR SAHU	79

List of Figures

Figure No./ Figure Caption	Page No.
Fig. 1.1: Working principle of PMEDM	3
Fig. 2.1: (a) Experimental setup with accessories for powder-mixed EDM, and (b) Close view of the machining area	14
Fig. 2.2: EDMed work surfaces of Inconel 718 obtained in (a) conventional EDM, and (b) graphite powder-mixed EDM	16
Fig. 2.3: Snapshot of EDMed work surfaces of Inconel 718 (obtained through PMEDM with SiC powder mixed kerosene as dielectric) along with copper tool electrode	18
Fig. 3.1: XRD spectra for 'as received' graphite powder	20
Fig. 3.2: SEM micrographs taken at different magnifications of 'as received' graphite powder	21
Fig. 3.3: Optimal images exhibiting crater morphology of the EDMed specimens obtained through (a) conventional EDM, and (b) graphite powder-mixed EDM	23
Fig. 3.4: SEM micrographs exhibiting irregularities of the EDMed work surfaces of Inconel 718 obtained in (a) conventional EDM, and (b) graphite powder-mixed EDM at I_P=30A	23
Fig. 3.5: SEM micrographs exhibiting severity of surface cracking of the EDMed work surfaces of Inconel 718 obtained in (a) conventional EDM, and (b) graphite powder-mixed EDM at I_P=30A	24
Fig. 3.6: SEM micrographs exhibiting existence of white layer onto the top of the machined surface obtained in (a) conventional EDM (WLT~31.77µm), and (b) graphite powder-mixed EDM (WLT~36.93µm) at I_P=25A	24
Fig. 3.7: XRD spectra for 'as received' Inconel 718	25
Fig. 3.8a: XRD spectra for the EDMed work surface of Inconel 718 produced at I_P=30A obtained through conventional EDM	26
Fig. 3.8b: XRD spectra for the EDMed work surface of Inconel 718 produced at I_P=30A obtained through graphite powder-mixed EDM	26
Fig. 3.9: EDS results for the EDMed work surface of Inconel 718 produced at I_P=25A for conventional EDM	33
Fig. 3.10: EDS results for the EDMed work surface of Inconel 718 produced at I_P=25A for graphite powder-mixed EDM	34
Fig. 3.11: Effect of peak discharge current on MRR	36
Fig. 3.12: Effect of peak discharge current on R_a	37
Fig. 3.13: Effect of peak discharge current on SCD: (a) SCD~0.0111µm/µm^2 for Conventional EDM at I_P=15A, (b) SCD~0.0133µm/µm^2 for **Conventional EDM** at I_P=25A, (c) SCD~0.0074µm/µm^2 for **Graphite powder-mixed EDM** at I_P=15A, (d) SCD~0.0106µm/µm^2 for Graphite powder-mixed EDM at I_P=25A	38
Fig. 3.14: Effect of peak discharge current on WLT (a) WLT **(Conventional EDM)** ~32.36µm, 33.21µm, 35.51µm and (b) WLT **(Graphite powder-mixed EDM)** ~33.94µm, 43.6µm, 47.23µm for I_P=15A, 20A, and 30A, respectively	40
Fig. 3.15: SEM micrographs exhibiting existence of white layer onto the top of the machined surface obtained in (a) conventional EDM (WLT~46.99µm), and (b) graphite powder-mixed EDM (WLT~33.94µm) at I_P=15A	40

Figure No./ Figure Caption	Page No.
Fig. 3.16: Effect of peak discharge current on TWR	41
Fig. 4.1: XRD spectra for ‘as received’ SiC powders	43
Fig. 4.2: SEM micrographs obtained at different magnifications of ‘as received’ SiC powders	44
Fig. 4.3: Surface morphology of EDMed surface (as observed under SEM) at I_P= 30A, T_{on}=1500µs and powder concentration 4g/l	46
Fig. 4.4: SEM micrograph exhibiting presence of white layer over the EDMed surface obtained at I_P= 30A, T_{on}=1500µs and powder concentration 4g/l (WLT ~ 34.18 µm)	46
Fig. 4.5: EDS elemental spectra for (a) ‘as received’ Inconel 718, (b) EDMed surface of Inconel 718 at I_P= 35A, T_{on}= 1500µs and powder concentration 0g/l, and (c) EDMed surface of Inconel 718 at I_P= 35A, T_{on}= 2000µs and powder concentration 2g/l	47
Fig. 4.6a: XRD spectra for ‘as received’ Inconel 718	48
Fig. 4.6b: XRD spectra for EDMed surface of Inconel 718 obtained at I_P= 35A, T_{on}= 1000µs and powder concentration 4g/l	48
Fig. 4.7: Mean S/N ratio plot for overall utility degree: Prediction of optimal setting. Predicted optimal setting: $A_1B_1C_3$ i.e. [I_P= 25A, T_{on}= 1000µs and powder concentration 4g/l]	52
Fig. 4.8: Effect of peak current on MRR	53
Fig. 4.9: Effect of pulse-on time on MRR	54
Fig. 4.10: Effect of peak current on R_a	55
Fig. 4.11: Effect of pulse-on time on R_a	55
Fig. 4.12: Effect of peak current on SCD	56
Fig. 4.13: Effect of pulse-on time on SCD	57
Fig. 4.14: Effect of peak current on WLT	57
Fig. 4.15: Effect of pulse-on time on WLT	58
Fig. 4.16: Effect of powder concentration on MRR	59
Fig. 4.17: Effect of powder concentration on R_a	60
Fig. 4.18: Effect of powder concentration on SCD	61
Fig. 4.19: Effect of powder concentration on WLT	61

List of Tables

Table No./ Table Caption	Page No.
Table 1.1: Types of dielectrics/powders used in literature for PMEDM	9
Table 2.1: Chemical composition of Inconel 718 [40]	13
Table 2.2: Properties of Inconel 718	14
Table 2.3: Properties of graphite powder	14
Table 2.4: Parameters kept at constant values	16
Table 2.5: Properties of SiC powder	17
Table 2.6: Domain of experiments: Parameters and values	18
Table 2.7: Design of Experiment (DOE) and collected response data	19
Table 3.1: Computation of crystallite size (L) for 'as received' graphite powder along different crystallographic directions	22
Table 3.2: Precipitates/intermetallic compounds observed at the EDMed work surface	28
Table 3.3: The variation of crystallite size (L), and dislocation density (ψ) for (1) 'as received' Inconel 718, and EDMed work surface of Inconel 718 obtained by using (2) Conventional EDM, and (3) Graphite powder-mixed EDM at **I_p=15A**	30
Table 3.4: The variation of crystallite size (L), and dislocation density (ψ) for (1) 'as received' Inconel 718, and EDMed work surface of Inconel 718 obtained by using (2) Conventional EDM, and (3) Graphite powder-mixed EDM at **I_p=25A**	31
Table 3.5: The variation of crystallite size (L), and dislocation density (ψ) for (1) 'as received' Inconel 718, and EDMed work surface of Inconel 718 obtained by using (2) Conventional EDM, and (3) Graphite powder-mixed EDM at **I_p=30A**	32
Table 3.6: Average crystallite size (L_{avg}) of the EDMed specimens as compared to 'as received' work material	42
Table 4.1: Computation of crystallite size (L) for 'as received' SiC powder along different crystallographic planes (corresponding directions)	45
Table 4.2a: The variation of crystallite size (L), and dislocation density (δ) for (1) 'as received' Inconel 718, (2) EDMed work surface of Inconel 718 obtained at (I_P= 35A, T_{on}=1000µs and powder concentration 4g/l)	49
Table 4.2b: The variation of crystallite size (L), and dislocation density (δ) for (1) 'as received' Inconel 718, (2) EDMed work surface of Inconel 718 obtained at (I_P= 35A, T_{on}=1000µs and powder concentration 4g/l)	50
Table 4.2c: The variation of crystallite size (L), and dislocation density (δ) for (1) 'as received' Inconel 718, (2) EDMed work surface of Inconel 718 obtained at (I_P= 35A, T_{on}=1000µs and powder concentration 4g/l)	51
Table 4.3: Computed utility values and overall utility degree	51
Table 4.4: Mean response table	52

Abbreviations

APM-EDM	Abrasive Powder-Mixed Electro-Discharge Machining
CNT	Carbon nanotube
DOE	Design of Experiment
ECM	Electro-Chemical Machining
EDD	Electro-Discharge Drilling
EDM	Electro-Discharge Machining
EDS	Energy Dispersive X-ray Spectroscopy
FWHM	Full-Width Half-Maximum
GRA	Grey Relational Analysis
Grey-PCA	Principal Component Analysis-based grey technique
HA	Hydroxyapatite
HB	Higher-is-Better
(L)	Crystallite size
(L_{avg})	Average crystallite size
LB	Lower-is-Better
MMCs	Metal Matrix Composites
MRR	Material Removal Rate
OA	Orthogonal Array
PMEDM	Powder-Mixed Electro-Discharge Machining
(PMND)-EDM	Powder-Mixed Near-Dry-EDM
PSO	Particle Swarm Optimization
R_a	Roughness average
R_{max}	Peak-to-valley roughness
SCD	Surface Crack Density
SEM	Scanning Electron Microscope
TOPSIS	Technique for Order Preference by Similarity to Ideal Solution
TWR	Tool Wear Rate
WLT	White Layer Thickness
XRD	X-ray Diffraction Microscopy
μEDM	Micro-Electro-Discharge Machining
(ϖ)	Micro-strain
(ψ)	Dislocation density

CHAPTER 1

Background and Rationale

1.1 Introduction

Inconel 718 is an austenitic nickel-chromium based super alloy [1], which finds wide application in nuclear reactor, marine engineering, chemical processing and aerospace [2-3]. Inconel 718 exhibits excellent mechanical properties like high temperature resistance, high resistance to corrosion and high strength even at elevated temperatures [2, 4, 5].

As mentioned in Tool Engineers Handbook [6], the term 'machinability' refers to 'easiness of machining'. Machinability can be judged by some indices which, in general, include material removal efficiency, tool life, surface integrity, consumed energy, etc. However, fabrication of complex shapes by this alloy with good dimensional accuracy as well as surface finish is indeed difficult to achieve by standard machining routes. Inconel 718 is therefore termed as '*difficult-to-machine*'. Due to its underprivileged thermal conductivity, high cutting temperature is evolved at the tool-tip. This results in reduction of tool life. High cutting forces generated during machining promotes severe vibration of the machine tool which deteriorates surface finish of the end product. The strong work-hardening tendency of this alloy invites another challenge to execute machining operation efficiently.

In contrast to conventional machining, a non-traditional route like Electro-Discharge Machining (EDM) is found comparatively more suitable for machining of this alloy. However, EDM performance on Inconel 718 is highly influenced by the electrical parameters such as peak current, gap voltage, pulse duration, duty cycle, and polarity. Material properties of tool/workpiece including melting temperature, electrical and thermal conductivity etc. do play important role towards sound execution of EDM operation [7]. However, poor material removal rate and inferior surface finish limit the application of conventional EDM of Inconel 718. In order to overcome this, application of abrasive (conductive/ semi-conductive) powder added to the dielectric fluid was recommended in literature [8-11].

In PMEDM, abrasive powders (conductive/semi-conductive type) when added to the dielectric media increases thermal and electrical conductivity of the working medium. Enlarged discharge gap followed by reduction in energy density improves process stability.

Multiple discharges take place for a single pulse input. The sparking is uniformly distributed amongst the suspended powder particles; therefore, reduced energy density stimulates formation of wide and shallow craters. The process improves material removal efficiency and offers favorable surface finish as compared to conventional EDM. Desired mechanical properties can also be achieved at the machined surface through PMEDM. However, properties of powder particles, powder concentration, particle size etc. play important role in determining success of the PMEDM process. Advantages of PMEDM include:

1. Any material (electrically conductive) can be machined, regardless of its strength, hardness toughness and microstructure.
2. Complicated die contours can be produced with precise dimension and good surface finish.
3. PMEDM process is totally burring free.
4. The PMEDM can overcome some of the shortcomings of conventional EDM like low efficiency to material removal, inferior surface quality, and excessive tool wear [10].
5. Application of powder mixed dielectric fluid results in wide discharge gap and reduced energy density [11].
6. In PMEDM process, reduction of dielectric strength leads to occurrence of early electric discharges. Discharge process appears more stable and consequently process performance is improved.
7. Mirror-like surface finish can be achieved by PMEDM with appropriate powder, particle size and concentration.
8. Machined surface produced by PMEDM corresponds to improved wear and corrosion resistance whilst compared to conventional EDM.
9. Secondary finishing operations are substantially eliminated.

1.2 State of Art

During EDM operation, material removal takes place due of thermal impact of a series of repetitive spark discharges occurring within the gap between the tool electrode and the workpiece; both immerged in a dielectric medium. However, poor thermal conductivity of Inconel 718 limits the performance of EDM operation. Therefore, research is being carried out to identify effective ways in order to improve EDM performance while using Inconel 718 as workpiece material. Since, EDM characteristics greatly depend on the performance of the

dielectric medium; considerable attention is being paid to modify properties of dielectrics or to introduce foreign particles (powder) suspended in the dielectrics. The latter is known as 'Powder-Mixed EDM' (PMEDM).

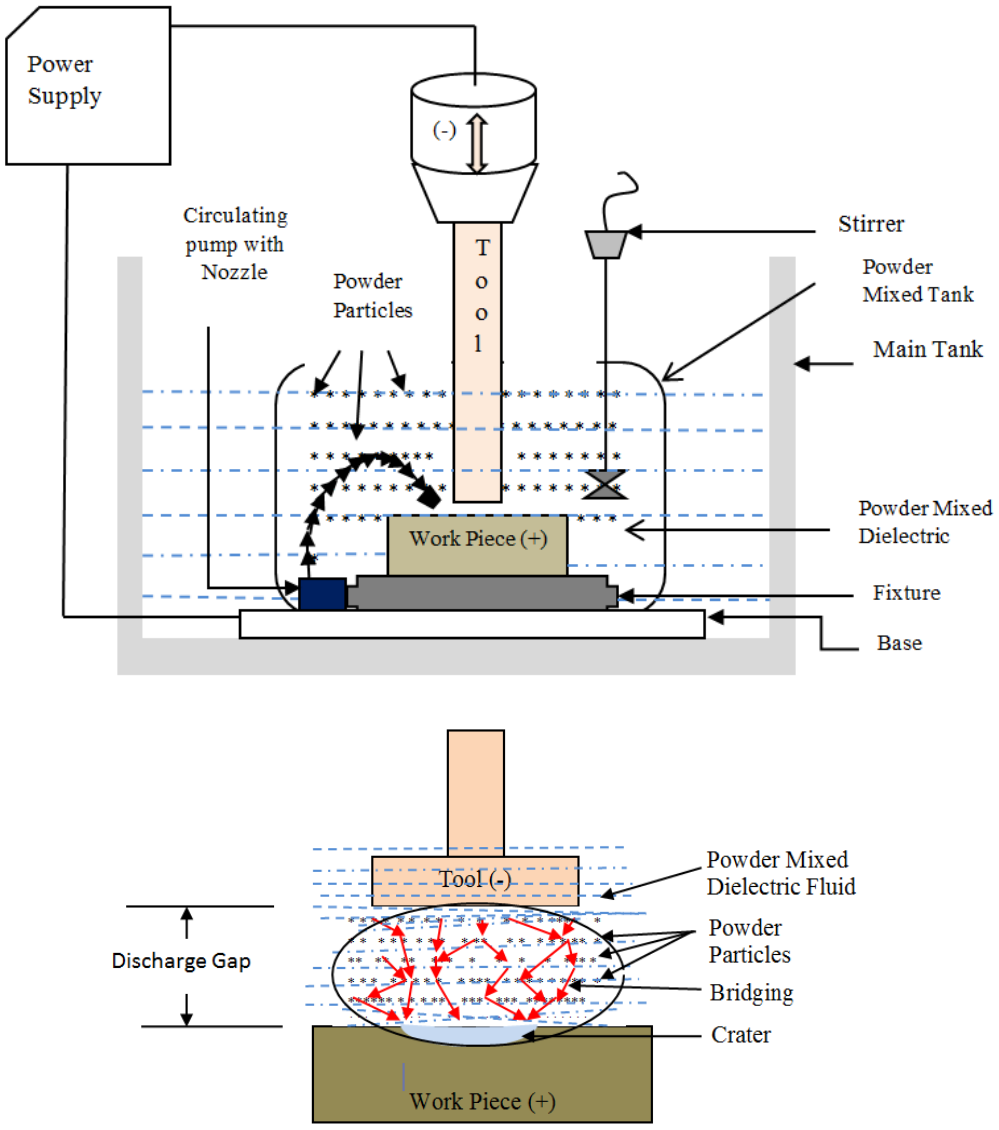

Fig. 1.1: Working principle of PMEDM

When an electric potential is applied between two electrodes; the powder particles fill up the spark gap. Being sufficiently energized, these powder particles start acting as conductors and form zigzag fashioned chain like structure within the spark gap. Due to the 'bridging effect' [11], the insulating strength of the dielectric fluid falls down. As a consequence, gap size is increased. Due to easy short circuiting, discharge frequency is increased causing more material to be eroded out. The addition of powder particles also modifies the shape of the

plasma channel favorably. Discharge energy is distributed uniformly within the widened and enlarged channel. This consequences formation of wide and shallow craters and also improves surface finish of the end product.

Tzeng and Lee [11] analyzed influence of aluminum, chromium, copper, and silicon carbide powder characteristics on PMEDM performance of SKD-11 tool steel. The following factors: particle concentration, particle size, particle density, electrical resistivity, and thermal conductivity of powders were found significantly affecting material removal efficiency and rate of tool wear. For a constant particle concentration, the tiniest suspended particle achieved improved Material Removal Rate (MRR) and, reduced Tool Wear Rate (TWR). Kansal et al. [12] optimized material removal efficiency and surface roughness by selecting an appropriate setting of the process parameters including pulse duration, duty cycle, peak current and powder (Si powder) concentration during EDM on EN-31 tool steel. Peças and Henriques [13] observed dependency between electrode area and features of surface quality (viz. surface roughness and craters morphology) during PMEDM. Significant performance improvement was observed for the powder-mixed EDM as compared to conventional EDM. In another paper, Peças and Henriques [14] reported improved polishing performance of EDM by using silicon powder added dielectric media. Favorable results were obtained in terms of reduced crater dimension, less white layer thickness and superior surface finish. Adequate control on the powder concentration along with flushing flow was found necessary for improved polishing effect. Kung et al. [15] studied material removal efficiency and electrode wear ratio for the case of aluminum powder-mixed EDM of cobalt-bonded tungsten carbide (WC-Co) workpiece. The following input parameters: discharge current, pulse duration, grain size, and powder concentration were considered towards evaluation of machinability.

Jahan et al. [16] achieved desired surface characteristics in micro-EDM (μEDM) of cemented WC–Co. The characteristics of the machined surface were assessed in purview of surface topography, crater dimension, roughness average (R_a) and peak-to-valley roughness (R_{max}). It was observed that application of semi-conductive graphite nanopowders suspended in the dielectric medium remarkably achieved superior surface finish, enhanced volumetric material removal efficiency and reduced electrode wear ratio. Substantial improvement in surface topography as well as crater distribution was observed due to the enlarged spark gap and uniform discharging fashion in powder-mixed μEDM. Kumar and Batra [17] examined aspects of surface modification for different die steel materials during tungsten powder-mixed EDM. Adequate transfer of tungsten and carbon at the work surface was observed resulting improvement in micro-hardness. Bhattacharya et al. [18] obtained suitable

parametric settings to achieve rough as well as finish machined surface for EN31, H11, and HCHCr die steel materials for PMEDM process. It was observed that application of copper tool with aluminum powder added in the dielectric could maximize material removal rate. Graphite powder-mixed EDM showed lesser MRR but provided superior surface finish.

Singh and Yeh [19] applied grey relation analysis towards optimizing multi-response characteristics of Abrasive Powder-Mixed Electro-Discharge Machining (APM-EDM) of aluminum Metal Matrix Composites (MMCs). Apart from electrical parameters, powder concentration, abrasive size etc. were considered therein. Mai et al. [20] examined the upshot of carbon nanotube (CNT) powder addition to the dielectric on surface integrity and machining efficiency during EDM. Significant reduction in average surface roughness was observed for the machined part. Additionally, defects of the recast layer and micro-cracks were found comparatively less in magnitude for the case of PMEDM. Bai et al. [21] studied the relationship between processing parameters and material removal rate during Powder-Mixed Near-Dry (PMND)-EDM. Improved MRR was noticed with increased peak discharge current, pulse duration, flow rate, and air pressure; MRR got decreased with increase in pulse-off time as well tool rotational speed. However, as powder concentration increased, it was found that MRR initially increased to somewhat and then assumed a decreasing trend.

Prihandana et al. [22] investigated application potential of molybdenum disulfide (MoS_2) powder-mixed dielectrics on the performance of µEDM on Inconel 718 workpiece. It was observed that MoS_2 powder-suspended dielectric media (with appropriate size and concentration) could produce superior quality micro-holes. Kolli and Kumar [23] reported that improved material removal efficiency, satisfactory surface finish and reduced tool wear rate could be achieved while executing B_4C powder-mixed EDM of Ti-6Al-4V alloy. Singh et al. [24] focused on the advantage of powder-mixed EDM on Co 605 super alloy using graphite tool electrode. Results indicated that desired micro-hardness and surface finish could simultaneously be achieved therein. Razak et al. [25] investigated the role of concentration and particle size for silicon carbide powder-mixed EDM aiming to improve performance characteristics like MRR, surface finish, TWR, machining time and cost. Kumar [26] studied on development of mirror-like surface finish of the EDMed D2 steel using CNTs added with the dielectric. It was observed that specified amount of CNTs added into the dielectric fluid could enhance machining rate and refine surface finish. Additionally, concentration of additives and peak current were found to be the most significant process variables.

Batish et al. [27] reported that an optimal powder concentration could improve the process performance to the maximum extent. Use of powder, mixed with dielectric medium, caused

effective spark length to be enlarged thus forming larger overcut. Singh et al. [28] experienced significant improvement (~48.43%) in the MRR while machining Al 6061/10% SiC through EDM process using tungsten powder-added kerosene as dielectric media. Superior surface finish and reduced recast layer thickness were noticed. Al-Khazraji et al. [29] examined the favorable effect of using SiC powder-mixed dielectric during EDM on white layer thickness, total heat flux generated and the fatigue life of the part component. Ekmekci and Ekmekci [30] examined machinability of Ti-6Al-4V alloy using hydroxyapatite (HA) powder suspended in deionized water (as dielectric media) during the EDM process. The procedure was found beneficial due to migration of powder particles; an HA-rich layer was formed on the work surface resulting improved biocompatibility of the work material. Kuriachen and Mathew [31] studied the advantages of SiC particle suspended dielectric for machining of Ti-6Al-4V using tungsten carbide electrode.

Baseri and Sadeghian [32] studied effects of parameters: concentration of the TiO_2 nanopowder, energy input and tool rotational speed on MRR, tool wear, and surface roughness. It was concluded that appropriate nanopowder mixed with the dielectric media along with suitable tool rotation speed could enhance EDM efficiency. Prabhu and Vinayagam [33] applied Genetic Algorithm (GA) coupled with full factorial experimental design technique towards optimizing machining yields for CNT mixed EDM of AISI D2 tool steel. Li et al. [34] introduced SiC abrasive-mixed EDM with magnetic stirring. Improved hardness of the formed layer was achieved due to formation of TiC and $TiSi_2$ at the machined surface of Ti-6Al-4V. Prakash et al. [35] reported significant improvement in biocompatibility of β-Ti alloy while machined by Si powder-mixed EDM. Additionally, enhancement of the machining performance in regards of high material removal efficiency and less tool wear rate was noticed.

Talla et al. [36] studied application potential of aluminum powder-mixed kerosene dielectric media during EDM of aluminum/alumina MMC. Authors optimized MRR and surface roughness by using principal component analysis-based grey technique (Grey-PCA). Tripathy and Tripathy [37] attempted PMEDM of H-11 die steel using copper electrode. Authors applied Taguchi method in combination with Technique for Order of Preference by Similarity to Ideal Solution (TOPSIS) and Grey Relational Analysis (GRA) for optimizing multiple performance characteristics: MRR, surface roughness, and electrode wear ratio. Mohanty et al. [38] applied desirability function approach and Particle Swarm Optimization (PSO) algorithm for optimizing MRR, surface roughness, and TWR in the context of PMEDM.

Dubey and Singh [39] optimized MRR using desirability function approach during chromium powder-mixed EDM of AA7075/B_4C composite.

In this context, it is to be noted that powder type, shape/size of powders, powder concentration, thermo-physical properties of powders play vital role on performance of PMEDM. Different types of powders were used during PMEDM on different work materials along with variety of dielectrics. Results are summarized in Table 1.1.

1.3 Problem Statement: Coverage of the Present Dissertation

In view of several difficulties faced during traditional machining (turning, drilling, milling etc.) of Inconel 718; increased attention is being paid on execution of non-traditional machining operations like Electro-Discharge Machining (EDM), Electro-Chemical Machining (ECM), Electro-Discharge Drilling (EDD) etc. on Inconel 718 to achieve desired intricate contour, complex shape, and high dimensional accuracy of the EDMed part component. However, poor material removal efficiency and inferior surface finish limit application of such non-traditional processes especially on Inconel 718 super alloys. Amongst various non-traditional routes, EDM is very popular. But, Inconel 718 possesses very low thermal conductivity which adds complexity for the EDM process to progress efficiently. EDM process is controlled by various electrical and non-electrical parameters. Electrical parameters include: gap voltage, peak discharge current, pulse-on duration, pulse-off duration, duty factor, polarity etc. Non-electrical parameters include dielectric flushing circulating pressure, types of dielectrics, electrode material etc. Adequate knowledge and precise control over process parameters may result in satisfactory EDM performance. Previous researchers recommended various ways to improve EDM performance further. Few of them suggested use of conductive/ semi-conductive powders (added to the dielectric media) to improve performance of the EDM process. Application of powder-mixed EDM was elaborately studied with respect to titanium and its alloys. Limited studies were documented in literature on assessing performance of powder-mixed dielectrics during EDM of Inconel 718 super alloys. Moreover, in published works related to PMEDM, the authors mainly focused on MRR, surface roughness, and tool wear rate as machining performance indices. Aspects of surface integrity were reported, however, quantitative evaluation of surface topographical features including surface metallurgy is still lacking.

In the present work, an attempt was made to assess machinability of Inconel 718 for EDM using graphite powder mixed dielectric media. Machinability was assessed in purview of multiple process-performance indicators including material removal efficiency, tool wear rate and surface integrity. Morphology along with topographical features of the machined surface (viz. roughness average, crack density, depth/thickness of white layer, residual stress, and micro-hardness) obtained in graphite powder-mixed EDM were studied in detail and compared to that of conventional EDM. Aspects of material migration, formation of intermetallic compounds, and grain refinement as affected by the EDM process were also studied. Detailed analysis on quantitative metallurgical aspects of the machined surface including crystallite size, micro-strain, dislocation density and variation obtained thereof as resulted by the thermo-mechanical effect of the EDM process was also covered in this work.

In continuation to the previous work, an additional set of experiments was performed to determine an optimal value of particle concentration along with peak discharge current and pulse-on duration for satisfactory machining performance during PMEDM of Inconel 718. PMEDM experiments were carried out using SiC powder-mixed kerosene (as dielectric media). Optimal setting of process parameters was determined in purview of maximum material removal efficiency, simultaneously with minimum surface roughness, surface crack density, and white layer thickness. L_9 orthogonal array design of experiment was used. Experimental data were analyzed through utility theory in conjugation with Taguchi's optimization philosophy. Direct (main) effects of process parameters (peak discharge current, pulse-on duration, and particle concentration) on influencing machining performance characteristics were graphically presented. Apart from surface integrity, elemental analysis, and metallurgical analysis were also performed to study effects imposed by PMEDM process on the machined specimen while compared to 'as received' parent material.

Table 1.1: Types of dielectrics/powders used in literature for PMEDM

Reference	Author(s) and Year	Work Material	Name/Type of Dielectric Fluid Used	Particle Type/Size
[11]	Tzeng and Lee (2001)	Steel SKD-11	Kerosene	Aluminum (Al), Chromium (Cr), Copper (Cu), and Silicon Carbide (SiC) Particle size: 0.07–0.08 µm, Concentration: 0.25, 0.5, 1.0 g/l
[12]	Kansal et al. (2005)	N-31 Steel (Comparable to AISI 52100)	Kerosene	Silicon (Si) powder. Particle size: 20–30 µm
[13]	Peças and Henriques (2008)	AISI H13	Castrol SE fluid 180	Si powder with 2g/l concentration Average particle size: 10 µm
[14]	Peças and Henriques (2008)	AISI H13	Castrol SE fluid 180	Si powder with 2g/l concentration Average particle size: 10-15 µm
[15]	Kung and Horng (2009)	94WC-6Co	Mineral oil (TOTAL EDM44)	Al powder Average particle size: 1.5–2.5 µm, Concentration: 10, 15, 20 g/l
[16]	Jahan et al. (2011)	WC–10 wt.% Co	Total FINA ELF EDM 3	Graphite powder Average particle size: 55 nm Concentration: 1.0 g/l
[17]	Kumar and Batra (2012)	OHNS die steel, D2 die steel, H13 die steel	Kerosene	Tungsten (W) powder Particle size: 30–40 µm Concentration: 15 g/l
[18]	Bhattacharya et al. (2012)	EN 31, H11, HCHCr	Kerosene, Refined mineral oil (transformer oil)	Graphite, Aluminum powders Concentration: 2 g/l

Table 1.1 (Continued)

Reference	Author(s) and Year	Work Material	Name/Type of Dielectric Fluid Used	Particle Type/Size
[19]	Singh and Yeh (2012)	Aluminum alloy (AA6061)	SEO-250 Oil	SiC powder Powder concentration: 8, 10, 12 g/l Particle size: 74, 45, 37 µm
[20]	Mai et al. (2012)	NAK80 steel	Kerosene, Kerosene with dispersed CNT, Al, Si, and Graphite powders	Concentration of additives: 3 g/l Carbon Nano Tube (CNT) diameter: 40–60 nm, Length: 1–3µm
[21]	Bai et al. (2013)	Steel 45	Commercial grade mineral oil	Silicon powder Powder concentration: 0, 3, 6, 9, 12, 15 g/l
[22]	Prihandana et al. (2014)	Inconel 718	Kerosene	Molybdenum disulfide (MoS_2) Powder size: 10 nm, 50 nm, and 2µm Powder concentration: 0, 5, 10 g/l
[23]	Kolli and Kumar (2014)	Titanium alloy Ti-6Al-4V	Spark Erosion 450 EDM oil	Boron carbide (B_4C) powder Concentration: 1–20 g/l
[24]	Singh et al. (2015)	Superalloy Super Co 605	EDM oil	Graphite powder Concentration: 10 g/l
[25]	Razak et al. (2015)	Ti-6Al-4V	Kerosene	SiC powder Concentration: 5, 10, 15 g/l Size: 10, 20, 30 µm
[26]	Kumar (2015)	AISI-D2 die steel	Kerosene	CNT Concentration: 0–6 mg/l

Table 1.1 (Continued)

Reference	Author(s) and Year	Work Material	Name/Type of Dielectric Fluid Used	Particle Type/Size
[27]	Batish et al. (2015)	Hot die steel (H11), high carbon high chromium (HCHCr), and AISI 1045 steel	Kerosene and commercial EDM oil	Si ,Graphite ,W powders Concentration: 0, 5, 10 g/l
[28]	Singh et al. (2015)	AA6061/10%SiC Composite	Kerosene	Tungsten powder Concentration: 4 g/l Size: 10-15μm
[29]	Al-Khazraji et al. (2016)	AISI D2 steel	Kerosene	SiC micro powders Grain size: 95.502 μm
[30]	Ekmekci and Ekmekci (2016)	Ti-6Al-4V alloy	Water	Hydroxyapatite powder Concentration: 15 g/l
[31]	Kuriachen and Mathew (2016)	Ti-6Al-4V	Deionized water	SiC powder Size: 600 nm Concentration: 5, 15, 25 g/l
[32]	Baseri and Sadeghian (2016)	H13	Water	Nanopowder TiO_2-US3500 Concentration: 0, 1, 2, 3 g/l Size: 20 nm
[33]	Prabhu and Vinayagam (2016)	AISI D2 tool steel material	Kerosene	CNT Size: Outer diameter: 10-20 nm Length: 10-30 μm
[34]	Li et al. (2017)	Ti-6Al-4V	Kerosene	SiC powder Concentration: 12 g/l
[35]	Prakash et al. (2017)	Ti35Nb-7Ta-5Zr β-Titanium Alloy	Hydrocarbon oil	Si powder Concentration: 4 g/l

Table 1.1 (Continued)

Reference	Author(s) and Year	Work Material	Name/Type of Dielectric Fluid Used	Particle Type/Size
[36]	Talla et al. (2015)	Aluminum/alumina MMC	Kerosene	Al and alumina powder Concentration: 4 g/l Size: 15µm, 90µm
[37]	Tripathy and Tripathy (2016)	H-11 die steel	EDM oil	Cr powder Size: <53µm
[38]	Mohanty et al. (2018)	Al-SiCp Metal matrix composite	EDM oil	Al_2O_3 powder Size: 20-30 µm
[39]	Dubey and Singh (2018)	AA7075 reinforced with 5% B_4C particles	EDM oil	Cr powder Size: 10-15µm Concentration: 4 g/l

CHAPTER 2

Experimental Details

Inconel 718 plates $(50 \times 50 \times 5) mm^3$ were used as work material. Chemical composition and properties of Inconel 718 were depicted in Table 2.1 and Table 2.2, respectively. PMEDM experiments were conducted in Die-sinking EDM (CNC Series) Setup (Model: ED30C; Make: Excetek Technologies Co., Ltd.; Country: Taiwan). Conventional EDM oil KYROS FERROLACe 3M, 110, 140 (Flash point: 275^0F; Density: 0.769 g/cc; Kinematic Viscosity at 40°C = 3.0-4.0 cSt) was used as dielectric medium. For execution of PMEDM, a specially designed setup was arranged (Fig. 2.1). In addition to the existing EDM setup, one submersible pump (Brand: Polo cool; Rating: 30W, 165-220 V/50 Hz; Make and Country: TMA International, New Delhi, India), a stirrer (Pure Copper Motor 6001F; Rating: 220 V, 50 HZ, 15W; Venus Aqua, Kolkata, India), a pressure gauge, and a nozzle were used. Descriptions of all equipment/instruments used in this work were provided in Appendix I along with specifications/technical details. Commercially available 99% pure copper rod (20 mm diameter) was used as tool electrode. Copper was selected as tool material due to its excellent thermal as well as electrical conductivity, and corrosion resistance. EDM operations were conducted by using graphite powder added to the EDM oil (as dielectrics). Properties of graphite powder were furnished in Table 2.3.

Table 2.1: Chemical composition of Inconel 718 [40]

Element(s)	% (by weight)	**Element(s)**	% (by weight)
Ni	50-55	**Si**	0.35
Cr	17-21	**C**	0.08
Fe	Balance	**S**	0.015
Mo	2.8-3.3	**P**	0.015
Nb	4.75-5.5	**B**	0.006
Co	1.0		
Mn	0.35		
Cu	0.2-0.8		
Al	0.65-1.15		
Ti	0.3		

Table 2.2: Properties of Inconel 718

Properties	Value
Density	8.19 g/cc
Specific gravity	8.19
Tensile strength(ultimate) at 23^0C	1375 MPa
Tensile strength (yield) at strain 0.2%	1100 MPa
Specific heat capacity	0.435 J/g.^{0}C
Thermal conductivity	11.4 W/m.K
Melting point	1260-1336^{0}C

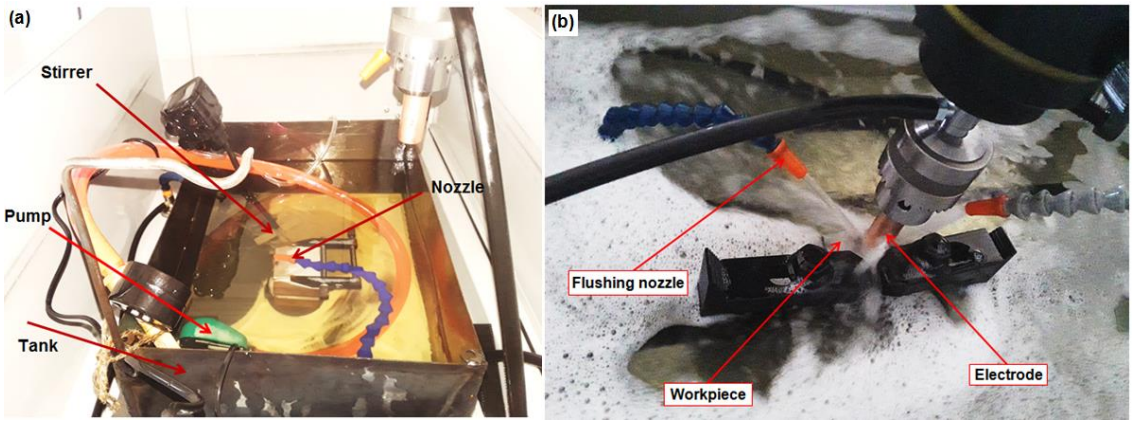

Fig. 2.1: (a) Experimental setup with accessories for powder-mixed EDM, and (b) Close view of the machining area

Table 2.3: Properties of graphite powder

Properties	Value
Density	2.15 g/cc
Thermal conductivity	119-165 W/cm-K
Melting point	3800K
Specific heat capacity	1.19 J/g-K

In PMEDM, a stirrer is generally used to ensure proper circulation of powder particles within the dielectric media kept in the container tank. But it was observed that stirrer alone was not sufficient to circulate the powder particle efficiently; as a result, some particles settled down at bottom of the container. Therefore, to ensure adequate circulation, two aquarium pumps were fitted (placed diagonally) in the container. The outlet of the pump was made slightly inclined towards the bottom of the container resulting into better circulation of the powder particles in the dielectric fluid. It was observed that by using stirrer alone, the powder was

circulated in a confined area; while application of two additional pumps, efficient circulation was noticed clearly.

The powder concentration selected herein was based on literature survey as well as trial experiments. From published works, it was found that satisfactory performance over conventional EDM could be achieved using powder concentration 0-10g/l. For example, Talla and Gangopadhyay [41] reported application of graphite, aluminum, and silicon powder (with concentration 0-8 g/l) for machining of Inconel 625. Singh et al. [28] used tungsten powder with concentration 4g/l for machining of aluminum based metal matrix composites. Kolli and Kumar [23] used B_4C powder added to dielectric media with concentration 1-20g/l for machining of Ti-6Al-4V. Graphite powder mixed with the dielectric fluid with concentration 10g/l was used for EDM of Co 605 super alloy [24]. AISI1045 steel was EDMed using Si, graphite and W powder with concentration 0-10g/l mixed with the dielectric fluid [27]. Singh and Yeh [19] machined aluminum metal matrix composite by using SiC powder mixed EDM with particle concentration 8-12g/l.

Initially trail experiments were performed with varying powder concentration. The change in EDM performance was experienced insignificant with concentration below 6g/l. On the contrary, concentration beyond this value was resulted in sedimentation of powders thus affecting overall machining performance. Therefore, 6g/l concentration was considered optimal and the same was kept constant throughout the experimentation. However, this was a rough estimation. A more practical approach would be to consider powder concentration varied simultaneously with other process parameters and to go for optimization of machining responses.

Apart from powder concentration, values of other constant parameters were furnished in Table 2.4.

Direct/interactive effects of important EDM factors: peak discharge current, pulse-on duration/pulse-off duration, duty factor, and gap voltage were amply covered in existing literature resource to exhibit their contribution on machining performance characteristics. Amongst all EDM factors (electrical and non-electrical), peak discharge current was found to be the most significant factor on influencing overall machining performance [42-43]. Spark energy is directly proportional to the peak discharge current. Owing to the fact that increase in number of factors and their levels of variation in turn increases number of experimental runs to be conducted; therefore, in the present work, peak current was considered as the only parameter of interest.

Table 2.4: Parameters kept at constant values

Parameters	Unit	Value
Gap voltage	[V]	230
Pulse-on time	[µs]	2000
Pulse-off time	[µs]	500
Flushing pressure	[kg/cm^2]	0.5
Polarity	-	Positive (work piece positive)
Gap between tool and workpiece	[µm]	50
Depth of cut	[mm]	0.75
Powder concentration	[g/l]	6

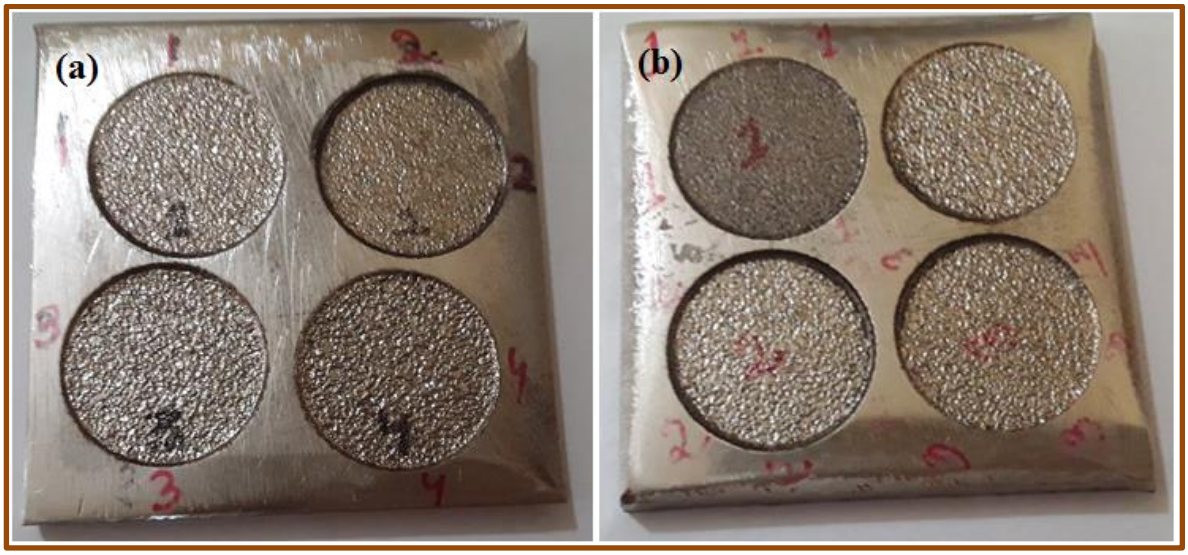

Fig. 2.2: EDMed work surfaces of Inconel 718 obtained in (a) conventional EDM, and (b) graphite powder-mixed EDM

PMEDM experiments were performed by varying peak discharge current into four discrete levels 15A, 20A, 25A, and 30A. A snapshot of the EDMed specimens was provided herein (Fig. 2.2). After experimentation, the following performance features were measured: MRR, TWR, R_a, Surface Crack Density (SCD), and White Layer Thickness (WLT). In order to compute weight loss of the work material as well as tool electrode the Weighing Machine (Model: Gold600; Make: Phoenix Electronics and Weighing Systems, India; Capacity: 600g; Accuracy: 0.01g) was used. Surface roughness values of the machined specimens were obtained by surface roughness tester (Model: SJ 210; Make: Mitutoyo) with cut-off length 0.8 mm. Surface cracks and well as white layer developed onto the EDMed work surface were viewed through Scanning Electron Microscope (SEM) (Make: JEOL, Model ID: JSM 6480 LV; Country of manufacture: Japan). The detailed procedure for determining SCD and WLT

could be obtained in the reporting by Upadhyay et al. [44]. Sample calculations on measurement of SCD and WLT were furnished in Appendix II, placed at the end of this thesis. In order to measure SCD and WLT, multiple micro-graphs were taken at different locations corresponding to a particular specimen. For each micro-graph, values of SCD and WLT were measured. Average of these values was considered for further analysis. Hence, the term 'SCD' and 'WLT' could be understood as 'average SCD' and 'average WLT', respectively, throughout the text.

X-ray Diffraction Microscopy (XRD) was performed for the machined surface as well as 'as received' parent material to study various metallurgical aspects in regards of phase, grain refinement, material migration and residual stress. XRD peak patterns were collected from XRD-Texture Measurement Machine (Make: BRUKER; Model: D8 ADVANCE with DAVINCI design; Country: Germany).

Additionally, chemical analyses of the specimens were done through Energy Dispersive X-ray Spectroscopy (EDS) using Scanning Electron Microscope (Make: JEOL; Model: JSM 6480 LV; Country: Japan).

The micro-hardness for each EDMed specimen (measured at a position approximately mid-depth of the white layer) was measured in Vicker's micro-hardness tester (Make: LECO; Model No. LM810; Country: USA). Indentations were made by applying 25gf load with a constant dwell time of 10s.

In the second phase of experiment, the same setup (as utilized before) was used for carrying out PMEDM of Inconel 718 work material. However, in this case, commercially available kerosene was used as dielectric media. Commercially available 99% pure copper rod (20 mm diameter) was used as tool electrode. Machining operations were conducted by using SiC powder added to the dielectric media. Properties of SiC powder were given below (Table 2.5).

Table 2.5: Properties of SiC powder

Properties	Value
Density	3.21 g/cc
Thermal conductivity	120 W/cm-K
Melting point	3170 K
Specific heat capacity	0.79 J/g-K

Experiments were conducted by varying two process parameters (electrical parameters) viz. peak discharge current and pulse duration (pulse-on time) along with powder concentration. These parameters were varied at three discrete levels as shown in Table 2.6. Powder concentration was varied from 0 (no powder) to 4g/l with intermediate value 2g/l. Values of other constant parameters (except pulse-on time) were same as furnished in Table 2.4. Experiments were performed as per L_9 Orthogonal Array (OA) design. After experimentation, the following performance features were measured: MRR, R_a, SCD and WLT. Experimental data were furnished in Table 2.7. A snapshot of the machined surfaces produced along with tool electrode was provided in Fig. 2.3.

Table 2.6: Domain of experiments: Parameters and values

Parameters	Unit	Notation	Levels of variation		
			1	2	3
Peak current (I_P)	[A]	A	25	30	35
Pulse-on time ($_{Ton}$)	[µs]	B	1000	1500	2000
Powder concentration	[g/l]	C	0	2	4

Fig. 2.3: Snapshot of EDMed work surfaces of Inconel 718 (obtained through PMEDM with SiC powder mixed kerosene as dielectric) along with copper tool electrode

Table 2.7: Design of Experiment (DOE) and collected response data

Sl. No.	L_9 OA DOE			Response data				Machining time [min]
	A	B	C	MRR [mm^3/min]	R_a [µm]	SCD [µm/$µm^2$]	WLT [µm]	
1	1	1	1	31.709	10.68	0.00644	32.65	3.35
2	1	2	2	36.450	11.18	0.01222	50.37	3.48
3	1	3	3	15.605	8.93	0.01555	52.43	13.38
4	2	1	2	40.951	11.25	0.01141	49.81	3.25
5	2	2	3	32.315	9.83	0.01487	40.74	7.33
6	2	3	1	28.893	10.43	0.01547	43.68	7.48
7	3	1	3	47.463	12.1	0.00866	44.64	3.37
8	3	2	1	37.657	12.15	0.01485	46.52	3.21
9	3	3	2	49.500	12.4	0.01295	56.54	2.59

CHAPTER 3

Application Potential of Graphite Powder-Mixed EDM: Comparison with Conventional EDM

3.1 Characterization of Graphite Powder Particles

A snapshot of 'as received' graphite powder (Mesh size 60; average particle size~250 μm) was provided in Fig. 3.1, along with its XRD peak pattern. Computation of average crystallite size was carried out based on Scherrer equation using Full-Width Half-Maximum (FWHM) of the peaks obtained in the XRD spectra (Table 3.1). The average crystallite size was obtained as 28.92 nm.

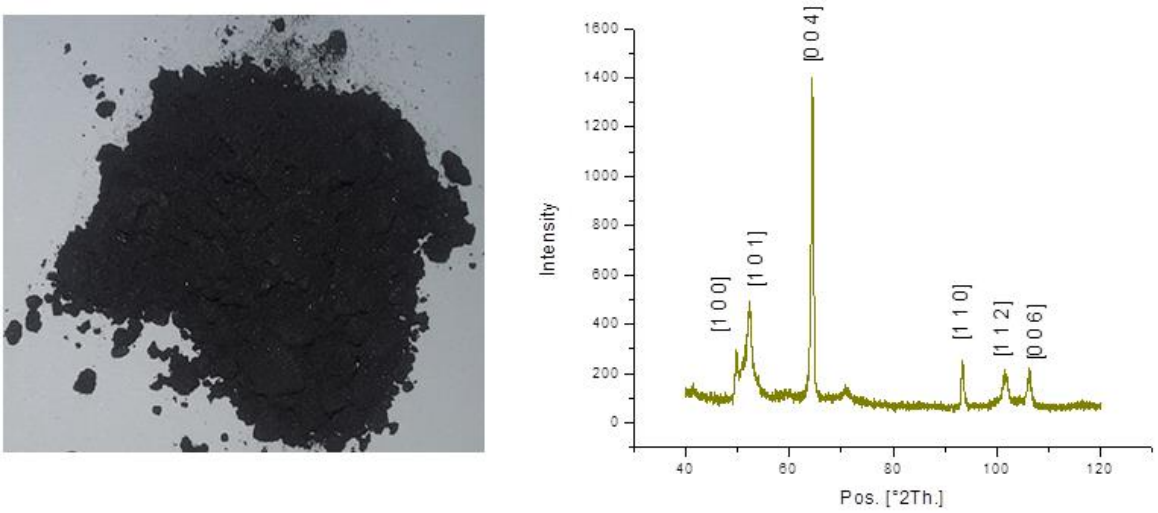

Fig. 3.1: XRD spectra for 'as received' graphite powder

It must be noted that a particle consists of several crystallites. The Scherrer equation for calculating crystallite size was provided below (Eq. 3.1). SEM micrographs (taken at different magnifications) of 'as received' graphite powder were also arranged in Fig. 3.2.

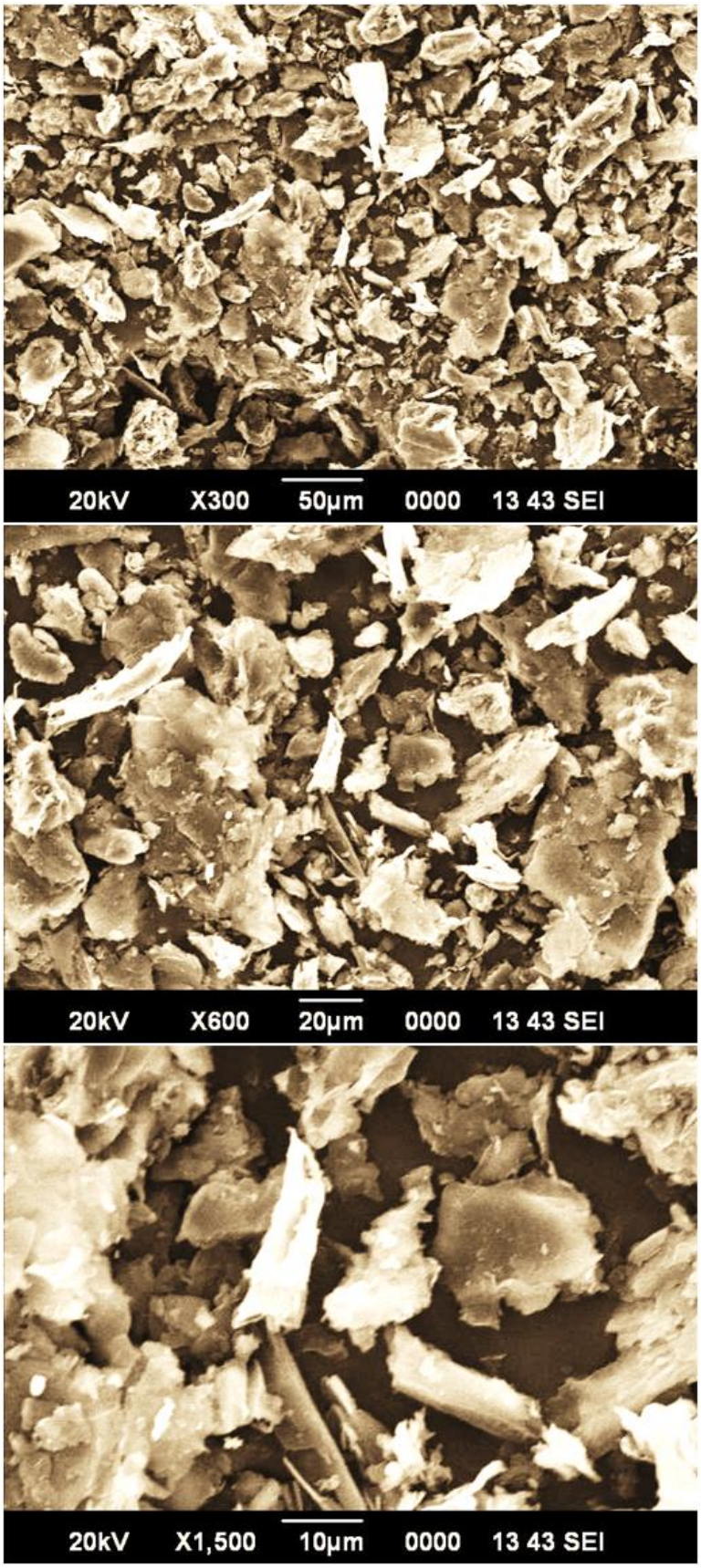

Fig. 3.2: SEM micrographs taken at different magnifications of ‘as received’ graphite powder

In this equation (Eq. 3.1), the notation L is the average size of the ordered (crystalline) domains; this is also termed as crystallite size.

The notation K is a dimensionless shape factor (considered a value 0.9); λ is the X-ray wavelength (λ_{Co} =1.7906A^0 for CoK_α); the term β_L (expressed in radians) is the broadening i.e. FWHM of the highest intensity peak, after subtracting instrumental broadening. The notation θ is the Bragg angle (in degrees) of X-ray diffraction.

$$L = \frac{K\lambda}{\beta_L \cos\theta} \tag{3.1}$$

Table 3.1: Computation of crystallite size (L) for 'as received' graphite powder along different crystallographic directions

Peak No.	Miller indices $[h,k,l]$ (Crystallographic direction)	$2\theta\ (^0)$	FWHM $(^0)$	Crystallite size (L) $[nm]$	Average crystallite size (L_{avg}) $[nm]$
1	[1 0 0]	49.6812	0.2362	42.96	28.92
2	[1 0 1]	52.3475	0.3936	26.06	
3	[0 0 4]	64.4543	0.4723	23.04	
4	[1 1 0]	93.2657	0.4723	28.39	
5	[1 1 2]	101.623	0.5510	26.44	
6	[0 0 6]	106.180	0.5760	26.61	

3.2 Surface Integrity

3.2.1 Surface Morphological Characteristics

Process performance can be evaluated by surface integrity of the end product. Surface integrity includes surface morphology as well topographical features. Surface irregularities like crater morphology, globules of debris, melted material deposition, spherical deposition, pockmarks (chimneys), cracks and white layer etc. describe morphology of the EDMed surface. On the other hand, topographical (measurable/quantifiable) measures include crack density, thickness/depth of white layer, residual stress, micro-indentation hardness along with metallurgy that includes phenomena of phase change, material migration, grain refinement, strain-effect etc. Hence, study of surface integrity is one of the vital parameters to assess quality of the EDMed end product.

In this context, first optical microscopy was carried out to examine crater morphology of the EDMed work surface obtained through conventional EDM and PMEDM both. As compared to conventional EDM, shallow craters of relatively large diameter were found attributed to the EDMed surface in case of PMEDM (Fig. 3.3). Formation of wide and shallow craters was expected to enhance surface finish for the specimen obtained by PMEDM.

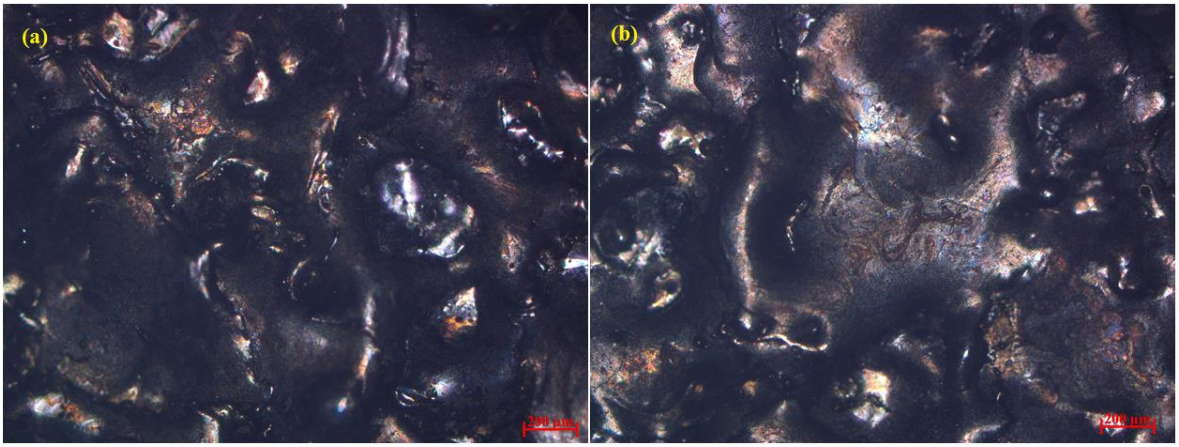

Fig. 3.3: Optimal images exhibiting crater morphology of the EDMed specimens obtained through (a) conventional EDM, and (b) graphite powder-mixed EDM at I_P=30A

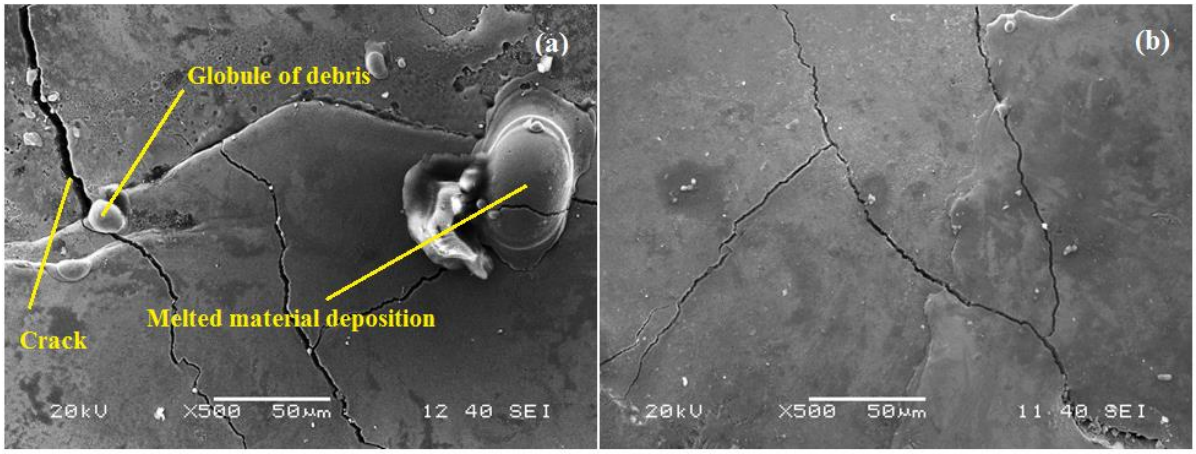

Fig. 3.4: SEM micrographs exhibiting irregularities of the EDMed work surfaces of Inconel 718 obtained in (a) conventional EDM, and (b) graphite powder-mixed EDM at I_P=30A

Surface morphology of the machined specimen was investigated by means of SEM micrographs of the EDMed work surface of Inconel 718 obtained in conventional EDM, and graphite powder-mixed EDM at I_P=30A (as shown in Fig. 3.4). Analysis revealed that the machined surface produced by conventional EDM was consisted of globules of debris, and surface cracks in abundance whilst compared to the case of PMEDM. The severity of surface cracking (crack opening width) was also found relatively high for the case of conventional

EDM (Fig. 3.5). Since, graphite powders (due to their conductivity) carried some amount of heat away from the machined zone; the extent of thermal stress developed at the machined surface was relatively less in magnitude. This reduced the degree of severity of surface cracking.

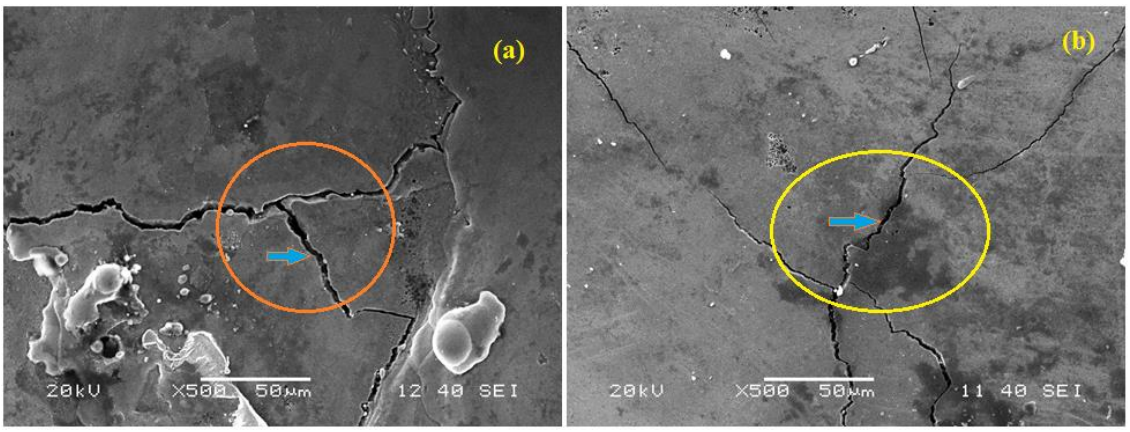

Fig. 3.5: SEM micrographs exhibiting severity of surface cracking of the EDMed work surfaces of Inconel 718 obtained in (a) conventional EDM, and (b) graphite powder- mixed EDM at I_P=30A

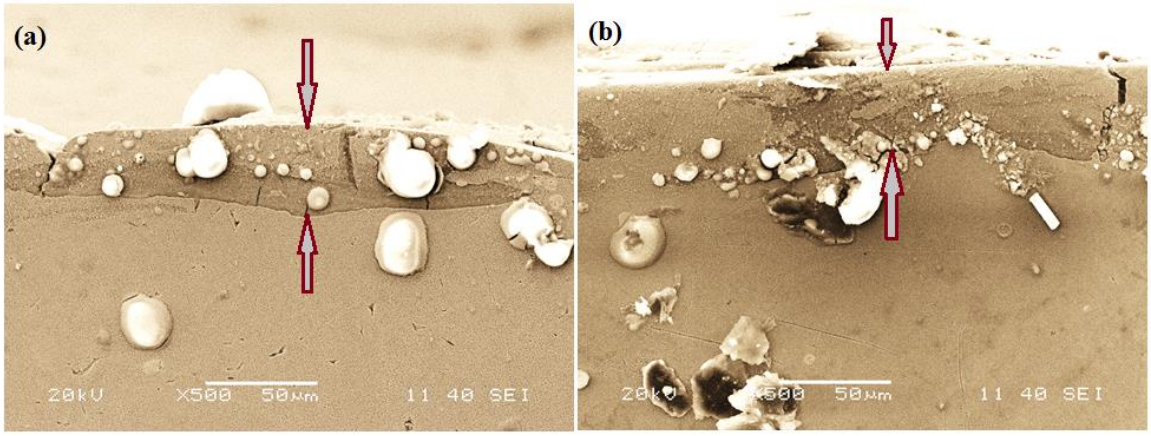

Fig. 3.6: SEM micrographs exhibiting existence of white layer onto the top of the machined surface obtained in (a) conventional EDM (WLT~31.77µm), and (b) graphite powder-mixed EDM (WLT~36.93µm) at I_P=25A

On the contrary, the machined surface obtained through PMEDM showed existence of thicker white layer whilst compared to the case of conventional EDM. Occurrence of discharge sparks in series improved material removal efficiency for the case of PMEDM. The process thus generated more debris from the work surface. Movement of debris might somewhat be restricted due to presence of locally agglomerated powders within the dielectric medium. Due to inefficient flushing, debris got stuck onto the machined surface forming deeper white layer (Fig. 3.6).

3.2.2 XRD Test Results: Metallurgical Characteristics

XRD analysis was carried out to identify various phases present within machined surface along with precipitates. Extent of grain refinement taking place during EDM operation was also understood by comparing peak patterns of the machined surface while compared to that of 'as received' parent material. Inconel 718 basically consisted of cubic nickel-chromium based solid solution matrix (Fig. 3.7). While comparing XRD spectra of 'as received' Inconel 718 to that of EDMed specimens (Figs. 3.8a-b); slight alternation in regards of peak positions, peak intensity, Full-Width-Half-Maximum (FWHM) etc. were observed. Extra peaks (one or more number) were also found attributed to the EDMed specimens due to formation of carbides/oxides or other intermetallic compounds. The formation of different intermetallic compounds in different crystallographic planes was depicted in Table 3.2. The values of crystallite size (L), micro-strain (ϖ) and dislocation density (ψ) corresponding to each specimen were also determined and provided in Tables 3.3-3.5.

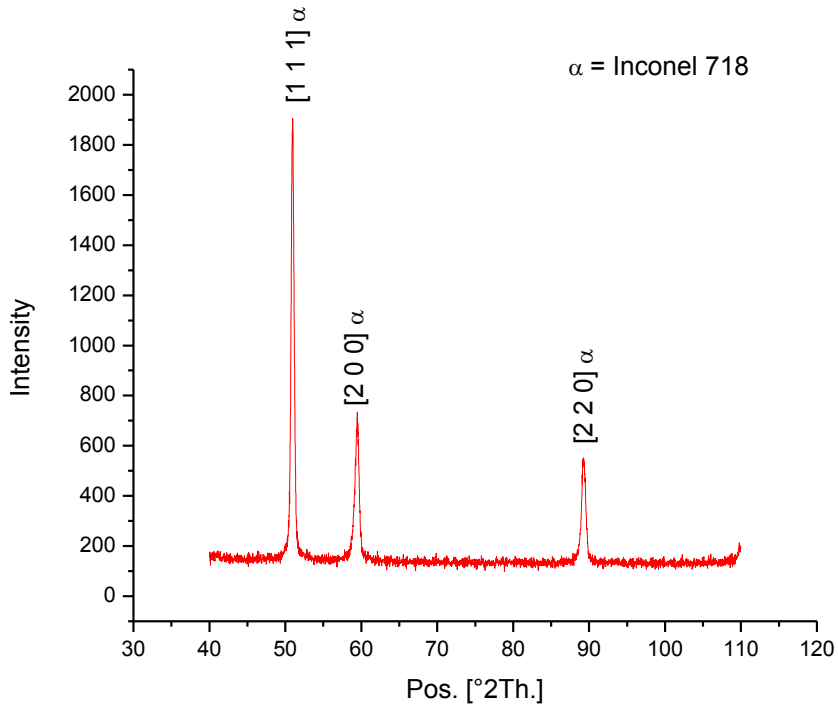

Fig. 3.7: XRD spectra for 'as received' Inconel 718

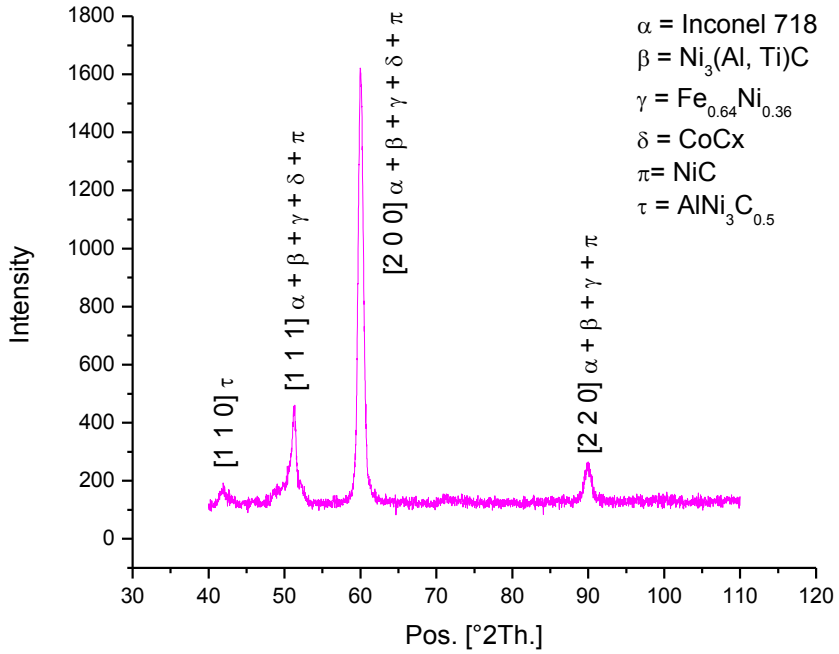

Fig. 3.8a: XRD spectra for the EDMed work surface of Inconel 718 produced at I_P=30A obtained through conventional EDM

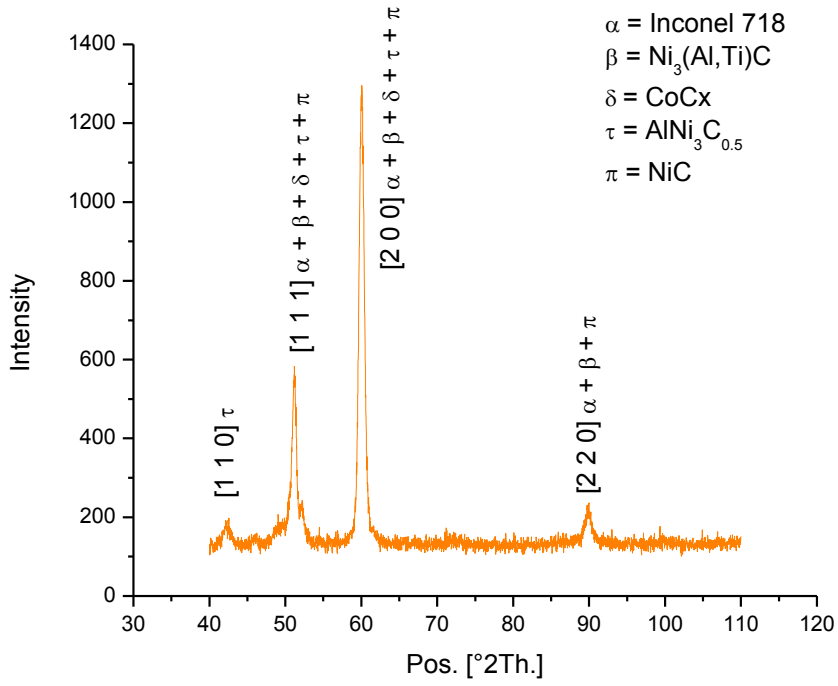

Fig. 3.8b: XRD spectra for the EDMed work surface of Inconel 718 produced at I_P=30A obtained through graphite powder-mixed EDM

Ignoring instrumental broadening and also peak broadening due to micro-strain; Scherrer equation (as shown in Eq. 3.1) was used to compute crystallite size. Though, a more practical approach is to consider three to four peaks from the XRD spectra and to compute an average crystallite size; however, in the present study, all computations were made based on the first two high intensity peaks of individual XRD spectra. Since, a comparative analysis was made in regards of crystallographic features like crystallite size, micro-strain and dislocation density etc. for different EDMed specimens; the calculation based on the measure of peak broadening corresponding to high intensity peaks was seemed quite justified.

For computing micro-strain, it was advised to consider peak broadening due to crystallite size concurrently with micro-strain. Thus, an accurate approach was to use Williamson-Hall plot by which crystallite size and micro-strain could be computed. However, in this work, for making a relative comparison on the strain developed in all EDMed specimens, the following equation (Eq. 3.2) was adopted (ignoring effect of crystallite size).

$$\varpi = \frac{\beta_{\varpi} \cos\theta}{4} \tag{3.2}$$

In this equation, ϖ refers to micro-strain; and β_{ϖ} denotes peak broadening due to micro-strain.

The dislocation density (ψ) can be computed as (Eq. 3.3):

$$\psi = \frac{15\beta_L \cos\theta}{4aL} \tag{3.3}$$

β_L = FWHM measured in radians

θ = Diffracting angle

a = The cell parameter (Lattice constant measured from XRD data)

Also, for cubic crystal structure, $a = d\sqrt{(h^2 + k^2 + l^2)}$, and

L = Crystallite size in nm

Also the notations h, k, l denote *Miller* indices representing a particular crystallographic direction.

During execution of EDM operation, discharge energy is utilized to facilitate removal of material from the workpiece. The debris along with wear-out material coming from tool electrode may react with the work material at the machining zone. Pyrolysis of dielectric fluid also contributes to carbon enrichment onto the machined surface. Moreover, powder particles added to the dielectric fluid may contribute to material migration onto the machined surface. Thus, XRD of the machined surface may exhibit presence of intermetallic

compounds, and carbide precipitates. As shown in Table 3.2, variety of carbides Ni_3(Al, Ti)C, CoCx, NiC, $AlNi_3C_{0.5}$ were found for the EDMed specimen surface at different crystallographic directions.

Table 3.2: Precipitates/intermetallic compounds observed at the EDMed work surface

EDMed specimen obtained through:	Elements identified at crystallographic directions			
	[1 1 0]	[1 1 1]	[2 0 0]	[2 2 0]
Conventional EDM	$AlNi_3C_{0.5}$	Ni_3(Al, Ti)C, $Fe_{0.64}Ni_{0.36}$, CoCx, NiC	Ni_3(Al, Ti)C, $Fe_{0.64}Ni_{0.36}$, CoCx, NiC	Ni_3(Al, Ti)C, $Fe_{0.64}Ni_{0.36}$, NiC
Graphite PMEDM	$AlNi_3C_{0.5}$	Ni_3(Al, Ti)C, CoCx, $AlNi_3C_{0.5}$, NiC	Ni_3(Al, Ti)C, CoCx, $AlNi_3C_{0.5}$, NiC	Ni_3(Al, Ti)C, NiC

As compared to 'as received' Inconel 718 work material, significant grain refinement was found attributed to all EDMed specimen surfaces which resulted in reduced crystallite size, and consequently increased strain and dislocation density at crystallographic direction [1 1 1] (Tables 3.3-3.5). However, grain growth was observed at crystallographic direction [2 0 0] for the EDMed specimens prepared by using conventional EDM at I_p=25A and 30A, respectively (Table 3.4 and Table 3.5). For these specimens, grain growth resulted in increased crystallite size (whilst compared to 'as received' parent material) and consequently decreased strain and dislocation density. This might be due to increased energy input which caused periodic heating and cooling of the workpiece. Considering two high intensity peaks as obtained from the XRD spectra at I_P=30A, the average crystallite size was determined (Table 3.6). It was observed that 'as received' Inconel 718 corresponded to average crystallite size (L_{avg}) of 43.77nm; whilst, EDMed work surfaces produced by conventional EDM, and graphite powder mixed EDM showed average crystallite size $(L_{avg})$of 48.55nm, 24.81nm, respectively. Whilst considering the average crystallite size (L_{avg})as an indicator of grain refinement; it could be inferred that overall effect of grain refinement was predominant for all EDMed surfaces prepared by graphite powder-mixed EDM than obtained in conventional EDM.

In graphite powder mixed EDM, increased thermal conductivity of the working medium (due to enlarged discharge gap) causes heat to be distributed uniformly in the working zone. Moreover, multiple discharges take place for a longer period of time. This in turn promotes

grain refinement of larger extent. Refined grain structure also take part in relieving thermal residual stresses. In PMEDM some amount of residual stress is also released due to mechanical abrasion effect of powder particles on the surface [45]. Therefore, propensity of crack formation is remarkably reduced for the specimen produced in PMEDM. Refined grain structure is expected to improve hardness, abrasion wear resistance and corrosion resistance of the machined specimen produced by PMEDM which is highly appreciating.

Table 3.3: The variation of crystallite size (L), and dislocation density (ψ) for (1) 'as received' Inconel 718, and EDMed work surface of Inconel 718 obtained by using (2) Conventional EDM, and (3) Graphite powder-mixed EDM at **I_p=15A**

Sl. No.	Data of the two high intensity peaks of XRD for different specimens	$2\theta\ (^0)$	FWHM $(^0)$	Crystallite size (L) $[nm]$	Miller indices $[h,k,l]$	Inter planner spacing between the atoms $(d)[A^0]$	Lattice constant $(a)[A^0]$	Dislocation density (ψ) $\times 10^4$	Micro-Strain (ϖ) $\times 10^4$
(1)	'As received' Inconel 718	50.997	0.1771	57.61	[1 1 1]	2.07939	3.6016	5.056	3.695
		59.414	0.3542	29.93	[2 0 0]	1.80633	3.61266	18.67	8.841
(2)	EDMed work surface of Inconel 718 obtained through conventional EDM	51.1584	0.3936	25.94	[1 1 1]	2.07327	3.591	25.0128	8.2427
		59.8793	0.5510	19.29	[2 0 0]	1.79358	3.587	45.2905	13.8839
(3)	EDMed work surface of Inconel 718 obtained through graphite powder-mixed EDM	51.1829	0.5510	18.53	[1 1 1]	2.07235	3.5894	49.0297	11.5453
		59.8326	0.7085	14.99	[2 0 0]	1.79485	3.5897	74.8652	17.8357

Table 3.4: The variation of crystallite size (L), and dislocation density (ψ) for (1) 'as received' Inconel 718, and EDMed work surface of Inconel 718 obtained by using (2) Conventional EDM, and (3) Graphite powder-mixed EDM at **I_p=25A**

Sl. No.	Data of the two high intensity peaks of XRD for different specimens	$2\theta\ (^0)$	FWHM $(^0)$	Crystallite size (L) $[nm]$	Miller indices $[h,k,l]$	Inter planner spacing between the atoms $(d)[A^0]$	Lattice constant $(a)[A^0]$	Dislocation density (ψ) $\times 10^4$	Micro-Strain (ϖ) $\times 10^4$
(1)	'As received' Inconel 718	50.997	0.1771	57.61	[1 1 1]	2.07939	3.6016	5.056	3.695
		59.414	0.3542	29.93	[2 0 0]	1.80633	3.61266	18.67	8.841
(2)	EDMed work surface of Inconel 718 obtained through conventional EDM	51.1632	0.3542	28.82	[1 1 1]	2.07309	3.5906	20.2567	7.4184
		59.7769	0.2880	36.88	[2 0 0]	1.79507	3.59014	12.3758	7.2419
(3)	EDMed work surface of Inconel 718 obtained through graphite powder-mixed EDM	51.0983	0.3542	28.82	[1 1 1]	2.07555	3.5949	20.2437	7.4076
		59.8823	0.3840	27.67	[2 0 0]	1.79220	3.584	22.0134	9.6764

Table 3.5: The variation of crystallite size (L), and dislocation density (ψ) for (1) 'as received' Inconel 718, and EDMed work surface of Inconel 718 obtained by using (2) Conventional EDM, and (3) Graphite powder-mixed EDM at **I_p=30A**

Sl. No.	Data of the two high intensity peaks of XRD for different specimens	$2\theta\ (^0)$	FWHM $(^0)$	Crystallite size (L) $[nm]$	Miller indices $[h,k,l]$	Inter planner spacing between the atoms $(d)[A^0]$	Lattice constant $(a)[A^0]$	Dislocation density (ψ) $\times 10^4$	Micro-Strain (ϖ) $\times 10^4$
(1)	'As received' Inconel 718	50.997	0.1771	57.61	[1 1 1]	2.07939	3.6016	5.056	3.695
		59.414	0.3542	29.93	[2 0 0]	1.80633	3.61266	18.67	8.841
(2)	EDMed work surface of Inconel 718 obtained through conventional EDM	51.2721	0.2755	37.08	[1 1 1]	2.06899	3.5835	12.268	5.784
		59.965	0.1771	60.03	[2 0 0]	1.79125	3.5825	4.681	4.47
(3)	EDMed work surface of Inconel 718 obtained through graphite powder-mixed EDM	51.1616	0.3542	28.82	[1 1 1]	2.07315	3.5908	20.256	7.418
		60.0669	0.5117	20.79	[2 0 0]	1.78850	3.577	39.097	12.943

3.2.3 Analysis of EDS and Micro-Hardness Test Results

From EDS analysis, it was observed that while compared to 'as received' Inconel 718 (~0.8 wt% C), the EDMed work surfaces obtained through conventional EDM as well as PMEDM both exhibited relatively high carbon content (as shown in Figs. 3.9-3.10). This was basically the consequence of dielectric cracking (pyrolysis) of the dielectric fluid (EDM-oil) which promoted carbon migration at the machined surface. This was further verified by the micro-indentation hardness test results (Refer Table 3.6 and Appendix III).

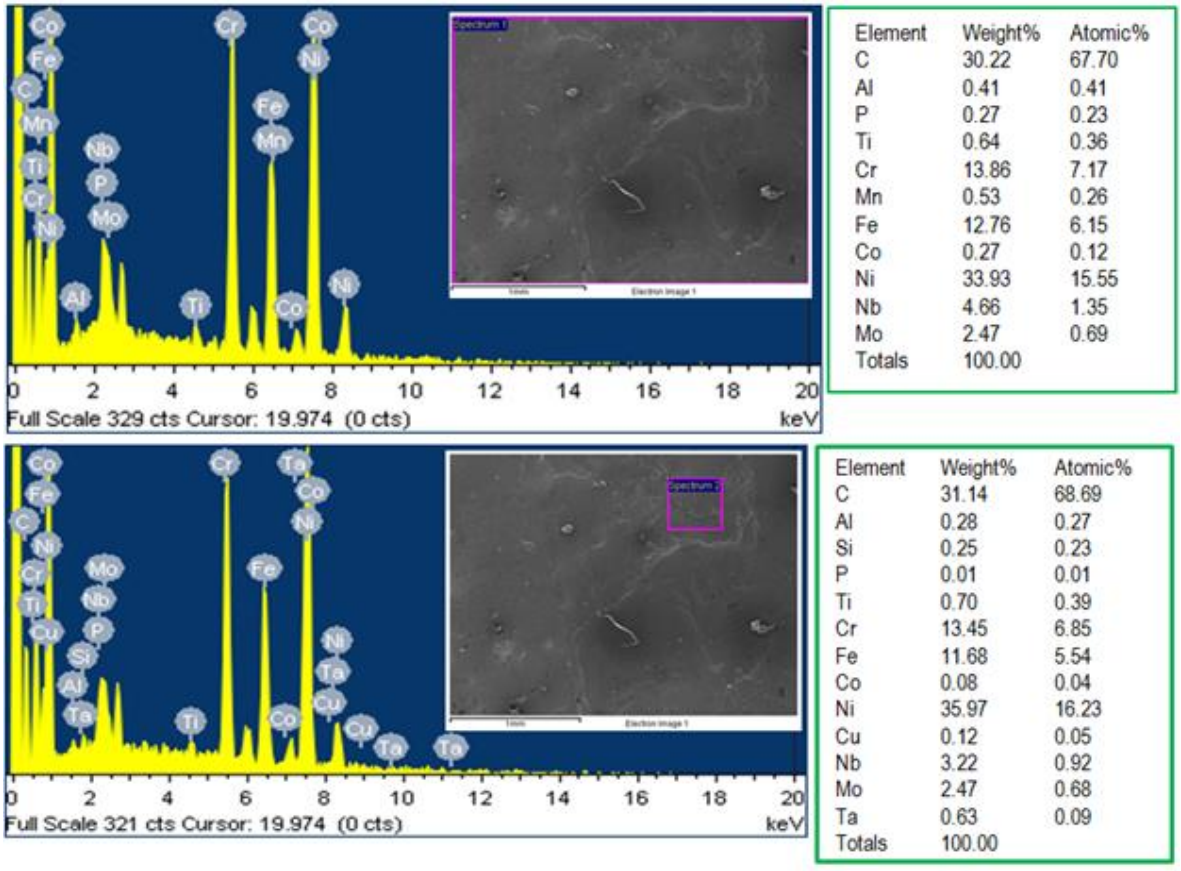

Element	Weight%	Atomic%
C	30.22	67.70
Al	0.41	0.41
P	0.27	0.23
Ti	0.64	0.36
Cr	13.86	7.17
Mn	0.53	0.26
Fe	12.76	6.15
Co	0.27	0.12
Ni	33.93	15.55
Nb	4.66	1.35
Mo	2.47	0.69
Totals	100.00	

Element	Weight%	Atomic%
C	31.14	68.69
Al	0.28	0.27
Si	0.25	0.23
P	0.01	0.01
Ti	0.70	0.39
Cr	13.45	6.85
Fe	11.68	5.54
Co	0.08	0.04
Ni	35.97	16.23
Cu	0.12	0.05
Nb	3.22	0.92
Mo	2.47	0.68
Ta	0.63	0.09
Totals	100.00	

Fig. 3.9: EDS results for the EDMed work surface of Inconel 718 produced at I_P=25A for conventional EDM

As compared to 'as received' Inconel 718 (which corresponded to average micro-hardness value MH~340 HV), the EDMed specimens produced at I_P=30A both in conventional EDM and PMEDM exhibited relatively high micro-hardness owing to the phenomenon of carbon enrichment during pyrolysis of the dielectric medium.

EDS analysis revealed that the amount of carbon enrichment was not uniform throughout the machined surface. It was noticed that majority of the EDMed surface produced through PMEDM, carbon content was found somewhat less as compared to conventional EDM; though it was just an experimental observation. However, during EDM with graphite powder

mixed dielectric, localized adhesion of suspended carbon particle onto the machined surface could attribute to sudden increase in carbon content at specific locations of the EDMed surface. Apart from this localized phenomena, it could be concluded that graphite powder-mixed EDM resulted in less carbon migration onto the machined surface whilst compared to convention EDM. This in turn reduced the probability of formation of hard carbide particles at the machined surface and thus reduced the propensity of surface cracking.

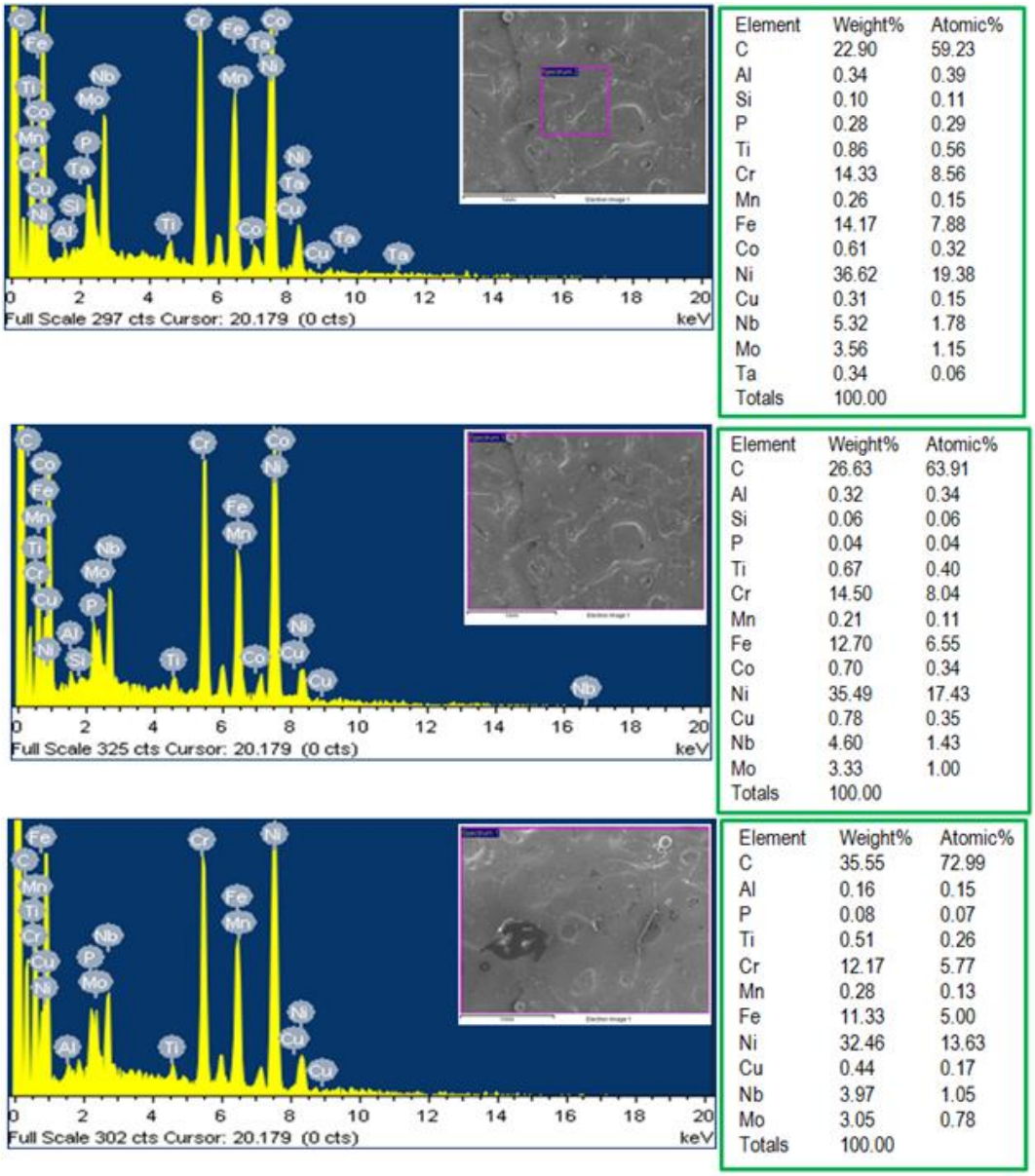

Fig. 3.10: EDS results for the EDMed work surface of Inconel 718 produced at I_P=25A for graphite powder-mixed EDM

This might be due to lesser extent of dielectric cracking during spark discharge. As addition of conductive graphite powder reduced dielectric strength of the working medium and thus stimulated early discharge to take place. Moreover, discharge energy was uniformly distributed at the working zone which resulted in heat dissipation in a more favorable manner from the discharging zone during the pulse-off time. As a consequence, early recovery of dielectric followed by de-ionization took place. The combined effects of these significantly dominated the amount of carbon migration at the machined surface. Therefore, lesser extent of carbon enrichment resulted in relatively less micro-hardness value (average MH~366.06 HV) for the EDMed specimen obtained in graphite powder-mixed EDM while compared to that of conventional EDM (average MH~476.03 HV).

With respect to 'as received' parent material, increased micro-hardness value as obtained in all EDMed specimens was due to formation of hard and low-conductive carbide layers onto the machined surface. Such carbide layers are found generally dispersed over the white layer. Therefore, white layer consists of re-solidified debris mixed with such carbides. Since, in the present work, all micro-indentations were made at positions approximately mid-depth of the white layer (measured from the top surface of the specimen); the micro-hardness value was influenced by the presence carbide distribution in the white layer. The dependency of surface hardness on the extent of white layer formed was clearly described in the work by Muthuramalingam et al. [46].

3.3 Effects of Peak Discharge Current

Increase in peak discharge current resulted in increased material removal rate because peak current is directly proportional to the energy input. More material was eroded from the workpiece leading to improved MRR. Increment of MRR with respect to increase in peak current was found more for the case of graphite powder mixed EDM whilst compared to conventional EDM (Fig. 3.11).

Addition of conductive powder particles promotes bridging effect that creates interlocking amongst the particles. Thus, they behave like a chain under the sparking area [8-11, 47-48]. Sparking intensity is remarkably increased within a discharge leading to faster erosion from the work material surface and consequently improved material removal rate. The 'series of discharge' as suggested by Zhao et al. [9] or 'multiple discharging effects' as explained by Chow et al. [49], favors the phenomenon of intensified electric field during powder-mixed EDM process. This is due to dispersion of the discharge energy in several increments

(sparking frequency increases) per single pulse. Consequently, the plasma channel is expanded and discharge energy is maintained consistent. Moreover, powder particles suspended in the dielectric fluid reduces gap voltage and insulating strength of the dielectric medium. Therefore, as compared to conventional EDM, a stable and uniform discharge takes place in PMEDM with enlarged spark gap.

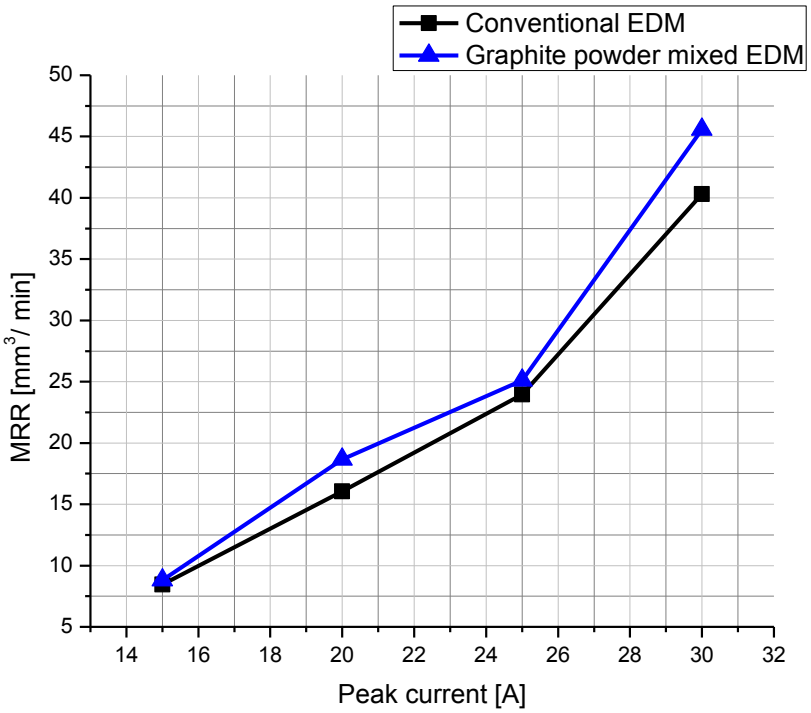

Fig. 3.11: Effect of peak discharge current on MRR

As explained by Baseri and Sadeghian [32], addition of powder particles in the dielectric fluid results in significant reduction of resistivity of the gap. This in turn improves conductivity of the working medium. This can easily be understood from the following (Eq. 3.4).

$$R_g = \frac{\rho_f L}{A} \tag{3.4}$$

In this equation, R_g is the gap resistance, ρ_f is the fluid density, A is the area between the tool and the workpiece, and L is the distance between the tool and workpiece. Thus, $R_g \propto L$. Therefore, increased spark gap ensures better flushing of the debris followed by series of desired discharges which causes improved MRR.

The abrasive powders present in the dielectric medium enhances efficiency to material removal which is simultaneously influenced by the mechanical thrust produced by gas bubble

explosion during evaporation of the working fluid and striking impact of the abrasive particles. This facilitates dislodging of work material from the work surface thus speeding up the material removal efficiency. As compared to conventional EDM, during PMEDM, increased peak current (which is a function of energy input) produces higher degree of erosive effect imposed by the abrasive powder particles. This in turn increases rate of material removal from the work surface.

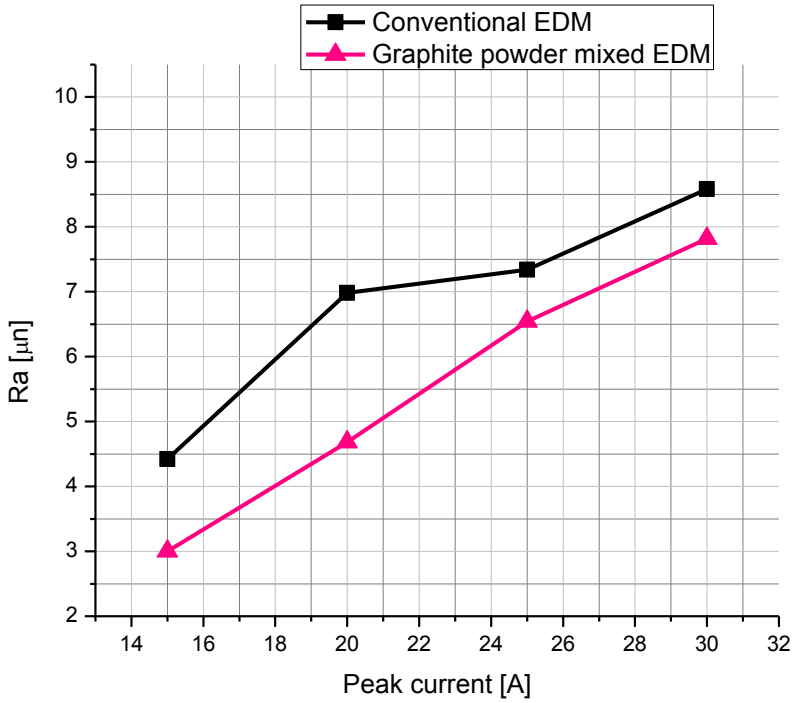

Fig. 3.12: Effect of peak discharge current on R_a

Regarding Fig. 3.11, it was observed that at Ip=15A and 25A, the improvement in MRR in PMEDM was appeared insignificant as compared to conventional EDM. This might be due to the fact of local agglomeration of powder particles which restricted removal of eroded material from the machined zone. The eroded material thus accumulated got engaged in 'rubbing action' with the machined surface. That was the reason why surface finish in case of PMEDM was appeared remarkably more appreciating as compared to conventional EDM (Fig. 3.12). Accumulation of eroded material in the vicinity of machined zone also increased the thickness of while layer developed (Fig. 3.14).

Increased energy input increases roughness of the machined surface due to high rate of material removal. In contrast to conventional EDM, superior surface finish was observed for the case of graphite powder mixed EDM (Fig. 3.12). Reduced degree of surface roughness of

the specimen produced by PMEDM was mainly due to formation of evenly distributed wide and shallow craters over the machined surface.

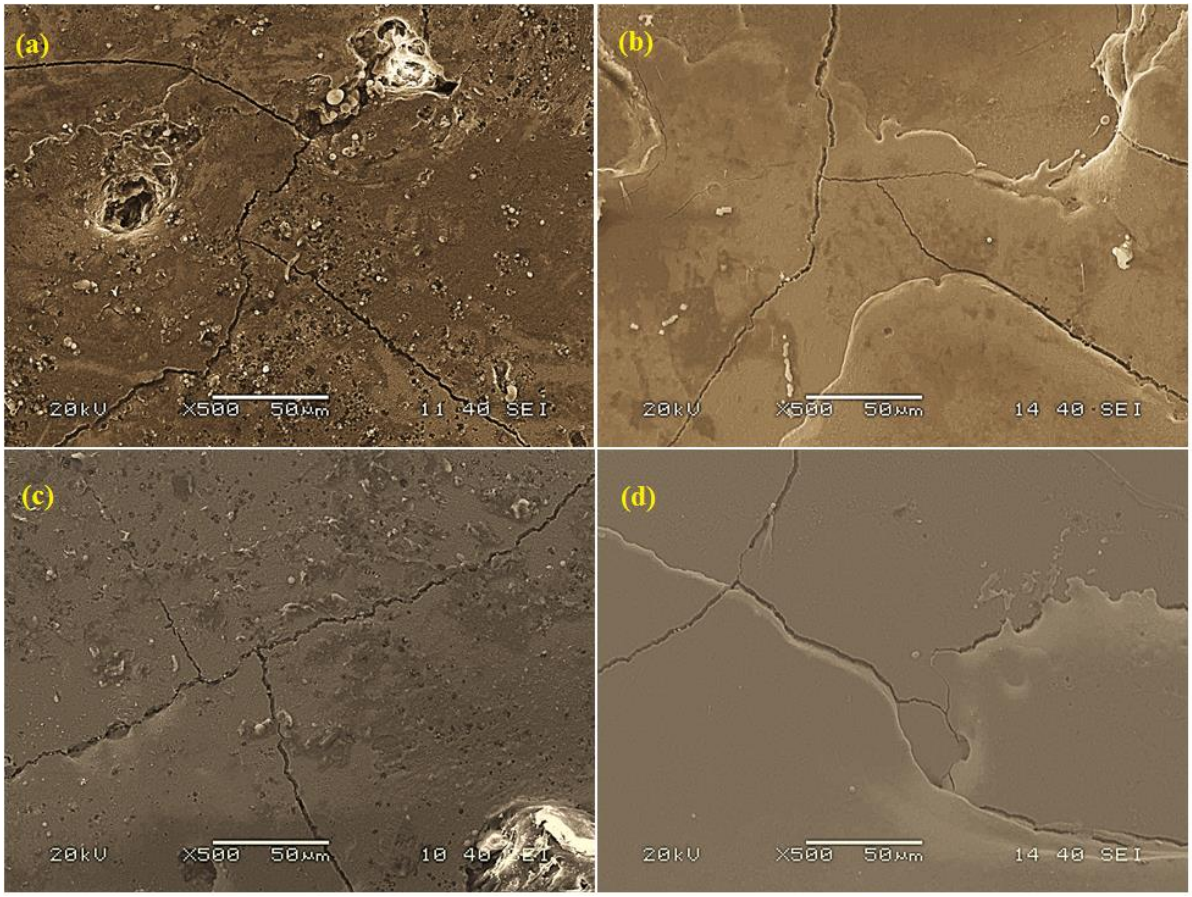

Fig. 3.13: Effect of peak discharge current on SCD: (a) SCD~0.0111µm/µm^2 for Conventional EDM at I_P=15A, (b) SCD~0.0133µm/µm^2 for **Conventional EDM** at I_P=25A, (c) SCD~0.0074µm/µm^2 for **Graphite powder-mixed EDM** at I_P=15A, (d) SCD~0.0106µm/µm^2 for Graphite powder-mixed EDM at I_P=25A

Due to the addition of powder particles, the discharge gap is enlarged which reduces the gap voltage as well as insulating strength of the dielectric medium. The discharge energy is evenly transferred with less impulsive forces and stresses that cause lesser degree of surface cracking. The widened discharge gap increases the discharge heat area reducing the discharge density. This facilitates formation of uniformly distributed, wide, and shallow craters. Thus, excellent surface finish is obtained in PMEDM [8]. Often, the abrasion effect of the powder particles at the work surface may also contribute towards enhancing surface finish. Such an abrasive action helps in reducing deposited debris and also undulations at crater boundaries. In graphite powder-mixed EDM, the low density graphite powders could mix uniformly

within the dielectric medium and float easily. The outstanding lubricating property of the graphite powder might favorably influence the surface finish to be appreciating.

Effect of peak discharge current on surface crack density was demonstrated in Fig. 3.13. Increment of peak current consequences increased energy input to the workpiece resulting evolution of huge thermal stress. When induced thermal stress exceeds ultimate tensile strength of the EDMed surface; cracks do initiate and propagate over the surface. Often, they penetrate through the depth of white layer continue towards bulk of the parent material. In the present work, crack density was found relatively less for the case of PMEDM whilst compared to conventional EDM.

In PMEDM, abrasive powder particles carry sufficient amount of heat generated during spark discharge. Wider spark gap facilitates easy removal of eroded material (debris) which also carries some amount of heat. Therefore, transfer of heat by the conductive abrasive particle is balanced by the rapid cooling of the workpiece. Thus, the machined surface produced by PMEDM experiences relatively less thermal stress than in conventional EDM. It was observed that the EDMed work surface produced in conventional EDM exhibited compressive residual strength (-336.4 ± 327.5 MPa) of higher magnitude as obtained for the case of PMEDM (~ 191.5 ± 147.3 MPa) which was found tensile in nature (Table 3.6). Reduced residual stress might be due to larger extent of grain refinement (refined structure and orientation of the grains) thereby relieving residual stress to some extent. Evolution of lesser residual stress in turn reduces chance of cracking to occur over the machined surface. Hence, surface crack density as well as severity of surface cracking (crack opening width) were found relatively less in case of graphite powder-mixed EDM. Surface cracking of lesser extent also contributed to superior surface finish.

Increased energy input causes more material to be eroded from the workpiece. Dielectric fluid appears increasingly inefficient to sweep away the debris from the machined zone. Hence, molten material gets resolidified forming white layer that adheres onto the machined surface. Thus, white layer appeared increasingly thicker as discharge current was increased gradually. Since, during execution of PMEDM, graphite powders, owing to their thermal conductivity, carried a percentage of the discharge heat energy; it was expected that the surface produced by PMEDM would exhibit presence of tiny white layer. However, specimens produced by graphite powder mixed EDM exhibited relatively thick white layer as compared to conventional EDM (Fig. 3.14). This might be due to localized effect of agglomeration of excess powder near the gap in the vicinity of the machined surface which restricted the debris to be flushed out properly. Therefore, molten material (debris) remained

in the same state for a longer period of time and solidified afterwards on the machined surface producing relatively thick white layer. However, very few sample exhibited dense (uniformly deposited) and thinner white layer whilst compared to conventional EDM (Fig. 3.15).

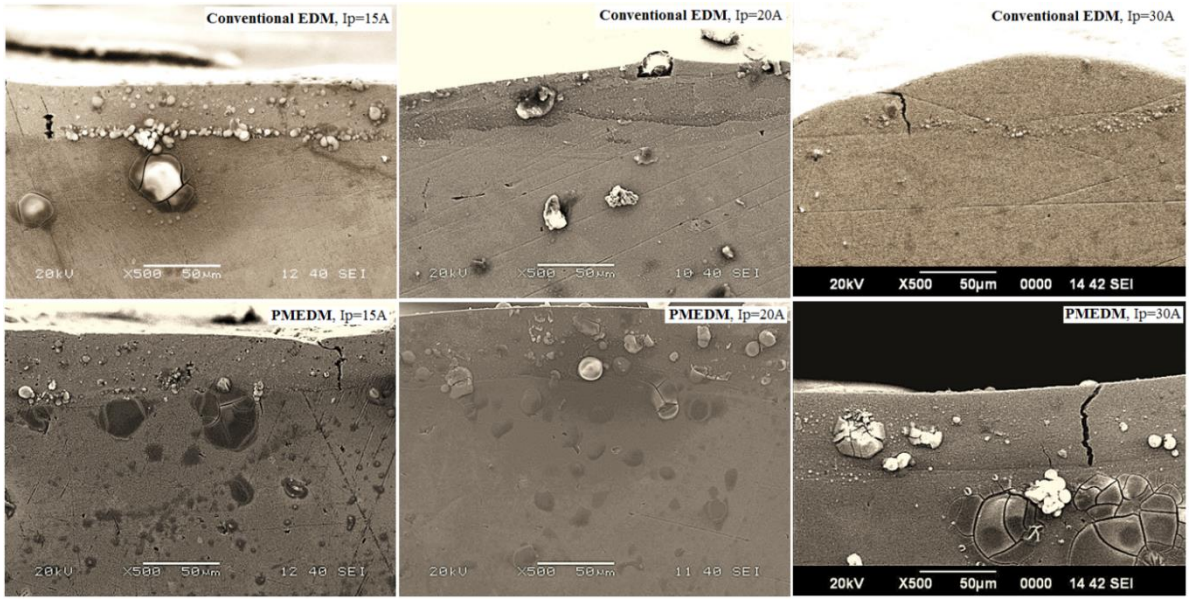

Fig. 3.14: Effect of peak discharge current on WLT
(a) WLT **(Conventional EDM)** ~32.36µm, 33.21µm, 35.51µm and (b) WLT **(Graphite powder-mixed EDM)** ~33.94µm, 43.6µm, 47.23µm for I_P=15A, 20A, and 30A, respectively

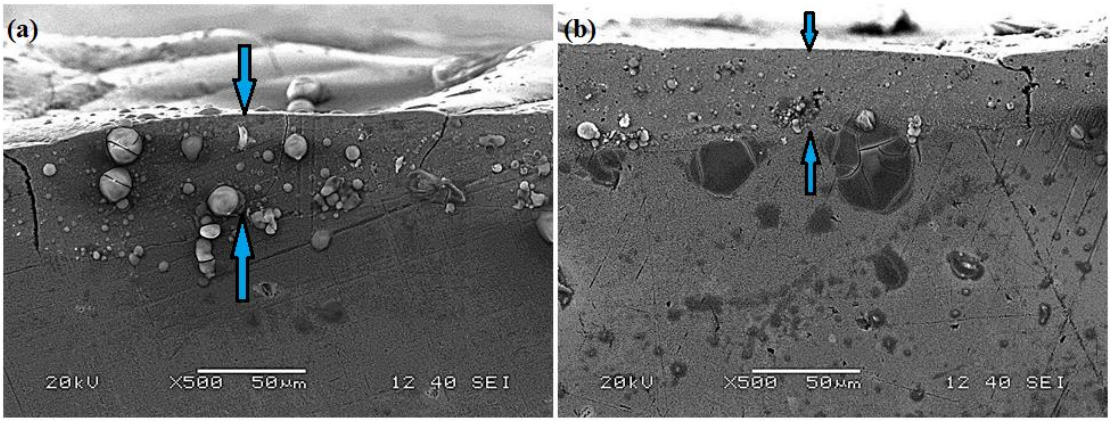

Fig. 3.15: SEM micrographs exhibiting existence of white layer onto the top of the machined surface obtained in (a) conventional EDM (WLT~46.99µm), and (b) graphite powder-mixed EDM (WLT~33.94µm) at I_P=15A

During EDM, intense heat is generated due to the spark discharge. Material removal is caused due to melting and evaporation of the workpiece. However, the spark not only melts the workpiece but also melts the tool as well. The melting of tool is called electrode wear. Tool wear rate is greatly influenced by thermal conductivity, melting point, and specific heat capacity of the tool material. Moreover, tool geometry and dielectric circulation flow rate also contribute towards tool wear. Increase in peak discharge current also resulted in increased tool wear.

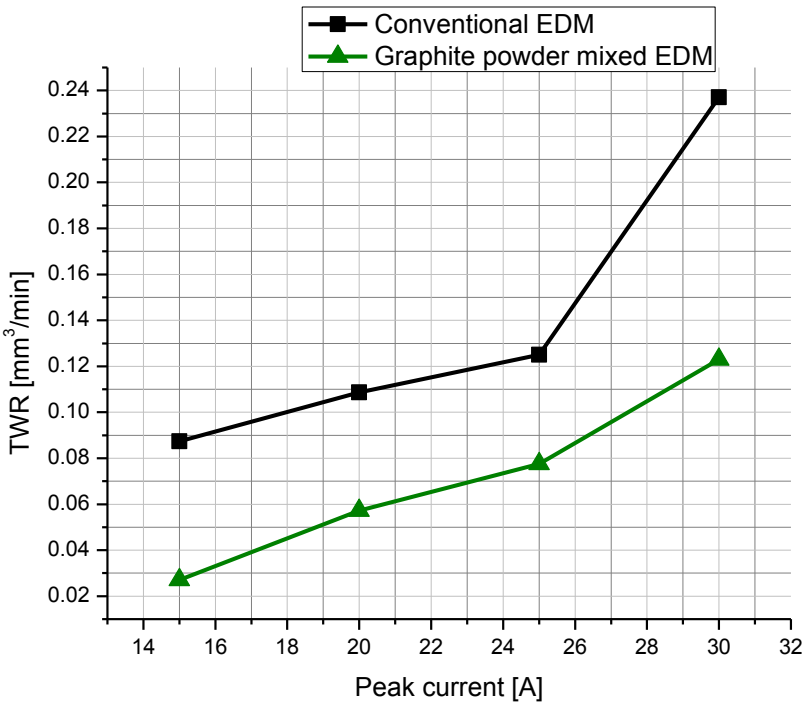

Fig. 3.16: Effect of peak discharge current on TWR

It was noticed that PMDEM could reduce tool wear substantially whilst compared to conventional EDM (Fig. 3.16). Tool wear rate of lesser extent can enhance tool life. During operation, heat is mainly transferred to both the workpiece as well as tool electrode. Pyrolysis of the dielectric medium generates pyrolitic carbon which adheres at the work surface as well as at the bottom surface and edge of the electrode mainly in the form of carbides. Deposition of hard, low conductive carbide layers in turn reduces thermal conductivity of the tool as a whole. These consequences rapid tools wear. In other words, such carbides deposited at the tool act as barrier towards heat conduction. Therefore, heat transfer can take place through bulk of the electrode material only after overcoming this barrier. This results in occurrence of tool wear and consequently poor tool shape retention capability. In contrast to conventional

EDM, addition of abrasive particles to the dielectric medium could reduce propensity of carbide deposition at the tool electrode. This in turn reduced the extent tool wear. Suspended powder particles in the dielectric media were frequently engaged in 'striking action' with the tool electrode. Since powder particles carried a significant amount of heat (due to their thermal conductivity), the thermally agitated powder particles to some extent restricted carbon atoms to be deposited over the tool electrode.

Similar to conventional EDM, in PMEDM also it was found that increased peak current resulted in increased degree of erosion of the tool electrode due to huge energy input. Consequently, tool wear rate assumed an increasing trend (Fig. 3.16).

Table 3.6: Average crystallite size (L_{avg}) of the EDMed specimens as compared to 'as received' work material

Sl. No.	Specimen	Average crystallite size (L_{avg}) [nm]	Residual stress [MPa]
(1)	'As received' Inconel 718	43.77	-371.1 ± 92.3
(2)	EDMed work surface obtained through conventional EDM (I_P=30A)	48.55	-336.4 ± 327.5
(3)	EDMed work surface obtained through graphite PMEDM (I_P=30A)	24.81	191.5 ± 147.3

CHAPTER 4

EDM of Inconel 718 with SiC Powder-Mixed Kerosene Dielectric Media: Effects of Powder Concentration

4.1 Characterization of SiC Powder Particles

A snapshot of the 'as received' SiC powder (Mesh size 400; average particle size~37 μm) was provided in Fig. 4.1, along with its XRD peak pattern. Computation of average crystallite size was carried out based on Scherrer equation using Full-Width Half-Maximum (FWHM) of the peaks obtained in the XRD spectra.

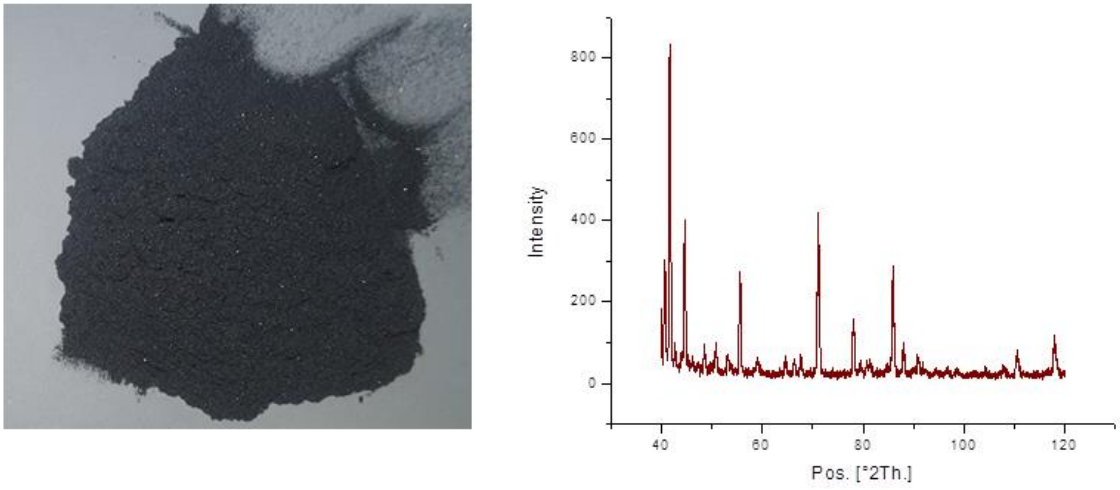

Fig. 4.1: XRD spectra for 'as received' SiC powders

The average crystallite size was obtained as 33.50 nm (Table 4.1). It must be noted that a particle consists of several crystallites. SEM micrographs (taken at different magnifications) of 'as received' SiC powder were also arranged in Fig. 4.2.

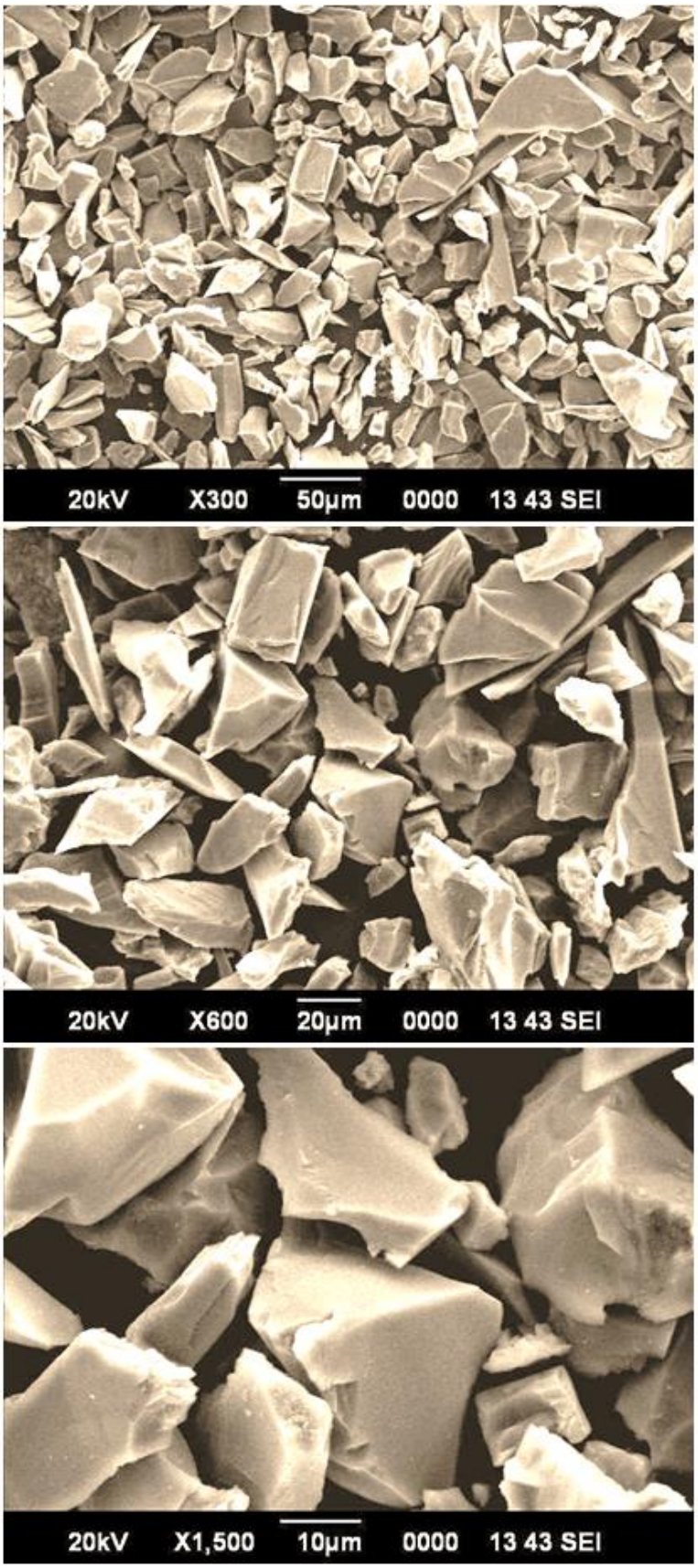

Fig. 4.2: SEM micrographs obtained at different magnifications of ‘as received’ SiC powders

Table 4.1: Computation of crystallite size (L) for 'as received' SiC powder along different crystallographic planes (corresponding directions)

Peak No.	Position $2\theta\ (^0)$	Height [cts]	FWHM $(^0)$	Crystallite size $(L)\ [nm]$	Average crystallite size $(L_{avg})\ [nm]$
1	40.6906	266.72	0.3542	27.72	33.50
2	41.6490	782.30	0.1378	71.50	
3	44.6457	356.25	0.4330	22.98	
4	55.6644	228.82	0.4330	24.05	
5	71.1812	348.35	0.4330	26.15	
6	78.0276	130.02	0.3936	30.11	
7	86.0011	218.32	0.3936	31.99	

4.2 Surface Integrity: Morphology and Topography

Surface morphology of the EDMed surface of Inconel 718 was found inferior (as compared to 'as received' Inconel 718) due to presence of pockmarks, globules of debris, uneven melted material deposition and surface cracks in abundance (Fig. 4.3). However, it was observed that intensity of such surface irregularities varied with respect to peak discharge current, pulse duration and concentration of powder particle in the dielectric media. White layer was also found (Fig. 4.4) over the EDMed surface of Inconel 718 due to resolidification of debris during pulse-off time. However, it was observed that in many cases, when PMEDM was executed using high powder concentration; there was the tendency of forming comparatively thick white layer. This might be explained due to the fact that at high powder concentration, local agglomeration of powders might restrict removal of debris from the machined surface; hence, resulting inefficient flushing. Due to restricted flow of debris; debris got accumulated in an increasing amount during successive occurrence of pulses. This increased the value of white layer thickness.

EDS elemental spectra for 'as received' Inconel 718 and the EDMed surface of Inconel 718 obtained at (I_P= 35A, T_{on}= 1500µs and powder concentration 0g/l) and at (I_P= 35A, T_{on}= 2000µs and powder concentration 2g/l) were exhibited in Figs. 4.5a-c. It was found that as compared to 'as received' Inconel 718; sufficient carbon migration took place at the EDMed surface leading to increase in the carbon percentage (weight%). The dielectric media (kerosene) was a hydrocarbon; during electric discharge, pyrolysis of kerosene produced free carbon which migrated over the machined surface. This was also found that as compared to

normal-EDM (no powder), increase in powder concentration (in case of PMEDM) resulted in increased carbon enrichment onto the machined surface.

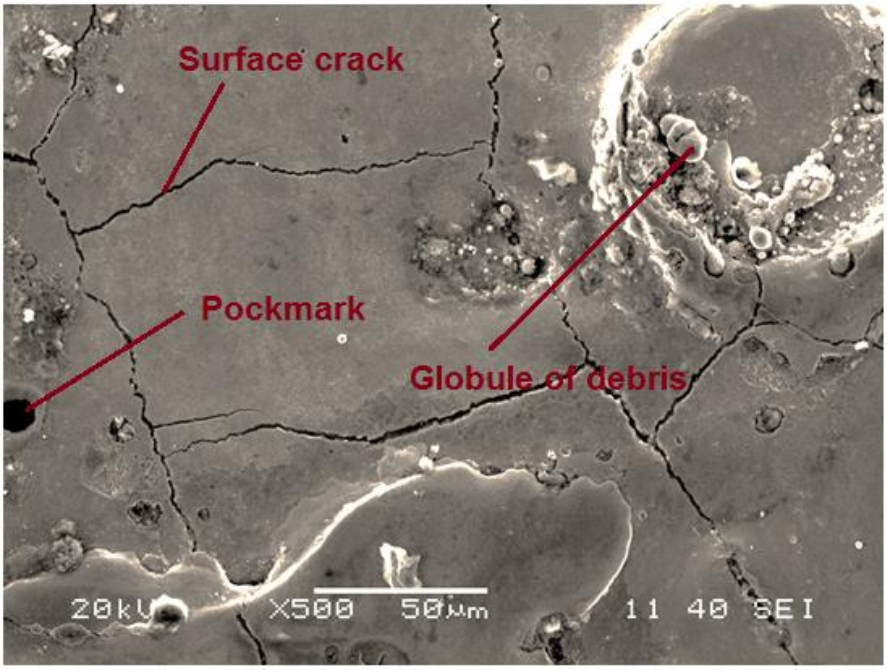

Fig. 4.3: Surface morphology of EDMed surface (as observed under SEM) at I_P= 30A, T_{on}=1500µs and powder concentration 4g/l

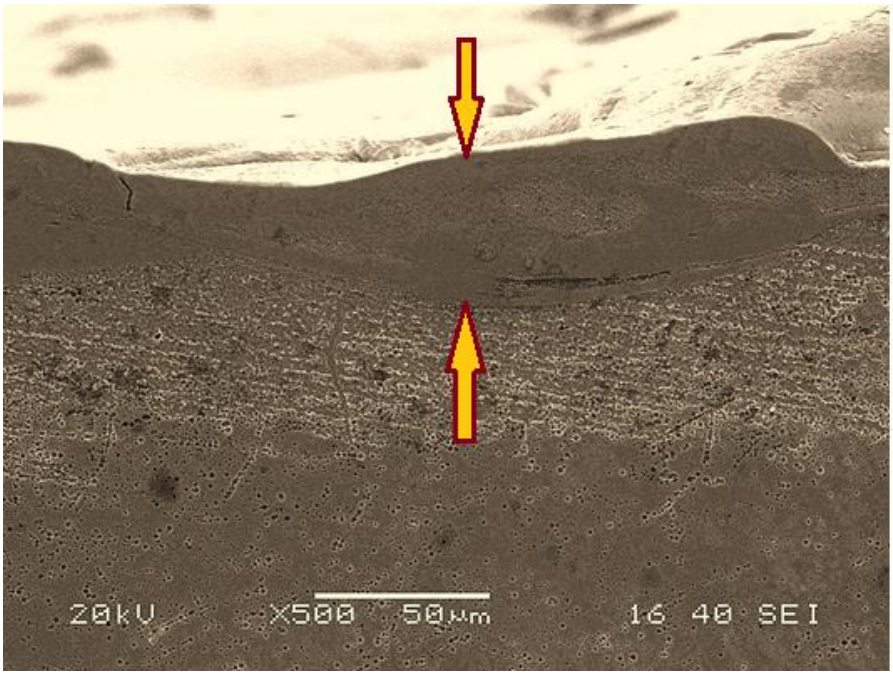

Fig. 4.4: SEM micrograph exhibiting presence of white layer over the EDMed surface obtained at I_P= 30A, T_{on}=1500µs and powder concentration 4g/l (WLT ~ 34.18 µm)

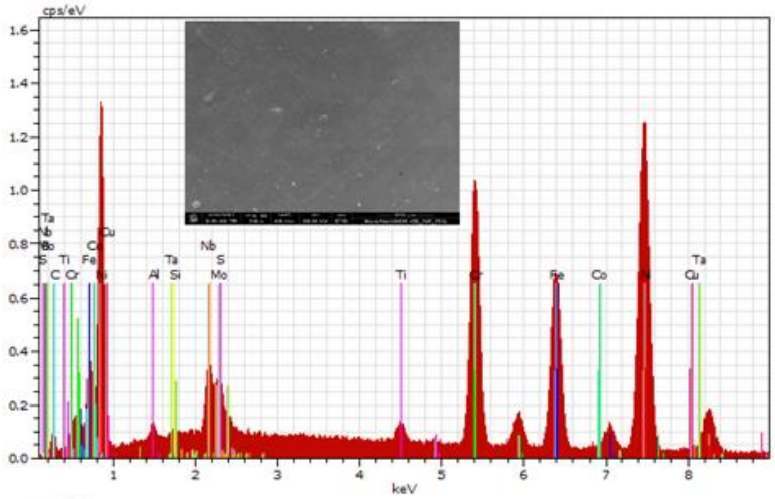

Element	% wt.
Ni	50.50
Fe	20.24
Cr	18.16
Nb	5.02
Mo	2.91
Ti	1.05
Al	0.62
Co	0.15
Si	0.08
Mn	0.07
Cu	0.06
C	0.05
P	0.008
Ta	0.003
B	0.003

(a)

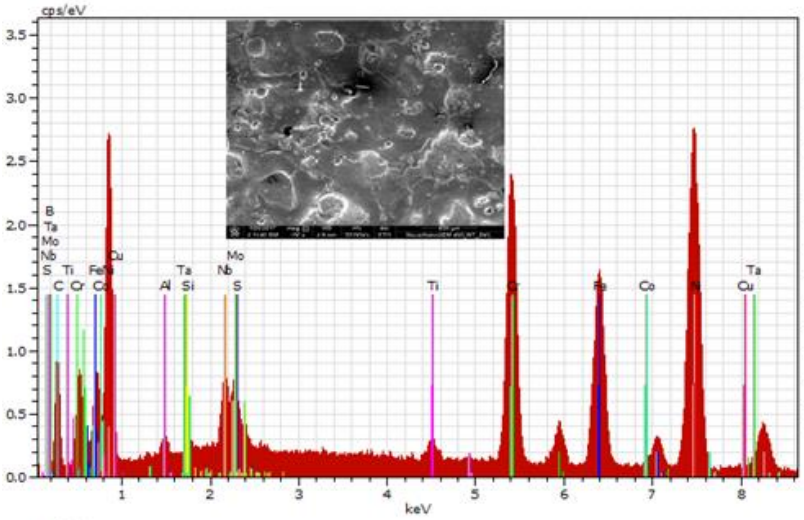

Element	wt.%
Ni	41.76
C	16.66
Cr	16.21
Fe	15.91
B	0.84
Nb	3.94
Mo	2.31
Ti	1.00
Al	0.56
Co	0.17
S	0.07
Cu	0.17
Ta	0.22
Si	0.19
Total	100

(b)

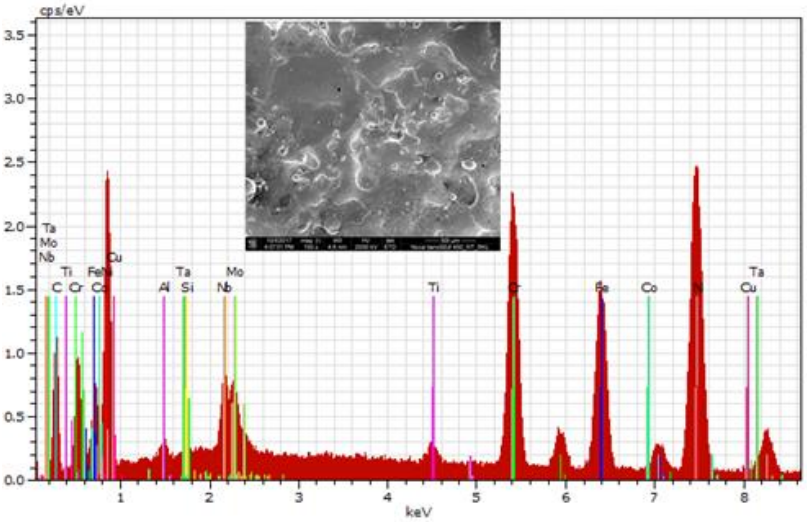

Element	wt.%
Ni	40.48
C	19.80
Cr	15.42
Fe	15.19
Nb	4.45
Mo	2.46
Ti	0.97
Al	0.63
Co	0.17
Cu	0.19
Ta	0.15
Si	0.10
Total	100

(c)

Fig. 4.5: EDS elemental spectra for (a) 'as received' Inconel 718, (b) EDMed surface of Inconel 718 at I_P= 35A, T_{on}= 1500µs and powder concentration 0g/l, and (c) EDMed surface of Inconel 718 at I_P= 35A, T_{on}= 2000µs and powder concentration 2g/l

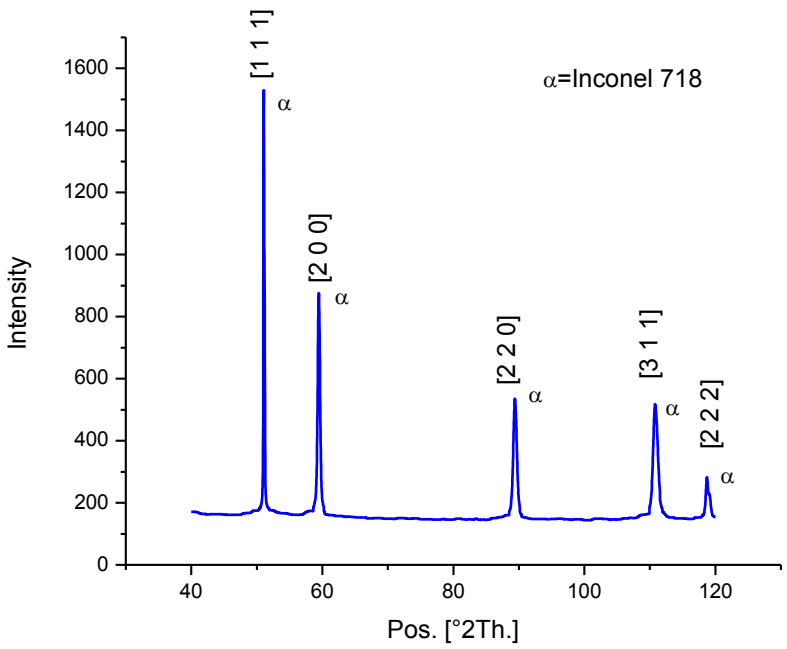

Fig. 4.6a: XRD spectra for 'as received' Inconel 718

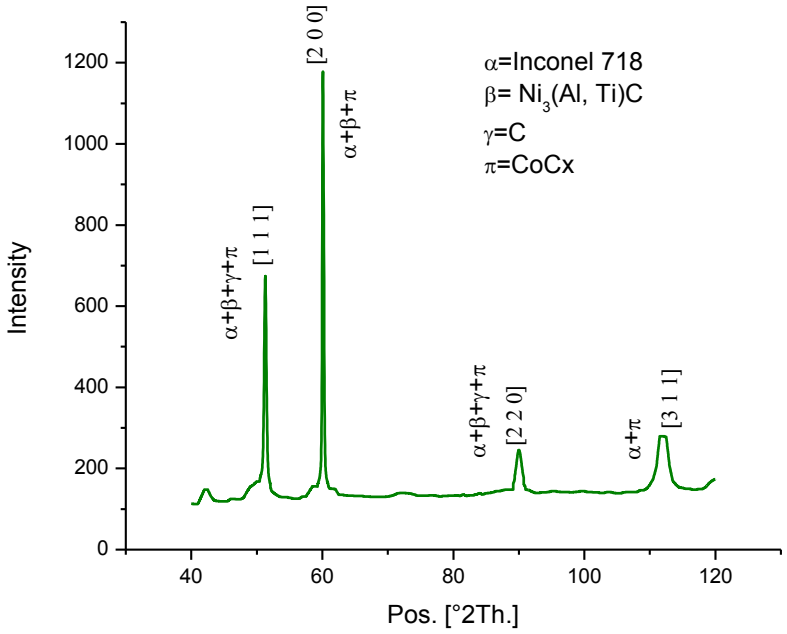

Fig. 4.6b: XRD spectra for EDMed surface of Inconel 718 obtained at I_P= 35A, T_{on}= 1000µs and powder concentration 4g/l

XRD spectra for the EDMed surface of Inconel 718 was compared to that of 'as received' Inconel 718. It was found that carbon migration onto the machined surface resulted in formation of few intermetallic compounds (specially carbides) viz. Ni_3(Al, Ti)C, free C, CoCx (Figs. 4.6a-b). While comparing the XRD peak pattern of the EDMed surface (obtained at I_P= 35A T_{on}=300µs and powder concentration 2g/l) to that of 'as received' Inconel 718; significant grain refinement was observed at crystallographic planes in the directions [111] and [220], respectively (Table 4.2a and Table 4.2c). However, for the crystallographic plane [200], grain growth was observed (Table 4.2b). It was also found that change in powder concentration did not promote any remarkable alteration in regards of phase constituents for the EDMed surface obtained in PMEDM as compared to the normal EDM (no powder).

Table 4.2a: The variation of crystallite size (L), and dislocation density (δ) for (1) 'as received' Inconel 718, (2) EDMed work surface of Inconel 718 obtained at (I_P= 35A, T_{on}=1000µs and powder concentration 4g/l)

Sl. No.	Data of the highest intensity peak of XRD for different specimens	$2\theta\ (^0)$	FWHM (β_L) $[rad]$	Crystallite size $(L)\,[nm]$
(1)	'As received' Inconel 718	51.0574	0.1181	86.41
(2)	EDMed work surface of Inconel 718 obtained at (I_P= 35A, T_{on}=1000 µs and powder concentration 4g/l)	51.2594	0.3542	28.84

Table 4.2a (Continued)

Sl. No.	Data of the highest intensity peak of XRD for different specimens	Miller indices $[h,k,l]$	Inter planner spacing between the atoms $(d)\,[A^0]$ (Obtained from *X'pert HighScore Software*)	Lattice constant $(a)\,[A^0]$	Dislocation density (δ) $\times 10^4$
(1)	'As received' Inconel 718	[1 1 1]	2.07710	3.5976	2.2496
(2)	EDMed work surface of Inconel 718 obtained at (I_P= 35A, T_{on}=1000 µs and powder concentration 4g/l)	[1 1 1]	2.06946	3.5844	20.2759

Table 4.2b: The variation of crystallite size (L), and dislocation density (δ) for (1) 'as received' Inconel 718, (2) EDMed work surface of Inconel 718 obtained at (I_P= 35A, T_{on}=1000µs and powder concentration 4g/l)

Sl. No.	Data of the highest intensity peak of XRD for different specimens	$2\theta\ (^0)$	FWHM (β_L) $[rad]$	Crystallite size $(L)\,[nm]$
(1)	'As received' Inconel 718	59.4273	0.3542	29.93
(2)	EDMed work surface of Inconel 718 obtained at (I_P= 35A, T_{on}=1000 µs and powder concentration 4g/l)	60.0712	0.1968	54.05

Table 4.2b (Continued)

Sl. No.	Data of the highest intensity peak of XRD for different specimens	Miller indices $[h,k,l]$	Inter planner spacing between the atoms $(d)\,[A^0]$ (Obtained from *X'pert HighScore Software*)	Lattice constant $(a)\,[A^0]$	Dislocation density (δ) $\times 10^4$
(1)	'As received' Inconel 718	[2 0 0]	1.80596	3.61192	18.67146
(2)	EDMed work surface of Inconel 718 obtained at (I_P= 35A, T_{on}=1000 µs and powder concentration 4g/l)	[2 0 0]	1.78838	3.57676	5.7833

4.3 Prediction of Optimal Setting: Effects of Process Factors

In this part of work, an attempt was made to determine an optimal setting of process parameters towards satisfying requirements of MRR, R_a, SCD, and WLT, simultaneously. Assuming that MRR corresponds to Higher-is-Better (HB); whereas, remaining response features correspond to Lower-is-Better (LB) requirement; utility theory coupled with Taguchi's optimization philosophy was explored herein to predict the most appropriate parameters setting. The basic formulation of utility based Taguchi method could be well articulated from the reporting by Singh and Kumar [50]. Procedural steps along with mathematical formulation of utility theory were provided in Appendix IV, at the end of this chapter.

Table 4.2c: The variation of crystallite size (L), and dislocation density (δ) for (1) 'as received' Inconel 718, (2) EDMed work surface of Inconel 718 obtained at (I_P= 35A, T_{on}=1000µs and powder concentration 4g/l)

Sl. No.	Data of the highest intensity peak of XRD for different specimens	$2\theta\ (^0)$	FWHM (β_L) $[rad]$	Crystallite size $(L)\,[nm]$
(1)	'As received' Inconel 718	89.3453	0.5117	25.31
(2)	EDMed work surface of Inconel 718 obtained at (I_P= 35A, T_{on}=1000 µs and powder concentration 4g/l)	89.9389	0.9600	13.56

Table 4.2c (Continued)

Sl. No.	Data of the highest intensity peak of XRD for different specimens	Miller indices $[h,k,l]$	Inter planner spacing between the atoms $(d)\,[A^0]$ (Obtained from *X'pert HighScore Software*)	Lattice constant $(a)\,[A^0]$	Dislocation density (δ) $\times 10^4$
(1)	'As received' Inconel 718	[2 2 0]	1.27323	3.601238	26.20291
(2)	EDMed work surface of Inconel 718 obtained at (I_P= 35A, T_{on}=1000 µs and powder concentration 4g/l)	[2 2 0]	1.26570	3.57994	91.82603

Table 4.3: Computed utility values and overall utility degree

Sl. No.	Utility values of individual responses				Overall utility degree	S/N Ratio of overall utility degree
	MRR	R_a	SCD	WLT		
1	5.5277	4.0937	9	9	6.9053	16.7837
2	6.6140	2.8394	2.4603	1.8939	3.4519	10.7612
3	0	9	0	1.2369	5.1184	14.1827
4	7.5218	2.6683	3.1605	2.0772	3.8569	11.7248
5	5.6753	6.3674	0.4565	5.3717	4.4677	13.0017
6	4.8026	4.7431	0.05266	4.2296	3.4569	10.7737
7	8.6723	0.6714	5.9760	3.8733	4.7982	13.6216
8	6.8680	0.5583	0.4702	3.1972	2.7734	8.8603
9	9	0	1.8679	0	2.7169	8.6815

Table 4.4: Mean response table

Level	Variation of mean S/N ratio of response expressed in [db] due to factorial variation		
	A [A]	B (µs)	C (g/l)
1	13.91	14.04	12.14
2	11.83	10.87	10.39
3	10.39	11.21	13.60
Delta	3.52	3.17	3.21
Rank	1	3	2

Response data (as obtained from Table 2.7 of Chapter 2) were converted into individual utility values. Next, utility values of individual responses were aggregated to compute the overall utility degree (Table 4.3). The overall utility degree was finally optimized (maximized) using Taguchi method. From the mean response (S/N ratio of overall utility degree) plot (Fig. 4.7); the optimal setting was predicted: $A_1B_1C_3$ i.e. [I_P= 25A, T_{on}= 1000µs and powder concentration 4g/l]; this was further verified by confirmatory test. From mean response table (Table 4.4), it was found that peak current appeared as the most significant parameter followed by particle concentration on influencing machining performance.

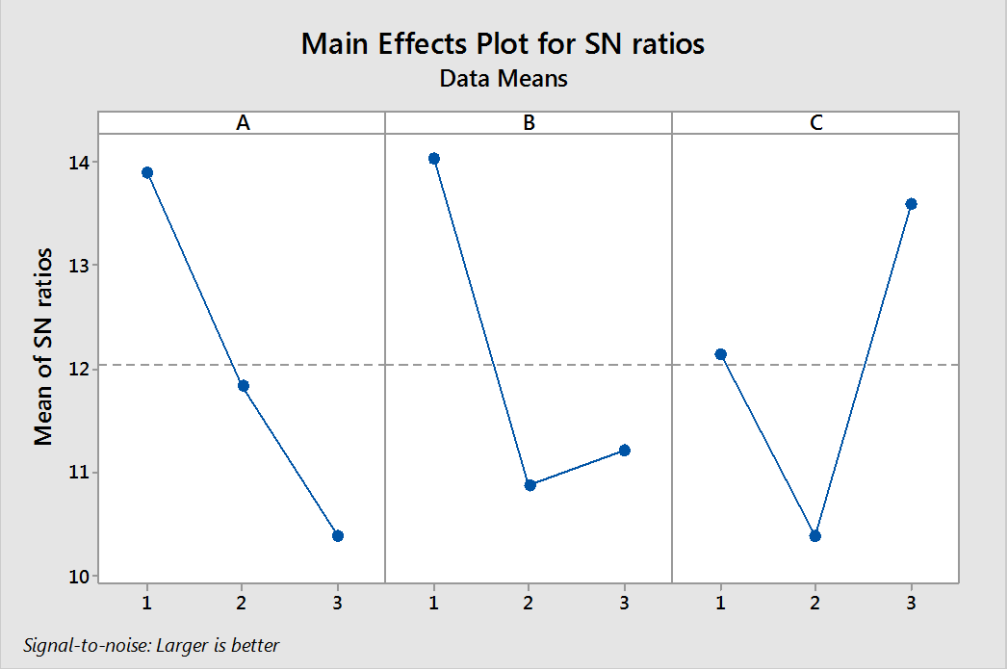

Fig. 4.7: Mean S/N ratio plot for overall utility degree: Prediction of optimal setting. Predicted optimal setting: $A_1B_1C_3$ i.e. [I_P= 25A, T_{on}= 1000µs and powder concentration 4g/l]

The orthogonal array design of experiment provides some advantages over full-factorial experimental design. Orthogonal array contains limited number of experimental runs while compared to full-factorial design and thus experimentation becomes less expensive and less time consuming. Additional advantage of orthogonal array is that it is capable of eliminating effects of insignificant factors (noise) and can extract direct (main) effect of individual process parameters followed by a prediction of optimal parameters setting. Therefore, apart from determining the optimal setting; results of Taguchi analysis were extended herein to understand parametric influence on different EDM performance indicators: material removal rate, surface roughness, crack intensity and thickness of the white layer.

Direct effect of peak discharge current on material removal rate was shown in Fig. 4.8. It was observed that with increase in peak current; material removal rate increased sharply. The intensity of discharge energy at the spark gap got increased with increased peak current which in turn enhanced the rate of material removal.

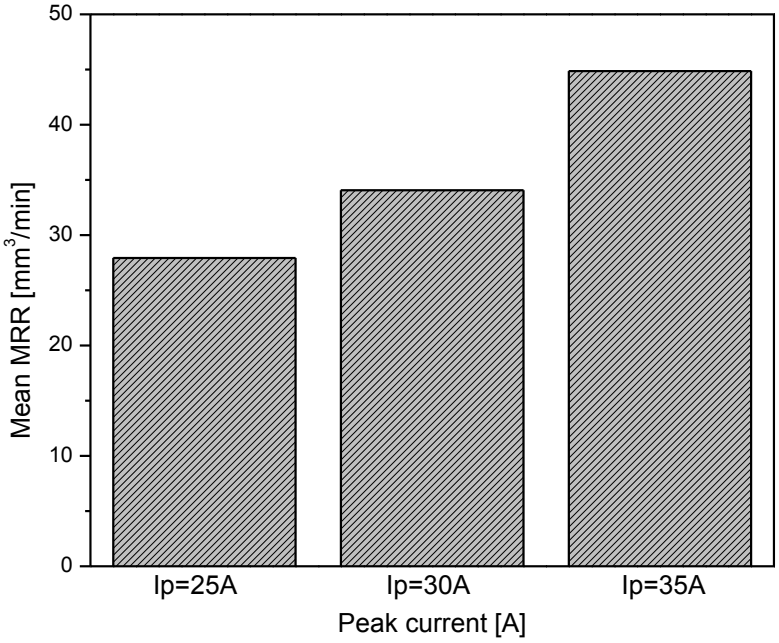

Fig. 4.8: Effect of peak current on MRR

It was noticed that with increase in pulse-on time, material removal rate assumed a decreasing trend (Fig. 4.9). Though, in practice, pulse-energy is increased with increase in pulse-on time. Therefore, it is expected that increased pulse-on time would cause high material removal rate. However, in the present experimental observation, it appeared opposite. This might be due to the fact that in the current experimental schema, pulse-off

duration as well as duty factor was not varied. Now, increased pulse-on duration resulted in more material erosion from the work surface; however, due to inefficient flushing; during pulse-off time, the situation obstructed eroded material to be swept away from the machining zone substantially; as a whole, material removal rate got decreased.

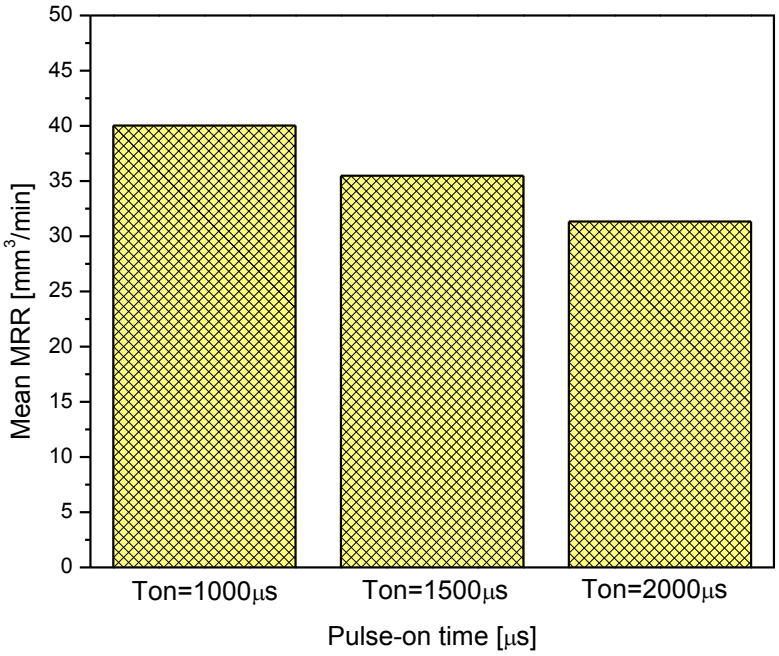

Fig. 4.9: Effect of pulse-on time on MRR

Direct effect of peak discharge current on surface roughness (R_a) was shown in Fig. 4.10. It was observed that surface roughness value increased with increased peak current. This happened due to the fact that with increase in peak current, the discharge energy was increased resulting more erosion from the work surface and thus higher value of surface roughness was obtained.

The effect of pulse-on time on R_a was also exhibited in Fig. 4.11. It was observed that increase in pulse-on duration resulted relatively superior surface finish. This might be due to the fact that at higher value of pulse-on time, eroded material could not be flushed away completely from the machining zone due to lack of time; as pulse-off duration was maintained constant. Therefore, in the vicinity of the spark gap, debris (eroded material) got accumulated and engaged in rubbing action with the machined surface. The situation played a vital role in reducing the value of roughness average.

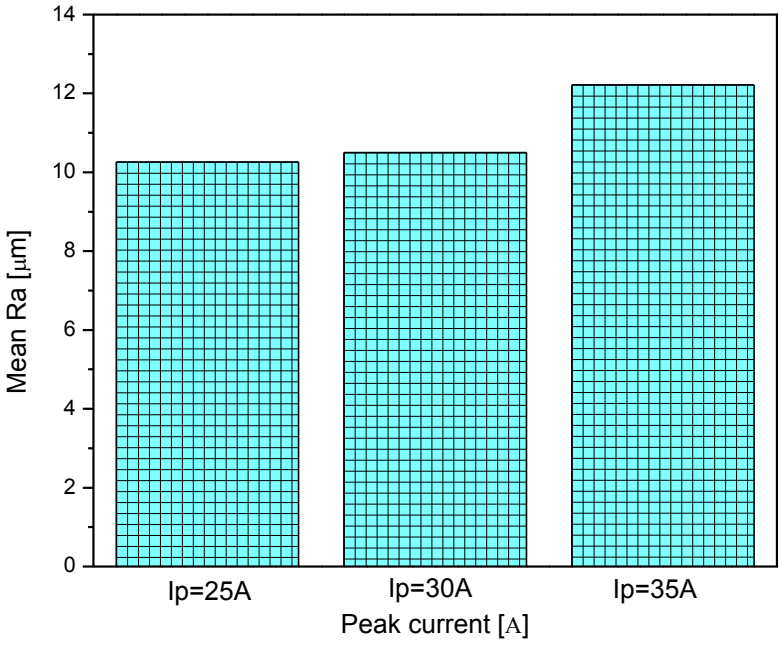

Fig. 4.10: Effect of peak current on R_a

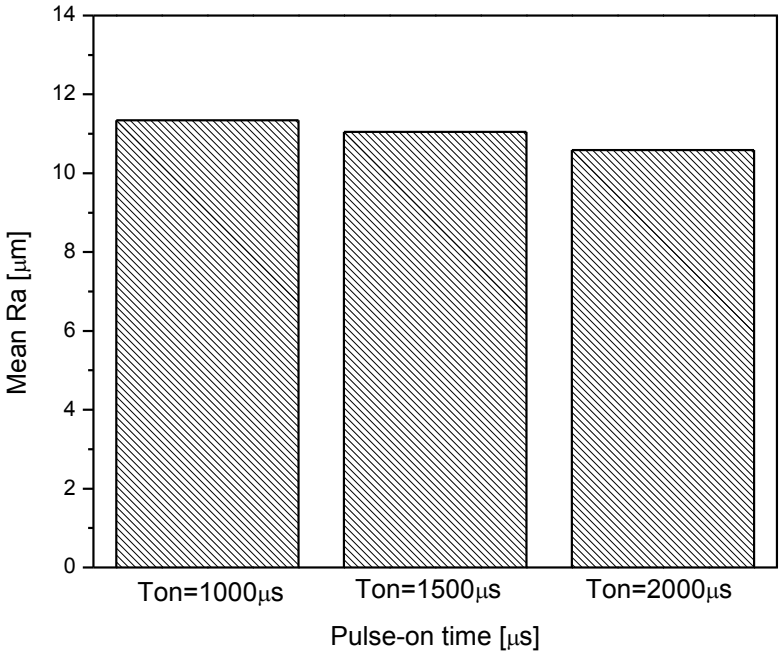

Fig. 4.11: Effect of pulse-on time on R_a

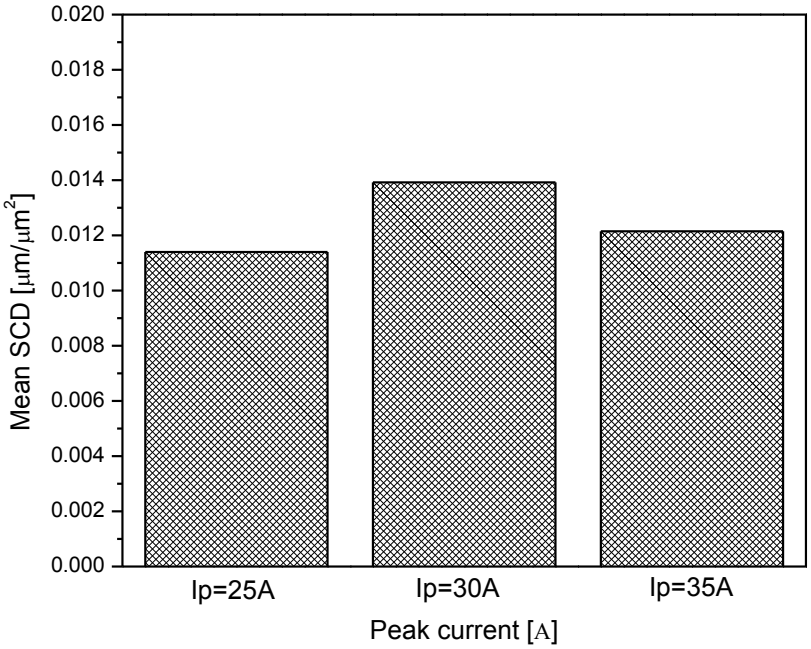

Fig. 4.12: Effect of peak current on SCD

Direct effect of peak discharge current on surface crack density was shown in Fig. 4.12. It was observed that when peak current was increased from 25A to 30A, surface crack density increased sharply; however, further increase in peak current (up to 35A), crack density assumed a decreasing trend. Increased peak current resulted in increased energy input; and hence, intense thermal stress at the machined surface. This situation enhanced propensity of surface cracking. However, the intensity of surface cracking depended not only on the energy input but also on the nature of formation of white layer and the growth of this layer. Crack density is measured as the total length of cracks developed on the surface divided by the surface area. Over the machined surface, there exists a layer called white layer which is formed due to re-solidification of the debris particles because they remain there in the vicinity of machined zone and not carried away due to insufficient flushing of the dielectric media. Initially, when peak current was varied from 25A to 30A, the rate at which white layer was formed appeared less as compared to the case when peak current was increased after 30A (rate of white layer formation was more; resulting thicker white layer). Therefore, crack density increased up to 30A of peak current; then it showed decreased value.

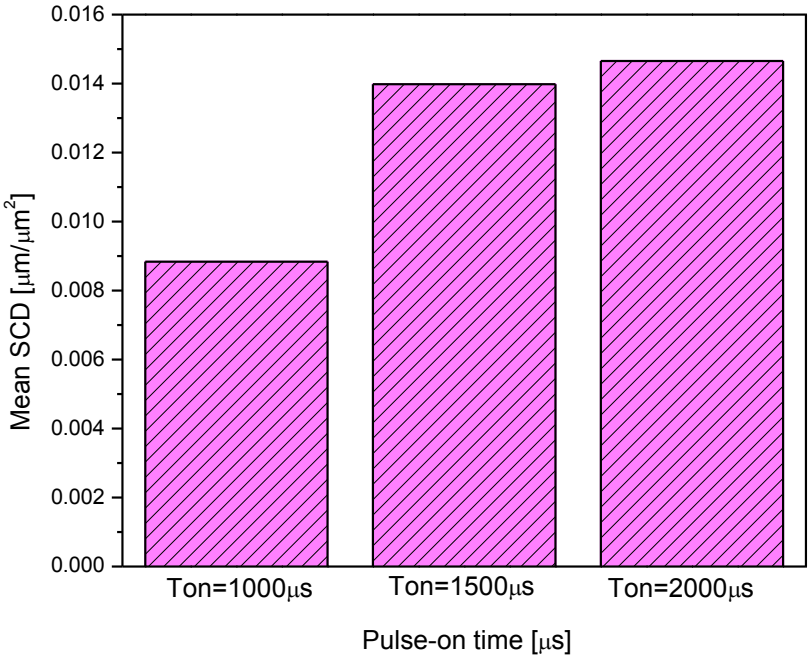

Fig. 4.13: Effect of pulse-on time on SCD

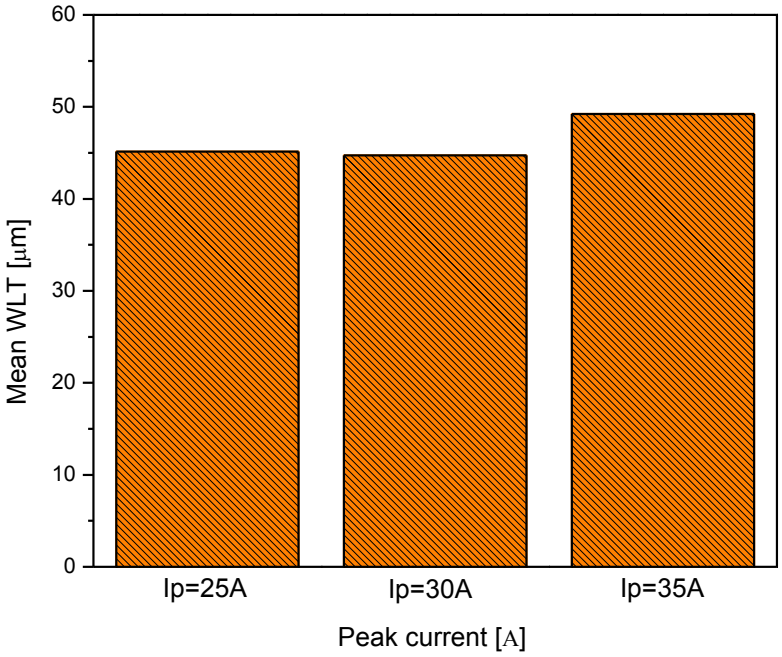

Fig. 4.14: Effect of peak current on WLT

The effect of pulse-on time on surface crack density was demonstrated in Fig. 4.13. It was noticed that crack density increased with increase in pulse-on time. Since eroded material was responsible of carrying a significant amount of heat from the machined surface; with increased pulse-on duration, inefficient flushing of debris resulted in more heat accumulation at the machined zone. The situation resulted in evolution of huge thermal stress; when such induced stress exceeded ultimate tensile strength of the machined surface cracking took place. Moreover, it is known that the extent of surface cracking is inversely proportional to the thermal conductivity of the work material. Due to dielectric cracking, the machined surface experienced significant carbon migration. Such carbon enrichment resulted in formation of hard carbides on the machined surface. Due to low thermal conductivity of carbides, severity of cracking got increased.

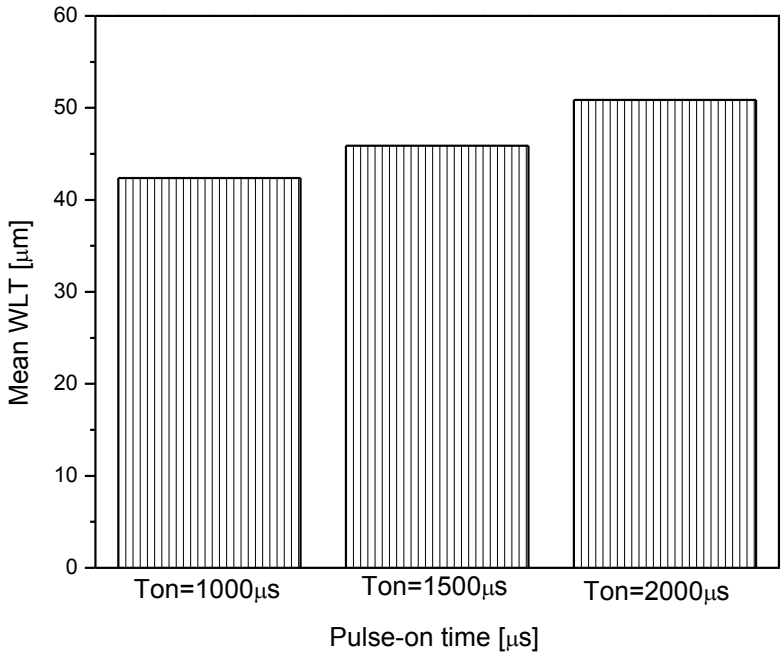

Fig. 4.15: Effect of pulse-on time on WLT

Direct effect of peak discharge current on white layer thickness was shown in Fig. 4.14. An average increasing trend of white layer thickness was experienced with increased peak current. Increased peak current resulted in more material to be eroded; however, dielectric media appeared increasingly inefficient to carry away entire debris. The remaining debris thus got solidified during pulse-off time and deposited over the machined surface in the form of white layer (or re-solidified layer).

Direct effect of pulse-on time on the thickness of white layer was shown in Fig. 4.15. It was observed that increased pulse-on time resulted in formation of relatively thick white layer. This could be explained by improper flushing of eroded material during constant pulse-off time. As pulse-on time was increased and thereby higher energy per spark was applied at the workpiece; more material was eroded from the work surface. However, material removal rate got reduced since pulse-off duration was not varied. This was because the entire debris could not be flushed away by the dielectric media. Hence, extra molten material got re-solidified on the machining zone forming thicker white layer.

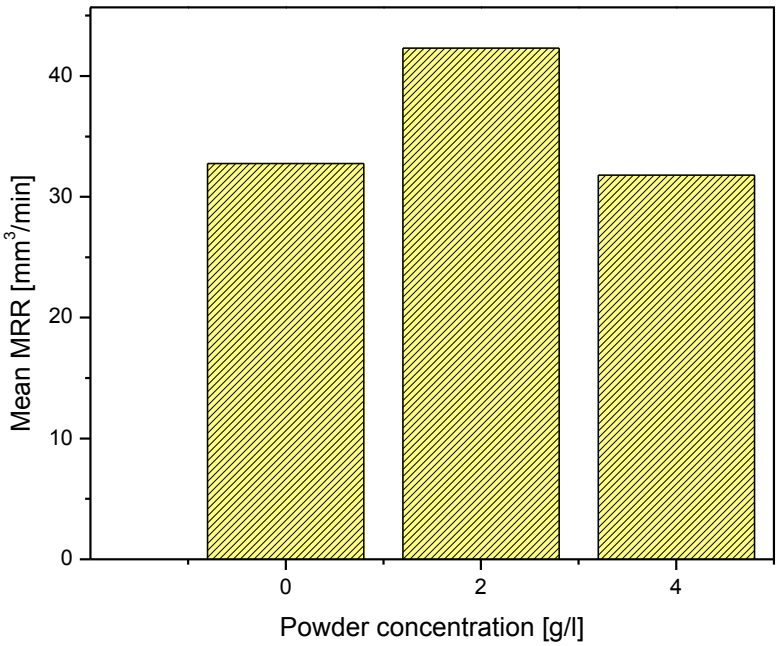

Fig. 4.16: Effect of powder concentration on MRR

Figs. 4.16-4.19 exhibited effects of powder concentration on mean response viz. MRR, R_a, SCD and WLT, respectively. It was observed that for constant energy input, increase in powder concentration caused increased material removal efficiency due to efficient discharge facilitated by the 'bridging effect' of dielectrics. However, after certain limit, increased powder concentration resulted in decreased MRR (Fig. 4.16). Increased powder concentration might cause local agglomeration of powder particles which further obstructed removal of debris adequately. This in turn reduced material removal rate.

Similar trend was noticed for surface roughness (Fig. 4.17). Increase in powder concentration improved MRR and thereby increased roughness value. However, after certain limit; further

increase in powder concentration resulted in reduced MRR value and consequently roughness of the machined surface. At high concentration of powders, local agglomeration of powders caused inefficient flushing. Increased powder particles (sharp edged SiC particles) and also debris tend to rub at the machined zone. Due to such rubbing action, surface finish got improved (surface roughness value gor decreased).

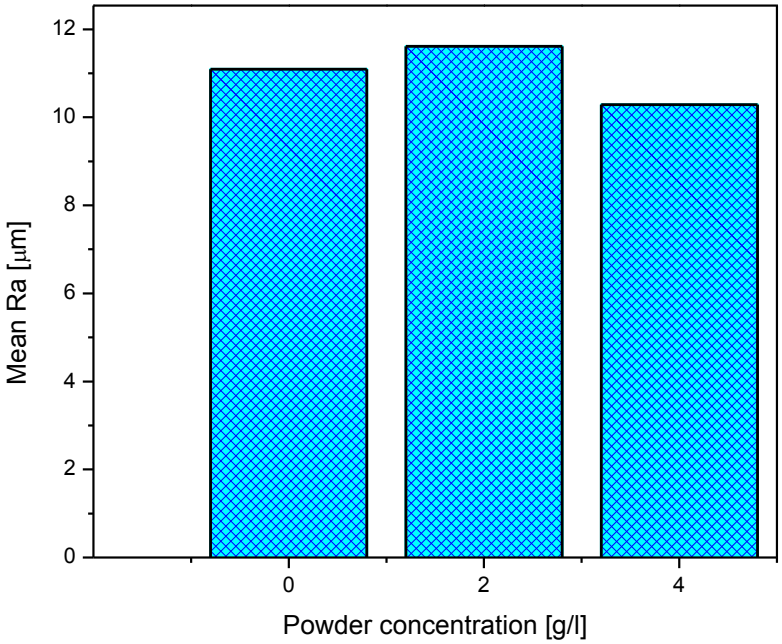

Fig. 4.17: Effect of powder concentration on R_a

It was observed that increase in powder concentration caused decrease in surface crack density up to certain value; further, increased concentration of powder particles into the dielectric media resulted in increased crack density (Fig. 4.18). The initial deceasing trend (with increase in powder concentration) was due to the fact that conductive powder particles carried some portion of the released heat away from the machined zone. This in turn reduced the magnitude of thermal stress evolved at the machined surface. However, at high powder concentration local agglomeration of powders restricted such heat transfer. Heat was thus accumulated at the machined zone and thereby increased the magnitude of the thermal stress. When induced thermal stress exceeded ultimate tensile stress of the work surface; cracking took place.

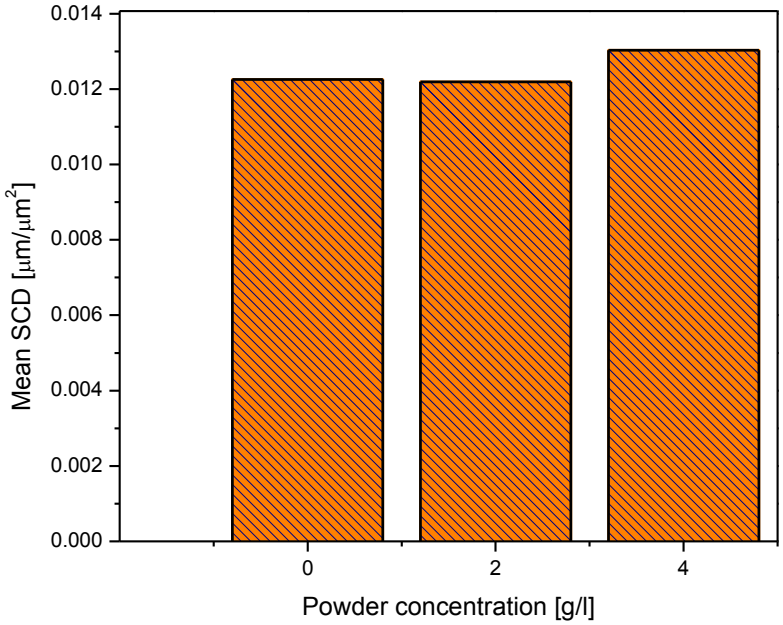

Fig. 4.18: Effect of powder concentration on SCD

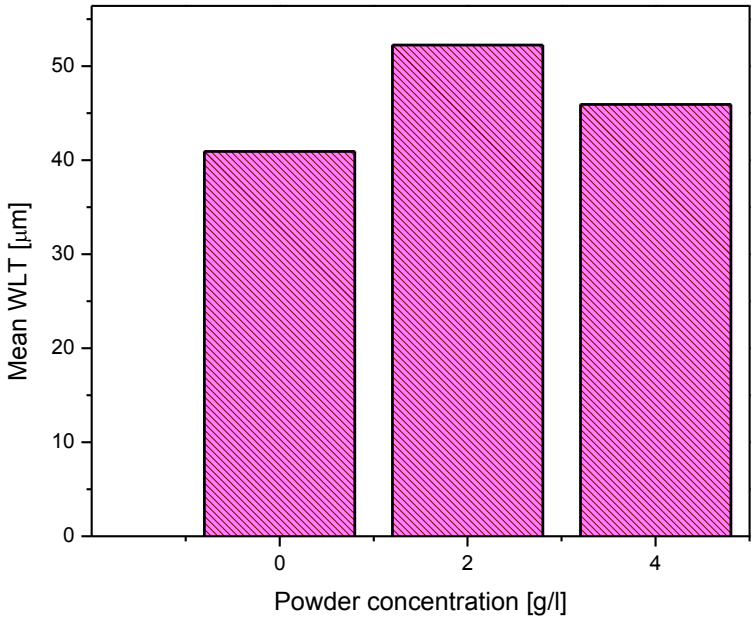

Fig. 4.19: Effect of powder concentration on WLT

The effect of powder concentration on WLT was found similar to that of MRR. At low powder concentration, MRR was high and hence thickness of the white layer got increased (Fig. 4.19). However, at high powder concentration, MRR tend to decrease which in turn resulted in formation of comparatively thin white layer.

CHAPTER 5

Summary and Conclusions

5.1 Conclusions

- ⇨ Use of graphite powder (average particle size ~250μm) added to the dielectric medium (with powder concentration~6g/l) was found beneficial than conventional EDM due to improved MRR, reduced tool wear rate, superior surface finish, and reduced degree of surface cracking.
- ⇨ Maximum improvement in MRR was observed (~13.08%) at 30A. The most satisfactory surface finish was obtained at 20A (R_a ~49.15% reduced than conventional EDM). The minimum tool wear rate was noticed at 30A (~92.68% less than conventional EDM).
- ⇨ As compared to conventional EDM, thickness of white layer was found relatively more for the case of PMEDM. Insufficient flushing due to accumulation of localized agglomerated graphite powders might restrict the eroded material (debris) to be carried away efficiently. This lead to formation of thicker white layer.
- ⇨ Lesser extent of carbon migration at the machined surface was observed during PMEDM. This reduced the amount of hard carbides ($AlNi_3C_{0.5}$, Ni_3(Al, Ti)C, NiC etc.) formed on the machined surface and consequently suppressed the probability of forming severe surface cracks.
- ⇨ The specimen produced by PMEDM exhibited relatively less micro-hardness and residual stress as well, when compared to conventional EDM.
- ⇨ For the case of graphite powder-mixed EDM of Inconel 718, grain refinement of greater extent was observed at the machined surface whilst compared to the case of conventional EDM.

- ⇨ Within selected experimental domain, the most appropriate parametric combination as determined in the *second phase of work* was: [I_P= 25A, T_{on}= 1000µs and powder concentration 4g/l]. Thus, it was found that at low energy input, application of SiC powder (added to kerosene dielectric media) with concentration 4g/l was experienced favorable for achieving improved (maximum) MRR, and reduced R_a, SCD as well as WLT. At low energy input, the effects of adding powder in the dielectric media was found relatively more beneficial as compared to high energy input. Since, at high energy input, there might be a possibility of fusion (melting) of powder particles adversely affecting the 'bridging effect'; local agglomeration of powder particles may cause insufficient flushing of the removed material from the machined surface.
- ⇨ No significant phase alteration was noticed at the EDMed work surface during PMEDM whilst compared to normal EDM. Formation of intermetallic compounds like Ni_3(Al, Ti)C, CoCx was found taking place during EDM operation.
- ⇨ As compared to 'as received' Inconel 718, significant grain refinement was observed for the EDMed surface (produced at I_P= 35A, T_{on}=1000 µs and powder concentration 4g/l) at crystallographic plane in the direction [1 1 1]. Such grain refinement resulted in decreased crystallite size and increased dislocation density.
- ⇨ Significant carbon migration onto the EDMed work surface was noticed due to dielectric cracking of kerosene dielectric media.
- ⇨ Amongst the parameters investigated (peak current, pulse-on time and powder concentration); peak current appeared as the most significant parameter followed by powder concentration.
- ⇨ Effects of powder concentration on MRR, R_a, SCD and WLT were studied in this work for better understanding of process physics during PMEDM.

In this work, two separate research problems are solved. First, deals with graphite powder-mixed EDM of Inconel 718, in which, graphite powders are added/dispersed into normal EDM oil. Parametric appraisal (especially, effect of peak discharge current) is studied on MRR, TWR, and aspects of surface integrity of the EDMed part product. On the other hand, second phase of work attempts to determine an optimal powder concentration for desired output. In this part, SiC macro-powders are added to kerosene dielectric, and then PMEDM is executed on Inconel 718. Hence, it appears difficult to compare results of two distinct studies. Aforesaid two research problems differ in type of dielectric used, type of additives, and

experimental domain. Moreover, particle size, thermal/mechanical/physical properties of powders play important role on the performance of PMEDM.

5.2 Scope for Future Research

The limitations of the present work were also pointed out below. These issues may be considered as future scope of the work.

- ⇨ Effects of variation of particle size of the powder were not examined.
- ⇨ Apart from peak discharge current, effects of other electrical parameters (viz. gap voltage, pulse duration, duty factor etc.) along with dielectric flushing circulation pressure might be studied to understand their influence on machinability of Inconel 718 during PMEDM.
- ⇨ Overcut is a major concern which dictates quality of the EDMed product. In PMEDM, there is a change of occurrence of larger overcut than in conventional EDM. Hence, optimal powder concentration, particle size along with EDM parameters needs to be identified properly.
- ⇨ In PMEDM, there is a chance that powder particles may be fused and stick over the machined surface. This may be in favor of imparting required mechanical properties of the EDMed surface. Hence, selection of powder particle depending on application aspects of the end product is worth of investigating in future.

Few other concerns in PMEDM are: (i) uncertainty on working life of the powder particles, (ii) uncertainty in ensuring adequate circulation of the suspended particles added to the working medium. Low density particles can ensure better suspension effect, (iii) separation of used abrasive powders from the debris (for reuse) is really difficult; hence, environmental issues come into picture.

References

[1] Special Metals Corporation: History, 2008, *http://www.pccforgedproducts.com*.

[2] Ezugwu EO, Fadare DA, Bonney J, Da Silva RB, Sales WF Modelling the correlation between cutting and process parameters in high- speed machining of Inconel 718 alloy using an artificial neural network. *International Journal of Machine Tools and Manufacture* 2005, 45(12): 1375-1385.

[3] Rajesha S, Sharma A, Kumar P On electro-discharge machining of Inconel 718 with hollow tool. *Journal of Materials Engineering and Performance* 2012, 21(6): 882-891.

[4] Zhou J, Bushlya V, Peng RL, Chen Z, Johansson S Analysis of subsurface microstructure and residual stresses in machined Inconel 718 with PCBN and Al2O3-SiCw tools. *Procedia CIRP* 2014, 13(13): 50-155.

[5] Amini MH, Fatemi A, Atefi R High speed turning of Inconel 718 using ceramic and carbide cutting tools. *Arabian Journal for Science and Engineering* 2014, 39(3): 2323–2330.

[6] ASTE Handbook Committee (1950) Tool Engineers Handbook, Mc Graw Hill, New York.

[7] Lee SH, Li XP Study of the effect of machining parameters on the machining characteristics in electrical discharge machining of tungsten carbide. *Journal of Materials Processing Technology* 2001, 115(3): 344-358.

[8] Furutania K, Saneto A, Takezawa H, Mohri N, Miyake H Accretion of titanium carbide by electrical discharge machining with powder suspended in working fluid. *Precision Engineering* 2001, 25(2): 138–144.

[9] Zhao WS, Meng QG, Wang ZL The application of research on powder mixed EDM in rough machining. *Journal of Materials Processing Technology* 2002, 129(1–3): 30–33.

[10] Li L, Gu L, Xi X, Zhao W Influence of flushing on performance of EDM with bunched electrode. *International Journal of Advanced Manufacturing Technology* 2012, 58 (1): 187-194.

[11] Tzeng YF, Lee CY Effects of powder characteristics on electro discharge machining efficiency. *International Journal of Advance Manufacturing Technology* 2001, 17(8): 586–592.

[12] Kansal HK, Singh S, Kumar P Parametric optimization of powder mixed electrical discharge machining by response surface methodology. *Journal of Materials Processing Technology* 2005, 169(3): 427–436.

[13] Peças P, Henriques E Electrical discharge machining using simple and powder-mixed dielectric: The effect of the electrode area in the surface roughness and topography. *Journal of Materials Processing Technology* 2008, 200(1-3): 250–258.

[14] Peças P, Henriques E Effect of the powder concentration and dielectric flow in the surface morphology in electrical discharge machining with powder-mixed dielectric (PMD-EDM). *International Journal of Advanced Manufacturing Technology* 2008, 37(11): 1120–1132.

[15] Kung K-Y, Horng J-T, Chiang K-T Material removal rate and electrode wear ratio study on the powder mixed electrical discharge machining of cobalt-bonded tungsten carbide. *International Journal of Advanced Manufacturing Technology* 2009, 40(1): 95–104.

[16] Jahan MP, Rahman M, Wong YS Study on the nano-powder-mixed sinking and milling micro-EDM of WC-Co. *International Journal of Advanced Manufacturing Technology* 2011, 53(1): 167–180.

[17] Kumar S, Batra U Surface modification of die steel materials by EDM method using tungsten powder-mixed dielectric. *Journal of Manufacturing Processes* 2012, 14(1): 35–40.

[18] Bhattacharya A, Batish A, Singh G, Singla VK Optimal parameter settings for rough and finish machining of die steels in powder-mixed EDM. *International Journal of Advanced Manufacturing Technology* 2012, 61(5): 537–548

[19] Singh S, Yeh MF Optimization of abrasive powder mixed EDM of Aluminum matrix composites with multiple responses using gray relational analysis. *Journal of Materials Engineering and Performance* 2012, 21(4): 481–491.

[20] Mai C, Hocheng H, Huang S Advantages of carbon nanotubes in electrical discharge machining. *International Journal of Advanced Manufacturing Technology* 2012, 59(1): 111–117.

[21] Bai X, Zhang Q-H, Yang T-Y, Zhang J-H Research on material removal rate of powder mixed near dry electrical discharge machining. *International Journal of Advanced Manufacturing Technology* 2013, 68(5): 1757–1766.

[22] Prihandana GS, Sriani T, Mahardika M, Hamdi M, Miki N, Wong YS, Mitsui K Application of powder suspended in dielectric fluid for fine finish micro-EDM of Inconel 718. *International Journal of Advanced Manufacturing Technology* 2014, 75(1): 599–613.

[23] Kolli M, Kumar A Effect of Boron Carbide powder mixed into dielectric fluid on electrical discharge machining of Titanium alloy. *Procedia Materials Science* 2014, 5: 1957-1965.

[24] Singh AK, Kumar S, Singh VP Effect of the addition of conductive powder in dielectric on the surface properties of super alloy Super Co 605 by EDM process. *International Journal of Advanced Manufacturing Technology* 2015, 77(1): 99–106.

[25] Razak MA, Abdul-Rani AM, Nanimina AM Improving EDM efficiency with Silicon Carbide powder-mixed dielectric fluid. *International Journal of Materials, Mechanics and Manufacturing* 2015, 3(1): 40-43.

[26] Kumar H Development of mirror like surface characteristics using nano powder mixed electric discharge machining (NPMEDM). *International Journal of Advanced Manufacturing Technology* 2015, 76(1): 105–113.

[27] Batish A, Bhattacharya A, Kumar N Powder mixed dielectric: an approach for improved process performance in EDM. *Particulate Science and Technology* 2015, 33(2): 150-158.

[28] Singh B, Kumar J, Kumar S Influences of process parameters on MRR improvement in simple and powder-mixed EDM of AA6061/10% SiC composite. *Materials and Manufacturing Processes* 2015, 30(3): 303-312.

[29] Al-Khazraji A, Amin SA, Ali SM The effect of SiC powder mixing electrical discharge machining on white layer thickness, heat flux and fatigue life of AISI D2 die steel. *Engineering Science and Technology, an International Journal* 2016, 19: 1400–1415.

[30] Ekmekci N, Ekmekci B Electrical discharge machining of Ti-6Al-4V in hydroxyapatite powder mixed dielectric liquid. *Materials and Manufacturing Processes* 2016, 31(13): 1663-1670.

[31] Kuriachen B, Mathew J Effect of powder mixed dielectric on material removal and surface modification in microelectric discharge machining of Ti-6Al-4V. *Materials and Manufacturing Processes* 2016, 31(4): 439-446.

[32] Baseri H, Sadeghian S Effects of nanopowder TiO2-mixed dielectric and rotary tool on EDM. *International Journal of Advanced Manufacturing Technology* 2016, 83(1): 519-528.

[33] Prabhu S, Vinayagam BK Optimization of carbon nanotube based electrical discharge machining parameters using full factorial design and genetic algorithm. *Australian Journal of Mechanical Engineering* 2016, 14(3): 161-173.

[34] Li L, Zhao L, Li ZY, Feng L, Bai X Surface characteristics of Ti-6Al-4V by SiC abrasive-mixed EDM with magnetic stirring. *Materials and Manufacturing Processes* 2017, 32(1): 83-86.

[35] Prakash C, Kansal HK, Pabla BS, Puri S Experimental investigations in powder mixed electric discharge machining of Ti–35Nb–7Ta–5Zrβ-titanium alloy. *Materials and Manufacturing Processes* 2017, 32(3): 274-285.

[36] Talla G, Sahoo DK, Gangopadhyay S, Biswas CK Modeling and multi-objective optimization of powder mixed electric discharge machining process of aluminum/alumina metal matrix composite. *Engineering Science and Technology, an International Journal* 2015, 18(3): 369-373.

[37] Tripathy S, Tripathy DK Multi-attribute optimization of machining process parameters in powder mixed electro-discharge machining using TOPSIS and grey relational analysis. *Engineering Science and Technology, an International Journal* 2016, 19(3): 62–70.

[38] Mohanty S, Mishra A, Nanda BK, Routara BC Multi-objective parametric optimization of nanopowder mixed electrical discharge machining of AlSiCp using response surface methodology and particle swarm optimization. *Alexandria Engineering Journal* 2018, 57(2): 609–619.

[39] Dubey V, Singh B Study of material removal rate in powder mixed EDM of AA7075/B_4C composite. *Materials Today: Proceedings* 2018, 5(2) Part 2: 7466–7475.

[40] Newton TR, Melkote SN, Watkins TR, Trejo RM, Reister L Investigation of the effect of process parameters on the formation and characteristics of recast layer in wire-EDM of Inconel 718, *Materials Science and Engineering*: A 2009, 513–514: 208–215.

[41] Talla G, Gangopadhyay S Effect of impregnated powder materials on surface integrity aspects of Inconel 625 during electrical discharge machining. *Proceedings of IMechE Part B: Journal of Engineering Manufacture* 2016, 1–14. (Published Online) DOI: 10.1177/0954405416666904.

[42] Ay M, Çaydaş U, Hasçalık A Optimization of micro-EDM drilling of Inconel 718 superalloy. *International Journal of Advanced Manufacturing Technology* 2013, 66(5): 1015–1023.

[43] Rahul, Abhishek K, Datta S, Biswal BB, Mahapatra SS Machining Performance optimization for electro discharge machining of Inconel 601, 625, 718 and 825: an integrated optimization route combining satisfaction function, fuzzy inference system and Taguchi approach. *Journal of the Brazilian Society of Mechanical Sciences and Engineering* 2017, 39(9): 3499-3627.

[44] Upadhyay C, Datta S, Masanta M, Mahapatra SS An experimental investigation emphasizing surface characteristics of electro-discharge machined Inconel 601. *Journal of the Brazilian Society of Mechanical Sciences and Engineering* 2017, 39(8): 3051-3066.

[45] Jahan MP, Rahman M and Wong YS Modelling and experimental investigation on the effect of nanopowder-mixed dielectric in micro-electrodischarge machining of tungsten carbide. *Proc IMechE, Part B: J Engineering Manufacture* 2010, 224(11): 1725–1739.

[46] Muthuramalingam T, Mohan B, Jothilingam A Effect of tool electrode resolidification on surface hardness in electrical discharge machining. *Materials and Manufacturing Processes* 2014, 29(11-12): 1374–1380.

[47] Wong YS, Lin LC, Rahuman I, Tee WM Near-mirror-finish phenomenon in EDM using powder-mixed dielectric. *Journal of Materials Processing Technology* 1998, 79(1-3): 30–40.

[48] Kozak J, Rozenek M, Dabrowski L Study of electrical discharge machining using powder-suspended working media. *Proceedings of the Institution of Mechanical Engineers Part B Journal of Engineering Manufacture* 2004, 217(11): 1597-1602.

[49] Chow HM, Yan BH, Huang FY, Hung JC Study of added powder in kerosene for the micro-slit machining of Titanium alloy using electro-discharge machining. *Journal of Materials Processing Technology* 2000, 101(1-3): 95–103.

[50] Singh H, Kumar P Optimizing multi-machining characteristics through Taguchi's approach and utility concept. *Journal of Manufacturing Technology and Management* 2006, 17(2): 255-274.

[51] Walia RS, Shan HS, Kumar P Multi-response optimization of CFAAFM process through Taguchi method and utility concept. *Materials and Manufacturing Processes* 2006, 21(8): 907-914.

[52] Singh H, Kumar P Optimizing multi-machining characteristics through Taguchi's approach and utility concept, *Journal of Manufacturing Technology Management* 2006, 17(2): 255-274.

APPENDIX I

List of equipment used along with specifications

[1] Die-Sinking EDM (CNC Series) (ED30C, Excetek Technologies Co., Ltd., Taiwan)

Specification		
X/Y Travel	[mm]	300 x 250
Z Travel	[mm]	300
Work Table	[mm]	650 x 350
Max. Workpiece size	[mm]	800 x 500 x 300
Max. Workpiece Weight	[kg]	550
Max. Electrode Weight	[kg]	120
Machine Weight	[kg]	1150
Outside Dimensions (Machine body+Travel+Tank+Generator)	[mm]	3050 x 1380 x 2090
Electrode Head to Work (Table Distance)	[mm]	270~550
Tank Capacity	Litre [l]	350

[2] Submersible Pump (Polo Cool, TMA International, New Delhi, India)

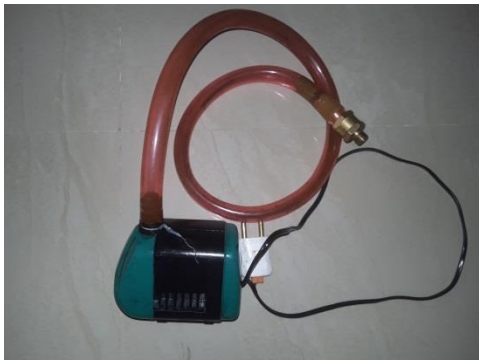

Technical parameters	
Voltage	165-220 V/50 Hz
Power	30 W
H-Max	7.5 F
Output	1800 l/h

[3] Stirrer (Venus Aqua, Kolkata, India)

Technical parameters	
Voltage	220 V, 50 Hz
Power	15 W
F-Max	880 l/h
Product Dimensions	21 x 6.3 x 10 cm; 222g
Item part number	Venus 6001F
ASIN	B0142RZBWI

[3] Pressure Gauge (Micro Stainless Steel Pressure Gauge, M/S Shubh Instruments, Mumbai, India)

Technical details:
Brand: Micro
Case and Bezel: SS304 Crimp Type / Snap Action Bayonet Type
Accuracy: ± 1% of full scale
Ranges: Pressure up to 0-7 bar
Size: 63 mm
Wetted Parts: Stainless Steel

[4] Sprit Level (Msldf300, CS Enterprises, Mumbai, India)

Precise Aluminum Frame and Magnetic Spirit Level

Technical details:
Size and Type: The bubbles shall be of cylindrical type having outside diameter of 9.0 + 1 mm and length 70 + 1.0 mm.
Accuracy: The accuracy of the spirit level shall be from 0.05 mm/M to 0.1 mm/M at 27°C.

Functional Requirements: The spirit level shall have the following technical features:

- ⇨ Base length: 200 mm + 1 mm
- ⇨ Base width: 20 mm + 0 – 1
- ⇨ Height: 25 + 1 mm
- ⇨ Bubble opening: 50 mm x 8 mm (length x width)
- ⇨ Sensitivity: 2 min. 30 s per 2 mm arc division of the dial
- ⇨ Least count of graduation: 2 mm
- ⇨ Weight (Without: 150g approx.)
- ⇨ Effective length of bubble: 20 + 1 mm

[5] Wight Balance (Gold600; Phoenix Electronics and Weighing Systems, India)

Specification	
Model	Gold600
Capacity	600g
Accuracy	0.01g
Platter Size	125 mm diameter

Main Features:

- ⇨ R. bright LEO display
- ⇨ 24 bit F -A ADC (High resolution)
- ⇨ Feather touch keyboard with audible indication during entry
- ⇨ Display intensity adjustable for longer halt, back-up
- ⇨ Memory Accumulation: Battery voltage display on screen

Accessories:

- ⇨ 6 V, / AH rechargeable SASS battery
- ⇨ Computer / Printer interface
- ⇨ Thermal Porter (with adaptor)
- ⇨ Green bright LED display

APPENDIX II

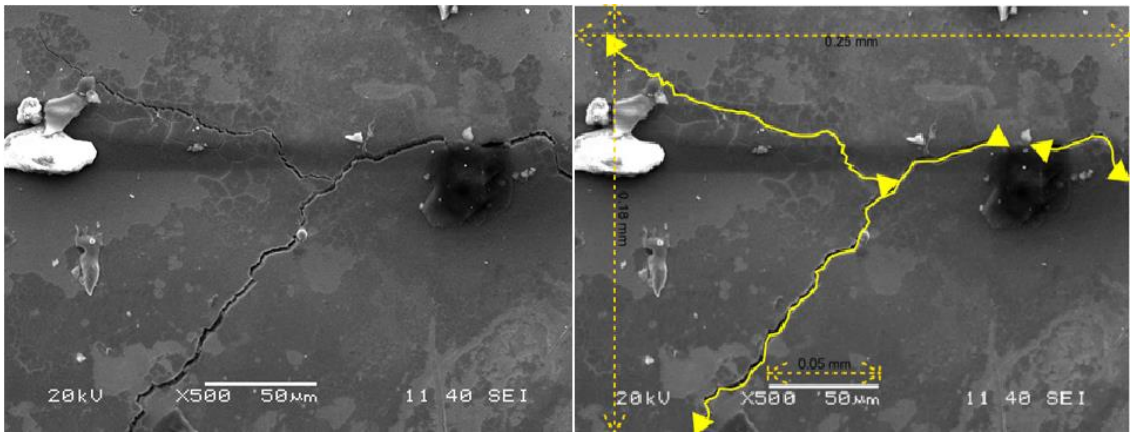

Measurement of crack density at the EDMed surface obtained at parameters setting [Ip=25A, Ton=1500µs, and powder concentration=2g/l]

$$SCD = \frac{Total\ crack\ length}{Micrograph\ area} = \frac{\sum_{i=1}^{n} L_i}{A} = 0.00911 \frac{\mu m}{\mu m^2}$$

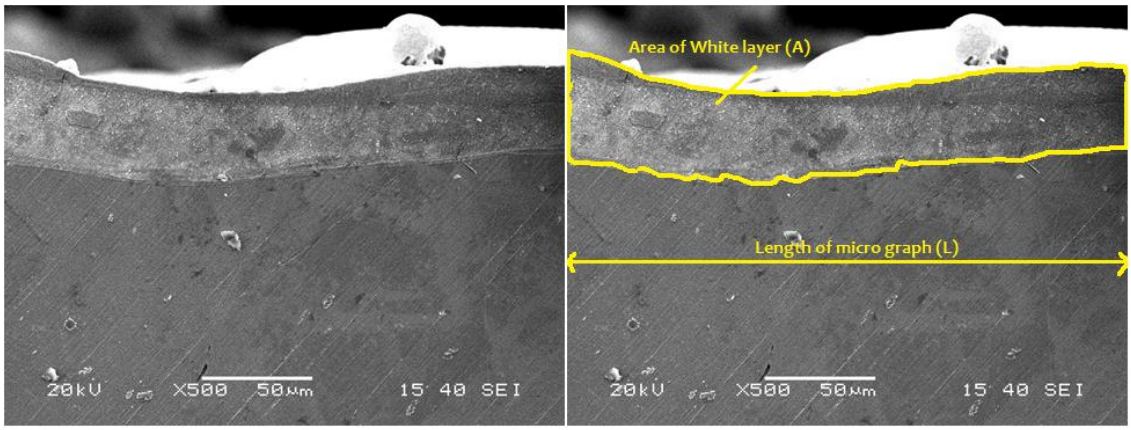

Measurement of white layer thickness for the EDMed surface obtained at parameters setting [Ip=35A, Ton=1000µs, and powder concentration=4g/l]

$$WLT = \frac{Area\ of\ white\ layer\ (A)}{Lenth\ of\ micrograph\ (L)} = \frac{10012.73}{252.083} = 39.72 \mu m$$

APPENDIX III

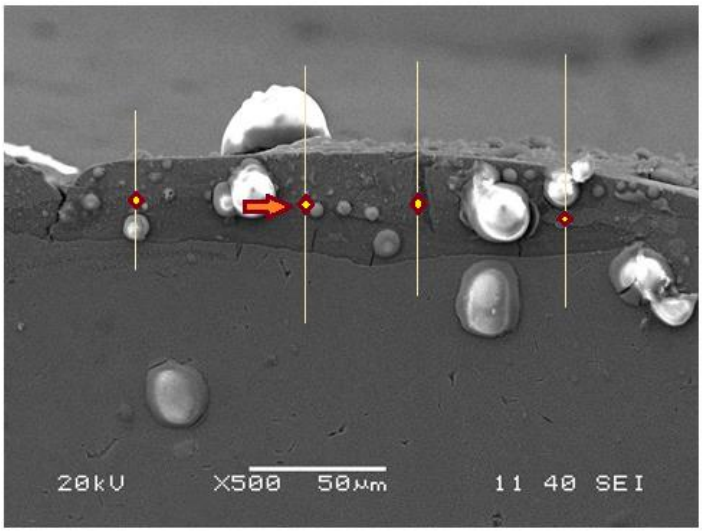

SEM micrograph of transverse-cut section of the EDMed specimen showing places of micro-indentation for hardness test: specimen obtained in conventional EDM at I_P=25A

APPENDIX IV

Utility Theory

Walia et al. [51] and Singh and Kumar [52] provided a comprehensive theoretical background of utility theory. Utility is suitability of a product with respect to consumers' expectations. The acceptability of a particular product depends on several criteria (may be conflicting to each other; ex. Higher-is-Better, HB; Lower-is-Better, LB). The theory provides a logical way to aggregate multiple criteria values into a unique index termed as overall utility degree. The most appropriate product should possess maximum value of overall utility degree.

It is, therefore, assumed that the overall utility degree of a particular product is the additive function of individual utility of each criterion.

Assuming the said EDM process was characterized by a total K criteria (ex. $K = 4$; i.e. MRR, R_a, SCD and WLT with reference to refer to Table 2.7 of Chapter 2); and, a total N settings (parametric combinations) were available for evaluation (ex. $N = 9$; in the present case). The 9 parametric combinations of L_9 OA were nothing but possible process environments; could be understood as candidate alternatives. Each process environment was capable of providing a product with a particular set of criteria values. The goal of utility theory was to select the best process environment to satisfy contradicting requirements of multi-criteria simultaneously.

If $x_i(k)$ is the value (experimental data) of k^{th} criterion in i^{th} experimental run $(i = 1,2,...,N)$ and there were a total of K criteria, then the joint utility function could be expressed as:

$$U_O(x(1), x(2),..., x(k),..., x(K)) = f(U(1), U(2),..., U(k),..., U(K)) \quad (4.1)$$

A preference scale for each criterion was constructed for determining its utility value. Two arbitrary numerical values (preference number) 0 and 9 were assigned to the just acceptable (the worst) and the most acceptable (the best) value of the criteria, respectively. The preference number (also called utility value) of a particular criterion could be expressed on a logarithmic scale as follows.

$$U_i(k) = A \times \log\left(\frac{x_i(k)}{\bar{x}(k)}\right) \quad (4.2)$$

Here $U_i(k)$ denoted utility value of k^{th} criterion in i^{th} setting;. $x_i(k)$ was the value of k^{th} criterion obtained at i^{th} setting; where, $(k = 1,2,..., K)$ and $(i = 1,2,..., N)$.

Also, $\bar{x}(k)$ was the just acceptable value of k^{th} criterion with the following condition i.e.

$\bar{x}(k) = \underset{i=1,2,...,N}{Min}\left[x_i(k)\right]$, if the requirement of k^{th} criterion: Higher-is-Better; else,

$\bar{x}(k) = \underset{i=1,2,...,N}{Max}\left[x_i(k)\right]$, if the requirement of k^{th} criterion: Lower-is-Better.

The value of A could be found by utilizing two boundary conditions that

if $x_i(k) = \bar{x}(k) \Rightarrow U_i(k) = 0$

and if $x_i(k) = x^*(k) \Rightarrow U_i(k) = 9.$

Here,

$x^*(k) = \underset{i=1,2,...,N}{Max}\left[x_i(k)\right]$, if the requirement of k^{th} criterion: Higher-is-Better; else,

$x^*(k) = \underset{i=1,2,...,N}{Min}\left[x_i(k)\right]$, if the requirement of k^{th} criterion: Lower-is-Better; $x^*(k)$ being the most acceptable value for k^{th} performance attribute.

Therefore, $A = \dfrac{9}{\log\left(\dfrac{x^*(k)}{\bar{x}(k)}\right)}$ (4.3)

The overall utility degree U_i^O for i^{th} process environment could be calculated as follows (assuming equal priority weight of individual attributes):

$$U_i^O = \frac{1}{K}\sum_{k=1}^{K} U_i(k);\ (i = 1,2,...,N; k = 1,2,...,K) \quad (4.4)$$

Based on U_i^O, the superiority of a particular parametric setting (process environment) could be evaluated which corresponded to maximum U_i^O; and, that setting could be treated as optimal setting. However, in the present work, the most favorable setting (with maximum U_i^O) could easily be identified from amongst 9 settings experimented as per L_9 OA. But this setting could not be treated as optimal because there might be a possibility that the maximum U_i^O could be obtained at a different setting beyond L_9 OA since full factorial designed experimentation was not performed. Therefore, overall utility thus obtained from L_9 OA experimentation needed to be extrapolated. This was done by Taguchi method. Hence, the advantage of exploring utility theory could well be understood by the fact that utility theory provided a basis for logical aggregation of multi-criteria into a single (criterion) index thus provided scope for applying Taguchi method for

optimization; because, traditional Taguchi method failed to solve multi-response optimization problems. Utility theory could eliminate dimensional effect and criteria conflict thereby combining utility values of individual responses into overall utility which corresponded to Higher-is-Better (HB) requirement.

Resume

Name: SANTOSH KUMAR SAHU

Father's Name: Mr. Udayanath Sahu

Mother's Name: Mrs. Rupabati Sahu

Address for Correspondence: At/Po- Knandasar, PS- Nalco, Dist- Angul, Odisha 759145

Phone No.: 06764-221666, **Mobile No.**: +91 9437383046, +91 7008358664

Email ID: 4chinu@gmail.com, sahunitrkl@gmail.com, sksahu_me@vssut.ac.in

EDUCATION

Degree	Examination Passed	Year of Passing	Institute	Board /University	Subject/Discipline /Specialization
X[10^{th}]	H.S.C. Exam	2000	P.T.C. High School, Angul	B.S.E. Odisha	MIL(O), Eng, Sci, Social Sci, Math
Under Graduate Degree	Diploma	2003	K.I.M.E.T. Chhendipada, Angul	S.C.T.E. &V.T., Odisha	Mechanical Engineering
Graduate Degree	B. Tech.	2007	S.I.ET., Dhenkanal	B.P.U.T. Odisha	Mechanical Engineering
Post Graduate	M. Tech. (Res)	2014	N.I.T., Rourkela	N.I.T., Rourkela, Odisha	Production Engineering
Doctoral Degree	Ph.D. (Engg.)	Thesis submitted	Jadavpur University	Jadavpur University, Kolkata	Mechanical Engineering

EXPERIENCE

Organization	Period		Designation
	From	To	
Kamalesh Construction Pvt. Ltd., Angul, Odisha	May 2007	July 2008	Mechanical Engineer
Orissa Engineering College, Bhubaneswar, Odisha	Aug 2008	July 2012	Assistant Professor
	Sept 2014	Aug 2017	Associate Professor
Veer Surendra Sai University of Technology (VSSUT), Burla, Sambalpur, Odisha	Sept 2017	Till date	Assistant Professor

SANTOSH KUMAR SAHU